AN ABSTRACT OF THE DISSERTATION OF

Jonathan James Halama for the degree of Doctor of Philosophy in Environmental Science presented on January 6, 2017.

Title: Penumbra: A Spatiotemporal Shade-Irradiance Analysis Tool with External Model Integration for Landscape Assessment, Habitat Enhancement, and Water Quality Improvement.

Abstract approved:

_____ _____

Robert E. Kennedy James J. Graham

Several solar energy models exist, but all models must balance: computational runtime, light complexity, and model output volume. These models span the spectrum of simplistic global solar energy equation sets to complex light ray-tracing models. Spatiotemporally inaccurate representations of solar energy may cause compounding simulation effects and introduce unknown modeling uncertainty. Within the current solar energy modeling spectrum was the need to advance large watershed area spatiotemporal irradiance modeling. A model utilizing methods simpler than ray-tracing that still accounted for the major environmental light reduction factors was needed. The model developed we called Penumbra. Penumbra provides solar energy reduction from topographic shadowing, forest shadowing, and cloud coverage at landscape scales. Penumbra was developed to function as a stand-alone model, but also be capable of integration within existing ecosystem models. Penumbra's intended audience include ecosystem modelers, land owners, watershed councils, county, state, and federal entities; any group needing an enhanced understanding of how light energy impacts processes within their landscapes. The questions being asked by my intended audience regard riparian zone restoration, fish habitat restoration, and improved forest management. To address these questions, a well-functioning shade|irradiance model capable of assisting with multiyear landscape assessments was needed.

Penumbra:
A Spatiotemporal Shade-Irradiance Analysis Tool with External Model Integration for Landscape Assessment, Habitat Enhancement, and Water Quality Improvement

by
Jonathan James Halama

A DISSERTATION

submitted to

Oregon State University

in partial fulfillment of
the requirements for the
degree of

Doctor of Philosophy

Presented January 6, 2017
Commencement June 2017

Doctor of Philosophy dissertation of Jonathan James Halama presented on January 6, 2017

APPROVED:

Co-Major Professor, representing Environmental Science

Co-Major Professor, representing Environmental Science

Director of the Environmental Science Graduate Program

Dean of the Graduate School

I understand that my dissertation will become part of the permanent collection of Oregon State University libraries. My signature below authorizes release of my dissertation to any reader upon request.

Jonathan James Halama, Author

ACKNOWLEDGEMENTS

The journey concluding to the completion of this dissertation was traveled sole, but far from alone. There were many companions along the trail, and I am grateful that each openly extended their assistance through support, knowledge, and guidance.

I first want thank all my family and friends for always supporting my efforts, even without always understanding why. The life of a researcher is not one of consistency, complacency, or continuance of empathy. A researcher's daily struggles of mental strain, odd hours, and a constant consciousness of the known unknowns are as heavily a burden on the family as the researcher, if not more.

I want to lovingly thank my wife, Kylee Halama, for her endless support of my efforts. She shared my burden equally. Without her, I would have lost my humanity in the pursuit of truth and science. As I pretend to simulate reality she continued to remind me of what reality truly is, and doing so with constant love and support.

I am grateful for the EPA research colleagues I have worked with over the years. The completion of this work, the successes, and all future potential is theirs as much as mine. I only stand with a completed dissertation due to the contributions of Dr. Robert B. McKane, Dr. Allen Brookes, Dr. Bradley L. Barnhart, Paul Pettus, Kevin Djang, and Patrick Wingo. Each contributed an extensive amount of time, expertise, and support through this endeavor.

I thank Oregon State University (OSU), U.S. Environmental Protection Agency (EPA), and Oak Ridge Institute for Science and Education (ORISE) for offering the many opportunities these organizations provide to aspiring researchers. Without their support, many scientific endeavors would never be initiated or completed. I thank them all for the years of direct and indirect support, plus their efforts harboring a culture of scientific exploration.

I want to explicitly thank Dr. Robert B. McKane, Dr. James J. Graham, and Dr. Robert E. Kennedy:

- Dr. Robert McKane supported my research efforts through years of emotional support and employment. He has been a remarkable mentor over the years, and one of the strongest supporters of my research ideas and ambitions. Without his

support this project would have never reached fruition. Beyond being a colleague, Dr. McKane became a close and dear friend. I thank him for everything he has done for me.

- Dr. James “Jim” Graham set the foundation of my spatial science knowledge and spatiotemporal modeling cognizance. He is an incredible educator and researcher. His approach to science and life extends beyond most people’s bounds. Anyone whom has the privilege to learn from Jim walks away with clearer and better understanding of why. Jim has been a friend, educator, and mentor for many years. I thank him for everything he has done for me.
- Dr. Robert E. Kennedy refined my research theory through continuous perspective shifts. I thank him for his continuous support, guidance, fortitude, and foresight. Dr. Kennedy agreed to step into an already progressing research project and help guide it to completion. His keen understanding of forestry research and environmental modeling, combined with open-mindedness and optimistic attitude helped maintain my projects momentum. That all led to this projects success. Robert has been an incredible mentor and become a close friend. I thank him for everything he has done for me.

CONTRIBUTION OF AUTHORS

Jonathan Halama formulated the project in chapters 2, 3, and 4. Dr. Robert E. Kennedy and Dr. James J. Graham both contributed greatly to the research implementation, management, execution, success, and authorship of all chapters.

TABLE OF CONTENTS

Page

1. Introduction 1

1.1 References 5

2. Penumbra: A spatially-distributed shade percent and incident ground-level irradiance model for simulating landscape scale solar energy 6

2.1 Abstract 6

2.2 Introduction 6

2.3 Modeling Theory 12

2.4 The Penumbra Model 12
2.4.1 Inputs 13
2.4.2 Processing Steps 14
2.4.3 Solar Angles 15
2.4.4 Walking Algorithm 15
2.4.5 Terrestrial Irradiance 16
2.4.6 Cosine Effect and Calibration on Terrestrial Irradiance 16
2.4.7 Solar Ray Height 16
2.4.8 Object Shade Reductions 16
2.4.9 Topographic Shade Reductions 17
2.4.10 Spatial Mask 18
2.4.11 Graphic Processing Unit (GPU) 18

2.5 Outputs 19
2.5.1 Object and Topographic Shade 19
2.5.2 Net Ground-Level Solar Energy 19

2.6 Calibration Process 20

2.7 Model Testing 20
2.7.1 Modeled versus Observed Solar Angle 21
2.7.2 Modeled versus Observed Global Irradiance 21
2.7.3 Model Calibration for Adjacent Forest and Open Sites 21
2.7.4 SNOTEL Site Calibrations 24

2.8 Landscape Scale Simulations 25

2.9 Discussion 27

2.10 Conclusion 28

2.11 References 30

2.12 Figures 33

2.13 Tables 51

2.14 Appendix 54

3. Improved Soil Temperature Modeling using Spatially-distributed Irradiance 55

3.1 Abstract 55
3.2 Introduction 55
3.3 Methodology 58
3.3.1 Global Irradiance Models: Previous and Current 58
3.3.2 Soil Temperature Model: Current Model and Improvements 59
3.3.3 Improved Soil Temperature Model 61
3.3.4 VELMA-Mimic Model 62
3.4 Soil Temperature Model Testing 65
3.5 Results 65
3.5.1 Penumbra Testing Using O'CCMoN Observed Data 66
3.6 Discussion 67
3.7 Conclusion 68
3.8 References 70
3.9 Figures 72
3.10 Tables 91

4. Dynamic landscape irradiance influenced by dynamic forest growth and disturbance 92

4.1 Abstract 92
4.2 Introduction 92
4.3 Model Integration 95
4.4 Site Description 97
4.5 Site Disturbance Scenarios 97
4.5.1 Historic Harvest 97
4.5.2 Suspended Harvest 98
4.5.3 Intensified Harvest 98
4.6 Watershed Simulations and Results 98
4.6.1 Historic Harvest Scenario (1990-2008) 99
4.6.2 Suspended Harvest Scenario (1990-2008) 99
4.6.3 Intensified Harvest Scenario (1990-2008) 100
4.6.4 Aggregated Results 100
4.7 Discussion 101
4.8 Conclusion 102
4.9 References 103
4.10 Figures 105
4.12 Appendix 115

5. Conclusion 116

6. Bibliography 119

LIST OF FIGURES

Figure Page

Figure 2-1: Shade modeling approach continuum. 33

Figure 2-2: Penumbra's solar ray approach to shade modeling. 33

Figure 2-3: Penumbra model framework. 34

Figure 2-4: Solar azimuth (α) and altitude (γ). 34

Figure 2-5: Walking Algorithm azimuth rise|run conversions. 35

Figure 2-6: Validation of Penumbra simulated azimuth and altitude angles. 36

Figure 2-7: Validation of Penumbra simulated extraterrestrial irradiance. 37

Figure 2-8: Moose Mountain Open site and Forest site. 38

Figure 2-9: Simulated versus observed PAR for Moose Mtn. Open site. 39

Figure 2-10: Simulated versus observed PAR for Moose Mtn. Forest site. 40

Figure 2-11: Static results for Moose Mountain Open and Forest sites. 41

Figure 2-12: Falls Creek EPA Crest to Coast Open and Forested Sites. 42

Figure 2-13: Simulated versus observed agreement for Falls Creek Open site. 43

Figure 2-14: Simulated versus observed agreement for Falls Creek Forest site. 44

Figure 2-15: Static results for Falls Creek Open and Forest sites. 45

Figure 2-16: SNOTEL sites: Meadows Pass and Mount Gardner. 46

Figure 2-17: Winter solstice irradiance across eastern Mashel River Watershed 47

Figure 2-18: Spring equinox irradiance across eastern Mashel River Watershed 48

Figure 2-19: Summer solstice irradiance across eastern Mashel River Watershed 49

Figure 2-20: Fall equinox irradiance across eastern Mashel River Watershed 50

Figure 3-1: Penumbra's uniform solar ray approach to shade modeling. 72

Figure 3-2: H.J.Andrews Experimental Forest Watershed-10 (WS10) site. 72

LIST OF FIGURES (Continued)

Figure Page

Figure 3-3: Oregon Crest-to-Coast Environmental Monitoring transect site locations.... 73

Figure 3-4: Comparison AST and AST3 for Cascade Head Open site soil layer 1..... 74

Figure 3-5: Comparison AST and AST3 for Cascade Head Open site soil layer 2..... 75

Figure 3-6: Comparison AST and AST3 for Cascade Head 14 Forest site soil layer 1. .. 76

Figure 3-7: Comparison AST and AST3 for Cascade Head 14 Forest site soil layer 2. .. 77

Figure 3-8: Comparison AST and AST3 for Moose Mountain Open site soil layer 1. 78

Figure 3-9: Comparison AST and AST3 for Moose Mountain Open site soil layer 2. 79

Figure 3-10: Comparison AST and AST3 for Moose Mountain Forest site soil layer 1.. 80

Figure 3-11: Comparison AST and AST3 for Moose Mountain Forest site soil layer 2.. 81

Figure 3-12: Comparison AST and AST3 for Soapgrass Open site soil layer 1. 82

Figure 3-13: Comparison AST and AST3 for Soapgrass Open site soil layer 2. 83

Figure 3-14: Comparison AST and AST3 for Soapgrass Forest site soil layer 1. 84

Figure 3-15: Comparison AST and AST3 for Soapgrass Forest site soil layer 2. 85

Figure 3-16: Comparison AST and AST3 for Toad Creek Open site soil layer 1. 86

Figure 3-17: Comparison AST and AST3 for Toad Creek Open site soil layer 2. 87

Figure 3-18: Comparison AST and AST3 for Toad Creek Forest site soil layer 1. 88

Figure 3-19: Comparison AST and AST3 for Toad Creek Forest site soil layer 2. 89

Figure 3-20: Location of field sites along stylized elevation profile, physical and biological characteristics across this transect, and names and major features of the various sites. 90

Figure 4-1: Penumbra-VELMA tightly-coupled model integration. 105

Figure 4-2: Mashel River Watershed land ownership and major sub-watersheds..... 106

Figure 4-3: Historic forest harvest pattern of the Mashel River Watershed. 107

LIST OF FIGURES (Continued)

Figure . Page

Figure 4-4: Intensified forest harvest pattern of the Mashel River Watershed scenario. 108

Figure 4-5: Initial 1990 state for the Penumbra-VELMA simulation..... 109

Figure 4-6: Historic scenario static result for the Penumbra-VELMA simulation..... 110

Figure 4-7: Suspended scenario static result for the Penumbra-VELMA simulation. ... 111

Figure 4-8: Intensified scenario static result for the Penumbra-VELMA simulation..... 112

Figure 4-9: Spatially summed and daily to monthly aggregated results..... 113

Figure 4-10: Monthly aggregated irradiance deltas for scenarios minus historic..... 114

LIST OF TABLES

Table Page

Table 2-1: List of Penumbra inputs, parameters, and outputs. 51

Table 2-2: List of Penumbra calibration parameters..... 51

Table 2-3: Converting azimuth and altitude angles to conform within Cartesian coordinate system..... 51

Table 2-4: Moose Mountain parameters, initial results, and calibrated results. 52

Table 2-5: Fall Creek parameters, initial results, and calibrated results.. 52

Table 2-6: SNOTEL 3-Meter results for four-day site calibration sequence..... 52

Table 3-1: VELMA soil temperature sub-model inputs variables.. 91

Table 3-2: O'CCMoN paired Open and Forest sites. 91

Table 3-3: VELMA-AST and VELMA-AST3 O'CCMoN results..... 91

1. Introduction

Ecosystem models provide insight into landscape health, resilience, and to some degree an expectation of the future due to system changes through landscape management (*Abdelnour et al., 2011*; *Fatichi et al. 2016*). The goals surrounding the development of these models, and how these models are utilized, vary dramatically. This is not to say ecosystem models are not useful, but rather these models are very useful within their limitations (*Johnson 2003*; *Guzy 2008*). The one constant across not only ecosystem models, but all models, is an attempt to simplify reality without compromising the representation of reality.

The most basic ecosystem models are plots of environmental relationships. Relationships of dependent and independent variables provide insights into how biotic and abiotic processes function. Tree growth is partially regulated by temperature and water availability (*Mellander et al., 2006*). Salmonid migration is in part successful by cold water refugia (*Brown et al., 2015*). Species distribution can be influenced by light availability (*Kelly et. al., 2003*). These relationships allow us to understand patterns and infer process-level controls for responses to independent variables. Relationships of this sort are typically developed from single location or plot level research.

Our environments are not this simplistic, but rather a complicated tapestry where any single aspect of an environmental phenomena can only be representative of one part of the bigger picture. Site data can be detailed and capture unique micro-scale processes, but only through geospatial variability and through long periods of observation do the data relationships begin to be indicative of reality.

The interplay of these environmental relationships can be constructed into meaningful process-based connections. Ecosystem models are the result of these associates. Built well, these models can provide representative and meaningful simulations of complex environmental processes. A meaningful simulation would be one backed by a validated model with known degree of uncertainty. The uncertainty surrounding a process-based ecological model can be introduced from several sources.

Here some issues surrounding ecological modeling are emphasized by conceptualizing how solar energy is utilized within such models. The first source of model

error spawns from the framework chosen to represent reality. For simplistic solar energy models a daily global irradiance value is often calculated. This representation possesses no landscape level spatial representation; therefore, this simplistic perspective should only be utilized at scales indicative of global irradiance. Solar irradiance models possessing a spatial representation are often spatially implicit. This is seen in models where data are aggregated over an area or stream segment. A point source within the area becomes representative of solar energy throughout the area. For some ecological variables, this assumption can be accurate, but shading effects on landscape solar energy are too complex in most environments to make such assumptions.

The second source of modeling error spawns from how detailed the model can represent reality, and any error persisting within the input data used to represent that reality. Ray-tracing models represent finite interactions of light within complex representations of tree structure (*Seidl et al., 2012*). At a local scale, these representations can produce detailed simulations of solar energy with high degrees of accuracy. At a landscape scale, the technology needed to capture data with such detail does exist, but these data do not ubiquitously exist. Ray-tracing models are also computationally demanding. For a landscape this computational demand makes the solar energy ray-tracing approach currently not feasible due to long computer runtime requirements.

The third source of modeling error spawns from how other modeling processes utilize solar energy data. An ecological model may contain a sub-model that was developed with the intent of being driven from spatially-distributed irradiance. With the proper irradiance input data, this sub-model may accurately represent the ecological process it was intended to simulate. Yet, the full model does not possess the irradiance data to drive the sub-model at such accurate levels. Due to the lack of proper spatially-distributed irradiance data, the sub-model fails to meet its accuracy potential. These modeling situations may result simulations that do not to their full potential, and create results that contain unexplainable error. Such simulation approaches introduce uncertainty to the modeling results.

A solar energy modeling niche existing between overly simplistic to overly complicated methods from the perspective of landscape scale process-based ecological

models. First, to fill this niche this study developed Penumbra, a landscape scale shade-irradiance model capable of: (1) producing spatiotemporal ground-level shade percent and irradiance data, (2) functioning with relatively limited model inputs that are nationally available, (3) functioning under flexible temporal runtime parameters, and (4) developed with flexible model coupling (loose and tight) for external model integration. Penumbra was validated against several independent sources of observed irradiance data to provide characterization of its modeling uncertainty.

Second, this study demonstrates how spatially distributed solar energy can improve an existing model's processes. This was accomplished through the inclusion of solar energy into VELMA (*Abdelnour et al., 2011*). VELMA is a spatially-distributed ecohydrological model with an existing soil temperature sub-model. The standard versus irradiance added soil temperature model results are tested against observed soil temperature data. These results provide solid reasoning for any spatiotemporal ecological model to either utilize Penumbra output data as input driver data, or evaluate model coupling with Penumbra, to improve components of its modeling workflow.

Third, this study provides an example of tight-model coupling with an established spatially-distributed ecohydrological model. This coupling of models allowed Penumbra to dynamically simulate landscape scale ground level irradiance resulting from the dynamic growth and disturbance of forest landscapes over two decades. These results provide an example theoretical case study of the informative data such an integration can be produce. Such simulations provide process-level details on solar energy response to forest growth and harvest, which could not feasibly be captured through experimentation or observation. Such integrations will allow for improved sub-modeling of soil temperature, stream temperature, habitat suitability, photosynthesis, snow dynamics, and any other ecological process where spatially distributed solar energy has a significant impact on environmental process.

Penumbra was developed to be, or be part of, a decision support tool framework. The inclusion of spatially-distributed solar energy provides a deeper understanding of how a landscape's morphology impacts the biological processes occurring within it. Even deeper, if one was to change the landscape, Penumbra can assist with an understanding of

how those changes will play out into the future, especially when integrated with another dynamic ecological model. Penumbra as a stand-alone model, or integrated with other ecological models, can provide stakeholders the ability to simulate and understand a variety of landscape management plans prior to implementation of management activities that can take years to decades to come to fruition.

1.1 References

Abdelnour, A., Stieglitz, M., Pan, F, McKane, R. (2011). "Catchment hydrological responses to forest harvest amount and spatial pattern." Water Resources Research 47(9): 1-18.

Brown, R., Ebersole, J., Brookes, A., Boxall, G., Massie, J. (2015). “Evaluating the Simulation of Metacommunities for Riverine Fishes (SMURF).” 145th Annual Meeting, Portland, Oregon, American Fisheries Society.

Caissie D. (2006). “The thermal regime of rivers: a review”. Freshwater Biology 51: 1389–1406

Fatichi, S., Vivoni, E. R., Ogden, F.L., Ivanov, V. Y., Mirus, B., Gochis, D., Downer, C. W., Camporese, M., Davidson, J. H., Ebel, B., Jones, N., Kim, J., Mascaro, G., Niswonger, R., Restrepo, P., Rigon, R., Shen, C., Sulis, M., Tarboton, D. (2016), “An overview of current applications, challenges, and future trends in distributed process-based models in hydrology.” USA, Journal of Hydrology, 537, pp. 45–60, doi:10.1016/j.jhydrol.2016.03.026.

Guzy, M. R., C. L. Smith, J. P. Bolte, D. W. Hulse and S. V. Gregory. (2008). “Policy research using agent based modeling to assess future impacts of urban expansion into farmlands and forests.” Ecology and Society 13(1): 37.

Johnson, S. L. (2003). "Stream temperature: scaling of observations and issues for modelling." Hydrological Processes 17(2): pp. 497-499.

Mellander, P.E., Stahli, M., Gustafsson, D., and Bishop, K. (2006) “Modelling the effect of low soil temperatures on transpiration by Scots pine”, Hydrological Processes., 20, pp. 1929–1944.

Seidl, R., Rammer, W., Scheller, R. M., Spies, T. A. (2012). "An individual-based process model to simulate landscape-scale forest ecosystem dynamics." Ecological Modelling 231: pp. 87-100.

2. Penumbra: A spatially-distributed shade percent and incident ground-level irradiance model for simulating landscape scale solar energy

2.1 Abstract

Landscape incident solar radiation is a significant environment driver, yet it can be complicated to model well. Several solar radiation models estimate the effects of irradiance by representing light at discrete point locations, over averaged zonal areas, or at polyline centers all to simplify the modeling of lights complexity. These modeling approaches have appropriate applications, but do not provide spatially-distributed or temporally dynamic representations of solar radiation throughout entire landscapes. We created Penumbra, a landscape-scale solar transmittance model, to address this deficiency. Penumbra simulates spatially-distributed ground-level shade and incident solar irradiance at flexible timescales. Penumbra directly models local and distant topographic shading, vegetation shading, and the influence of cloud coverage. Spatially resolved inputs of a digital elevation model, normalized digital surface model, and daily percent cloud coverage are used to estimate spatial variations (meters to landscapes) in incident solar irradiance at temporal resolutions ranging from one minute to one day. We validate Penumbra's accuracy against several independent irradiance datasets. Overall, Penumbra is a dynamic, spatially-distributed ground-level solar incident irradiance model that can be used as a stand-alone tool to produce maps of shade percentage and irradiance, or in combination with landscape-scale models to calculate subsequent radiation influences on the health and resilience of aquatic and terrestrial ecosystems.

2.2 Introduction

Solar energy drives most of Earth's ecosystems, and must be well characterized in environmental models of those systems. Solar energy is generally the largest energy input into ecosystems (*Trenberth, 2002*). Solar energy entering the atmosphere varies predictably with time of day, season, and location on the Earth, but estimating the energy that reaches the ground surface requires explicit modeling of shade. Shade, or the removal of portions of solar radiation projected toward the earth's surface, has high spatial and temporal variability. Important components which generate shade at a given location include both proximal and distal topography, surface structures such as buildings and vegetative

canopies, and cloud coverage. For some regions of the world cloud coverage can have significant impacts on the resulting solar energy reaching the earth's surface (*Hartmann, 1992*)

Spatiotemporally inaccurate representations of solar energy may cause compounding effects and introduce unknown modeling uncertainty. Ecological models each have their own unique focus, yet solar radiation typically is not treated explicitly. For example, site specific climate station data is often used to represent large-scale trends, though small-scale forest or stream system microclimates may greatly vary over short distances. Accurate representations of environmental drivers are especially crucial at scales for which processes are sensitive to microclimate variability (*Abdelnour et al., 2011*). No matter the modeling method taken, dynamic shade representation requires a balance between: computational runtime, light complexity, and amount of model output (*Rhodes, 2016*). Simulation methods used to account for solar energy in environmental models range from simplistic to complex (Figure 2-1).

The simplest solar energy simulation approach is to solely rely upon a global irradiance model. For soil temperature modeling this approach is taken by both Visualizing Ecosystem Land Management Assessments (VELMA) and the Soil & Water Assessment Tool (SWAT) (*Abdelnour et al., 2011*; *Neitsch et al., 2011*). Solar energy is represented as extraterrestrial irradiance or daily averaged irradiance as a single value per time step. This global approach has negligible modeling cost, but it oversimplifies spatial and temporal solar energy by omitting topographic shading, object shading, and cloud coverage effects.

Solar energy can be monitored at a point location using a pyrometer, pyrheliometer, or hemispherical image. These instruments provide detailed solar irradiance data describing local environmental shading and cloud coverage, but for only a single location per instrument. When these instruments are manually operated, the data can only represent short temporal periods due to the burden of collecting field data by personnel. Utilizing observed point location data is an approach taken by some ecological models for solar energy, as well as for many other climate variables. Though site data does account for the explicit local solar energy reductions due to shading, this approach forces spatially-distributed models to be treat the data as spatially homogeneous.

A variation on the site approach, taken by SHADE2, is to process field photos representing upstream site locations (*Li et al., 2012*) This approach assesses riparian canopy and overhanging tree shrubbery through solar angle assessment. Image scene orientation is assessed in the x and z dimensions, meaning perpendicularly across the stream and vertically from the stream surface to the top of the riparian canopy. SHADE2 provides excellent agreement to observed irradiance readings, yet mostly for East to West running streams (*Li et al., 2012*). Stream image collection also places a data capturing burden on researchers, and does not address the broader methodological issues of solar data extrapolation in space and time.

Some stream network models utilize a solar energy metric to characterize fish and vertebrate habitat, evaluate the thermal loading, or assess water quality metrics on individual streams and the network as a whole (*Brown et al., 2015*). Yet solar data are rarely monitored across landscapes at a reasonable grain size for landscape modeling. This data shortage forces some models to extrapolate observed data throughout the model space. To overcome this spatially homogenous data issue, some stream network and landscape models statistically extrapolate monitored site solar data across distant point locations. Spatial statistical models include the Spatial Stream Network (SSN) model (*Ver Hoef et al., 2014*). SSN geo-statistically interpolates point location data across a polyline network makes the solar energy spatially implicit (Figure 2-1). Spatial models can apply this approach to extrapolate solar energy across landscape polygons or gridded framework as well. However, when models extrapolate point data they ignore spatial shadowing effects from landscape objects or topography between the point locations. The assumption that one location can be a surrogate for another introduces modeling uncertainty (*Johnson, 2003*). These models are often limited by available data with significance, such as stream bank width, land use, or riparian coverage (*Detenbeck et al., 2016*).

Solar energy is a direct driver impacting forest and agricultural photosynthesis, stream temperature, and habitat suitability. Process-based, or mechanistic, models can simulate the mixed interactions of such environmental processes across landscapes well (*Fatichi et al., 2016*). Process-based models can be particularly helpful for policy making and land management of forest or agriculture based on vegetation developmental trends

due to resource availability (*Abdelnour et al., 2011*). Yet, Process-based models are often burdened by complexity resulting in runtime restrictions and memory allocation (*Fatichi et al., 2016*).

Ray tracing models take a complex, yet spatially explicit approach by simulating light rays directly. Ray tracing accounts for the complex temporal and spatial nature of solar energy by tracking discrete light path reflection, refraction, transmission, and absorption for each discrete simulation time step (*Glassner, 1989*). This method is computationally expensive due to the number of light rays and their potentially large number of landscape object interactions. Even over a small spatial extent at a small spatial grain, the computational requirements to run a simulation can become burdensome (*Heckbert et al., 1987*). Demonstrated by the iLand model, highly accurate light representations are feasible using ray tracing, but their applications have been limited to relatively small landscapes (*Seidl et al., 2012*). Moderate landscape-scale ray tracing simulations are currently not practical due to computational limitations on memory and machine performance, which combine into long model runtime requirements.

The HeatSource model confronted some ray tracing limitations by restricting shade assessment to only riparian shade (*Boyd and Kasper, 2003*). HeatSource is a stream assessment model that is widely used by states throughout the U.S. to design and implement stream temperature Total Maximum Daily Loads. Therefore, stream shading is one of several significant factors in the HeatSource workflow. Due to data demands and runtime constraints, HeatSource performs a limited ray tracing approach using light detection and ranging (LiDAR) data. HeatSource simulates landscape shadowing from the center point of stream reaches. From the center point, eight rays are traced thru the LiDAR point cloud for a fixed distance. This approach limits shade detection to the four cardinal and four intercardinal directions, and does not capture topographic shadowing. This method is also limited to study areas that contain LiDAR data, though that limitation is rapidly diminishing since airborne LiDAR is becoming more and more ubiquitous.

Despite their more realistic representation of shade, ray tracing models take longer to run than many ecosystem type models can tolerate, which makes integration of these model types impractical for dynamic models that focus on moderate to large landscapes.

Due to their large spatial extent, watershed models such as SWAT or VELMA could not expend the runtime overhead ray tracing requires over even moderately sized watersheds.

Overall, spatial models simulating stream networks or landscape scale areas must balance promptness, temporal capability, and spatial extent when simulating light. Simple to complex methods of simulating solar energy present either underrepresentation or model runtime and memory costs. Therefore, an environmental light simulation model is needed that can address the limitations of currently available environmental light simulation methods. An ideal landscape scale irradiance model would address the following design goals:

- Produce comprehensive ground-level irradiance and shade percent estimates as a function of spatiotemporal variations in tropospheric incident radiation and shadowing by topography, objects, and cloudiness.
- Minimize user burden through relatively limited model inputs and parameterization.
- Flexible temporal runtime parameters to simulate landscape solar energy at user-required temporal and spatial resolutions, including plot, watershed, and regional landscapes.
- Develop flexible model coupling (loose and tight) for external model integration.

The resulting model should be able to assess the major components that affect net solar energy across spatially heterogeneous landscapes in a spatially distributed manner. The model must perform within reasonable runtimes so it will not burden a coupled ecological model.

We developed Penumbra, a new shade and irradiance model that simulates ground-level irradiance across a wide range of scales in a computationally tractable fashion. The model incorporates tropospheric incident radiation, which varies based on time and local atmospheric conditions, topographical shading due to local and distant terrain features, and object shadowing due to buildings and vegetative canopies. Penumbra can be utilized as a standalone tool or integrated into other environmental models and falls within the current spectrum of available radiation modeling approaches (Figure 2-1).

Penumbra is designed to help scientists and stakeholders quantify radiative shifts across diverse landscapes through time to help understand potential consequences on human populations, aquatic environments, and terrestrial habitats in essentially any landscape. Penumbra accomplishes simulating these solar energy tasks under one of two states: stand-alone mode providing dynamic solar energy across a static landscape, or coupled mode where an ecosystem model provides Penumbra updates of a changing landscape and Penumbra's solar energy simulations respond accordingly.

Penumbra in stand-alone mode can produce maps of ground-level instantaneous irradiance, averaged irradiance over time, shade percentage, and incident power. These maps can provide users with an assessment of their landscapes the current energy state. This information can be especially useful for reference in decisions regarding vegetation management, stream management, and overall landscape health.

Penumbra in integrated mode can include spatial inputs of dynamically changing vegetative height and canopy structure to simulate changing shade patterns due to vegetation growth and light transmittance characteristics. Dynamic landscape models that simulate high-resolution processes over large spatial extents require long runtimes (*Abdelnour et al., 2011*). Penumbra leverages a tight-coupling model integration framework to increase runtime performance by eliminating the need to write shade or irradiance data to the hard disk for external models utilization. An additional Penumbra option is the utilization of the graphical processing unit (GPU) for reducing runtime burden.

In this paper, we describe and validate Penumbra. After presenting the model and describing its characteristics, we present stand-alone results using the 3-D visualization tool VISualizing Terrestrial-Aquatic Systems (VISTAS), which fluently renders the complex light phenomena that Penumbra simulates (*Cushing et al., 2015*). To validate the model, we compare Penumbra results against the Department of Energy (DOE) National Solar Radiation Data Base (NSRDB), the Environmental Protection Agency (EPA) Oregon Crest-to-Coast Environmental Monitoring transect (O'CCMoN) dataset, and Snow Telemetry (SNOTEL) sites containing measured hourly irradiance data (*NSRDB, 1990; Waschmann 2016; NRCS, 2016*).

2.3 Modeling Theory

Penumbra is a spatially-distributed, grid-based model capable of processing landscapes based on user-defined spatial inputs and temporal parameters. Penumbra's modeling approach is to simulate landscape scale irradiance as simply as possible while balancing that landscape's complex spatial structure to maintain a suitable level of accuracy. Penumbra's simplicity enables it to treat each grid cell as a black-box, whereas ray tracing modeling methods explicitly represent the detailed complexity of objects within each cell. Penumbra maintains a suitable level with accuracy through a spatially explicit assessment of the landscape. Any one cell's topography and object has the potential to cast shade upon any other cell.

The spatial representation of the landscape dictates the detail and accuracy of irradiance results. The cell resolution of a simulation dictates how detailed objects can be represented in the length-width, or X-Y, dimensions. An object's vertical z-dimension are implicit representations of reality, meaning the object's structure is a column with equal light transmittance from top to bottom. We acknowledge true objects like trees are more complex with structures allowing light through breaks in the tree crown and tree tops coming to points. The current dilemma though is at large landscape scales only LiDAR data is detailed enough to represent trees, but does not represent tree understory.

Penumbra simulations should be viewed as modeling a tree's light transmittance versus modeling a forest canopy's light transmittance. Landscapes represented with increasingly higher spatial resolution capture object structure in increasing detail. The use of LiDAR data to derive data inputs for Penumbra would allow modeling of light transmittance at the tree object scale. Conversely, many ecological models focus on landscape scale assessments. For these models, Penumbra could represent a landscape at lower spatial quality, such as gridded data at 10-meter or 30-meter resolution. At these resolutions, Penumbra would be modeling light transmittance through forest stands in aggregate.

2.4 The Penumbra Model

To computes solar energy at each the percent of the total potential illumination it utilizes three independent light reduction phases: topographic light reduction, landscape

object light reduction, and time-step data aggregation (Figure 2-2). These calculations are performed across a spatially gridded landscape for each cell independently.

Penumbra assumes that for any given time step the environmental lighting is received from a single distant source which is spatially uniform (*Angel, 2012*) (Figure 2-2). This assumption allows Penumbra to assess light ray interference as a reduction of the total available irradiance due to spatially explicit topographic and landscape object shading, and daily atmospheric conditions.

2.4.1 Inputs

Penumbra requires a small set of model parameters and spatial input data to run (Table 2-1). A start Julian day, stop Julian day, and years of simulation define the temporal grain and extent. Penumbra functions under two temporal grains: the frequency of solar angle assessments and the frequency of data aggregation for output. The sun's daily position is defined by the temporal frequency (Daily-Grain) of shadowing assessments and frequency of data aggregation. Penumbra's temporal grain can be set to one minute to a full day. Model outputs can be aggregated internally to any temporal extent equal to or greater than the temporal grain. Weekly or monthly simulations are possible by setting Penumbra's Day-Grain to 7 or 30, respectively.

A simulation's spatial resolution is defined by the input digital elevation data (DEM), which represents topographical features. A corresponding normalized digital surface model (nDSM) represents landscape object heights, and is coupled with an object transmittance model (nDSM-OTM) that includes a simple factor (0-1) for reducing light transmission through objects of a defined type. Currently, spatial input data must be provided in the ESRI ASCII Grid format (*ESRI, 2016*). Typical spatial resolutions vary from 1-meter data derived from LiDAR data up to the common 30-meter data available in a variety of forms at United States national extents.

When both a DEM and nDSM are provided, topographic and object shadowing are simulated; when only a DEM or nDSM is provided, only topographic or object shadowing will be simulated, respectively. Conversely, topographic and object percent shade can be simulated simultaneously, yet exported individually as topographic or object shade maps.

This unique model flexibility allows Penumbra users to isolate the effect of topographic shadowing or object shadowing within their landscapes of interest.

Each aspect of model irradiance reduction can be calibrated by the user. Due to Penumbra's mechanistic nature and spatiotemporal framework, estimates of solar energy accuracy can be improved by calibrating Penumbra to a study area's unique land cover, landscape, and local atmosphere. Table 2-2 lists each calibration parameter and model influence. All calibration parameters are scaled from one to zero, where one applies no change and any decimal value less than one retains that percent of influence on the data. All calibration parameters are applied to data in a spatially uniform and multiplicative manner.

These four calibration parameters exist to improve Penumbra simulation performance, yet not all have a strong influence on model performance. The TI_{CALI} and TR_{CALI} are essential calibration parameters. The degree to which the GR_{CALI} and CE_{CALI} improve model accuracy is terrain-specific and atmosphere-specific, and may provide only a minor improvement in overall simulation exactitude.

For a more complete representation of landscape shadowing and irradiance, additional spatial data may be provided but are not required. Each grid cell can correspond to a landscape object, such as Douglas-fir, Alder, or corn. The degree of light reduction (shading) for different landscape objects is defined by an input nDSM-OTM grid. If a transmittance map is not provided, Penumbra assigns a default transmittance that represents an average transmittance of light through forest canopies. Daily percent cloud coverage can be provided as a comma separated value (csv) file.

2.4.2 Processing Steps

Penumbra utilizes a simplified ray tracing method, called the Walking Algorithm, derived from the Marching Squares and Marching Cubes approaches (*Lorensen et al., 1987*). The Walking Algorithm traces a light ray's path from each DEM surface cell toward the sun using the sun's azimuth and altitude generating separate percent shade arrays for both object and topographic shade in parallel. The global solar energy sub-model computes the extraterrestrial irradiance per time step for a given location based on the study area's centroid latitude and longitude. Sky conditions reduce this global irradiance to a net global

irradiance. The topographic and object shade percentage arrays are multiplied against the net global irradiance to calculate a terrain level spatially distributed net irradiance.

2.4.3 Solar Angles

Solar azimuth and altitude are calculated at time intervals dictated by the simulation input daily temporal grain. Azimuth and altitude are calculated by:

$$Azimuth = \alpha = arccosine(EST * (\Delta JDay) - \lambda) \quad [1]$$

$$Altitude = \gamma = arcsine\big((cos\varphi * cos\delta * cos\Omega) + (sin\varphi * sin\delta)\big) \quad [2]$$

where latitude is φ, longitude is λ, declination is δ, hour angle is Ω, Earth sidereal time is EST, and ΔJDay is the current Julian day minus the January 1st, 2000* Julian day (Figure 2-4, Note: figure contains Equations 3 through 10).

Each origin cell's shading and net irradiance is computed by Walking Algorithm from that cell to a termination event. The Walking Algorithm itself is a set of methods which control the direction and distance of terrain evaluation. For a given starting cell the Walking Algorithm traverses the landscape evaluating each encountered cell to determine if it influences the starting cell. If yes, the encountered cell's transmittance is included in the assessment on the starting cell. The influence from all cells that affect the origin cell are accumulated to derived the percent shading and resulting net irradiance.

2.4.4 Walking Algorithm

At each time step the azimuth and altitude of the sun are applied to derive the rise, run, and sun ray elevation as discrete distances. The azimuth is applied from a nadir perspective to calculate the rise and run direction. Per time step, the rise and run are calculated once using the following equation sets under the four Cartesian angular conditions (Table 2-3), where α is the current solar azimuth and v is the assessment distance based on the walking algorithm's step distance.

As the Walking Algorithm traverses the landscape, each encountered cell is "stepped" across at a distance equal to ¼ the DEM's cell resolution. This stepped-distance can be modified by the user, though ¼ has stood as a good compromise between the Walking Algorithm representing a solar ray path across a gridded framework and computational demand. Reducing the stepped-distance would increase the number of assessments the Walking Algorithm would perform per cell.

The altitude determines the solar ray Vertical-Rise based on the same one quarter of the simulations cell resolution where γ is the current solar altitude and X_{TOTAL} is the Walking Algorithms current assessed distance from the origin cell to the current cell encountered.

$$Vertical_{SOLAR} = \tan \gamma * X_{TOTAL} \quad [11]$$

The benefit of the rise/run/elevation relationship over direct use of the azimuth and altitude is a reduction of repeated trigonometric calculations, which if repeatedly performed are computationally expensive.

2.4.5 Terrestrial Irradiance

The terrestrial solar irradiance (TSI; W/m^2) is calculated using the following equation (*Sun, 2015*), where S_{sun} is the solar constant and n is the Julian day.

$$TSI = Ssun * 2\pi * (n/265.25) \quad [12]$$

2.4.6 Cosine Effect and Calibration on Terrestrial Irradiance

The terrestrial irradiance is reduced to account for the solar altitude angle using the following equation, where Θ is the solar altitude and TSI (Equation 11). Calibration parameter TI_{CALI} is applied here.

$$TSIcos = cos\Theta * TSI * CTI \quad [13]$$

2.4.7 Solar Ray Height

As the Walking Algorithm traverses the landscape cell by cell, the ray's height is calculated using the Walking Algorithm's altitude (γ) and total distance assessed (Figure 2-5). The Solar Vertical Rise Component (VRC_{SOLAR}) represents the absolute height from the initial cell,

$$VRC_{SOLAR} = |\tan \gamma| * X_{TOTAL} \quad [14]$$

while the current Solar Ray Height ($Solar_{RH}$) represents the relative height between the ray's current height and the corresponding ground elevation (Figure 2-5),

$$Solar_{RH} = \text{Origin Cell Elevation} + VRC_{SOLAR} \quad [15]$$

2.4.8 Object Shade Reductions

As the Walking Algorithm encounters a new cell, that cell's landscape object interaction is assessed by subtracting the object's absolute elevation by the $Solar_{RH}$ to obtain z-dimensional difference between object height and solar ray (Figure 2-2).

$$\text{Object Delta Height } (O_{DH}) = \text{Solar}_{RH} - \text{Object Height} \quad [16]$$

If the O_{DH} is positive, the solar ray passed over the object. If the O_{DH} is negative, the solar ray penetrated through the object. As each landscape object's O_{DH} is encountered, that object's associated transmittance value is applied to the accumulated solar transmittance in a multiplicative manner.

When the Walking Algorithm is terminated, the resulting accumulated solar transmittance value is the origin cell's percent illumination. This value is tracked for shade and topographic light transmittance reduction separately. The multiplicative of the all encountered cell object transmittance reductions is assigned to the origin cell (Figure 2-2).

$$\text{Object Light Deduction } (O_{LD}) = \prod_{i=0}^{n} Object\ Transmittance \quad [17]$$

2.4.9 Topographic Shade Reductions

Topographic shadowing may occur upon the origin cell. Like object shadowing, as the Walking Algorithm encounters a new cell the potential interaction is assessed by subtracting the elevation from the Solar_{RH} to obtain a delta representing the z-dimensional difference between the terrain and ray (Figure 2-2).

$$\text{Terrain Delta Height } (T_{DH}) = \text{Solar}_{RH} - \text{Elevation} \quad [18]$$

If T_{DH} is positive, the solar ray is above the ground. If T_{DH} is negative, the solar ray penetrated the ground and the Walking Algorithm is terminated. Unlike object shadowing, the aggregation of topographic shadowing does not occur since direct light cannot attenuate through terrain. Instead the Topographic Light Deduction is calculated based on an inverse relationship between the number of cells walked (X_{TOTAL}) and the ground calibration factor (GR_{CALI}).

$$\text{Topographic Light Deduction } (T_{LD}) = (1/\ X_{TOTAL}) * GR_{CALI} \quad [19]$$

If X_{TOTAL} equals one (meaning only one cell was walked), the T_{LD} is equal to GR_{CALI}, or maximum topographic shade. Any number of additional cells walked would generate a weakening of topographic shade due to the inverse relationship of X_{TOTAL}. This effect accounts for indirect light scattering increasing the resulting light availability when large topographic shadowing occurs over the great distances.

2.4.10 Spatial Mask

Penumbra by default will assess every landscape cell within a rectangular spatial domain, not all cells provided to the model may be of concern to the model user. In this case, a landscape mask is an optional model input. For example, a watershed analysis would have irregular boundaries usually leading up to the edge of mountain or hill crests. Providing a spatial mask shortens the runtime due to Penumbra not simulating spatial data outside the defining spatial mask.

2.4.11 Graphic Processing Unit (GPU)

The use of a GPU for computational processing is an option in Penumbra. The GPU module replaces the Walking Algorithm, which is the most processing intensive aspect of Penumbra (*Rost et al.,* 2010, pp. 385-386). The GPU approach is based on a computer graphics process known as shadow mapping (term shadow coincidental), which simulates obfuscation of a surface or object from a light source by rendering a scene from the light source's viewpoint, and generating a lookup table from the subsequent render results (*Rost et al., 2010*) (pp. 385-386). The lookup table is known as a shadow map, and each point in the scene can test against the map by testing its distance from the light source versus the shortest distance recorded in the map (*Learning, 2016*).

As previously mentioned, Penumbra assumes that light rays are traveling along parallel paths; therefore, an orthographic projection can be used for the sun's viewpoint, guaranteeing that each ray into the scene only travels through a single row of pixels. The GPU utilizes "shaders" (GPU term "shaders" is coincidental to Penumbra's goal. GPU "shaders" are specific built-in instructions for GPU rendering processes) to both quickly render the shadow map and to perform the shadow lookup for each grid point in a massively parallel fashion (*Rost et al., 2010*, p. 698). However, there is an implicit overhead to moving data to and from the GPU memory. When processing small datasets, the central processing unit (CPU) bound Walking Algorithm will often exceed the GPU shadow mapping approach in runtime performance; when processing landscapes with many spatial or temporal units, the parallel nature of the GPU allows for the shadow mapping approach to produce superior runtime performance. For landscapes characterized at high resolution

or representing large spatial extents, and simulations set to a small temporal grain, the GPU is a viable option to shorten simulation runtime requirements.

2.5 Outputs

Penumbra can provide representations of landscape illumination as: object shade, terrain shade, total shade (object and terrain shade combined), or net solar energy. All these forms can be output in isolation or collectively. Shade outputs are all percentage based. Energy units are defaulted as Watts per meter^2, but the British Thermal Units/hour/meter^2 and micromoles/ meter^2/second (µmoles/m^2/s) are options.

2.5.1 Object and Topographic Shade

Penumbra internally tracks the deduction of energy as a percentage in the Object Light Deduction (O_{LD}) and Topographic Light Deduction (T_{LD}) arrays; not the percentage of shadowing by topography or objects. Shade maps are generated per aggregation output by inverting the O_{LD} and T_{LD} data to create Topographic Shade (T_{SHADE}) and Object Shade (O_{SHADE}) where 1 represents complete shade and 0 represents no shade.

$$T_{SHADE} = 1 - T_{LD} \quad [20]$$

$$O_{SHADE} = 1 - O_{LD} \quad [21]$$

Total shade ($Shade_{TOTAL}$) is calculated by taking the multiplicative of T_{LD} and O_{LD}.

$$Shade_{TOTAL} = T_{SHADE} * O_{SHADE} \quad [22]$$

2.5.2 Net Ground-Level Solar Energy

The net energy ($Energy_{NET}$) is the multiplicative outcome of $Shade_{TOTAL}$(Equation 21) and TSI_{Cos} (Equation 12). $Energy_{NET}$ is the result of the spatially distributed shadow reductions and all irradiance reductions (Figure 2-2).

$$Energy_{NET} = Shade_{TOTAL} * Irrad_{NET} \quad [23]$$

If only object shadowing is the focus, the $Energy_{NET}$ relies on the O_{LD} (Equation 16). If only topographic shadowing is the focus, the $Energy_{NET}$ relies on the T_{LD} (Equation 18). The typical focus is the total shadowing effect, in which $Energy_{NET}$ relies on the (Equation 21). Due to TSI_{Cos} incorporating the solar angles, sun cosine effect, $C_{CR,}$ along with $Shade_{TOTAL}$ representing all terrain shading, the $Energy_{NET}$ is the final spatially distributed terrain energy.

2.6 Calibration Process

Penumbra calibration is a multistep process. The first run is a baseline for comparison, and each subsequent run focuses on one additional calibration parameter. A Penumbra initial run has all calibration parameters set to 1.0, except GR_{CALI} which is set to 0.5. If GR_{CALI} is set to 1.0, the result would be no topographic shading. From the initial output, Penumbra's peak irradiance is calibrated to the observed peak irradiance using TI_{CALI} (Equation 23). The TI_{CALI} calibration calculation adjusts the percent difference between the Observed Peak Irradiance (Obs_{PI}) and the Simulated Peak Irradiance (Sim_{PI}). The observed value to derived (Obs_{PI}) would be the peak irradiance value within the observed data. TI_{CALI} helps account for regional atmospheric irradiance deductions.

$$TI_{CALI} = 1 - ((Sim_{PI} - Obs_{PI})/ Obs_{PI}) \quad [24]$$

For Penumbra runs two and three, the TR_{CALI} and GR_{CALI} calibration parameters are adjusted to improve topographic shading and object shading. Topographic and object shading can be collective in nature causing an interactive influence within the observed data. This interaction can make sequential calibration difficult due to TR_{CALI} or GR_{CALI} shifts impacting the opposing topographic or object shade results. General site knowledge can help guide the adjustment of these two calibrations parameters. The dominant influence should be calibrated first.

The Penumbra Cloud sub-model is a simplistic daily percent cloud coverage, where the percent of clouds observed is a direct reduction in available TSI_{COS}. Cloud coverage data can be obtained from many weather stations or assimilated by processing satellite imagery from data products captured by platforms such as Geostationary Operational Environmental Satellite (GOES). CE_{CALI} allows the model user to adjust the cloud coverage impact on CE_{CALI} to better represent the types of clouds their study area generally contains. Here we do not present simulations utilizing the cloud coverage option.

2.7 Model Testing

Penumbra's solar position, extraterrestrial irradiance, and simulated net irradiance were all tested individually to vet solar energy assessments in isolation. Each phase marks simulation moments where error can propagate through downstream calculations.

Penumbra's first three calibration parameters were utilized during the testing of net irradiance. CE_{CALI} was not modified due to the observed data being all clear sky days.

Penumbra was tested against observed solar energy data to guide model calibration and assess final model performance. The solar angles were tested using U.S. Navy Observatory data. The global irradiance model was tested using the National Solar Radiation Data Base (NSRDB) data. Two datasets containing measured solar energy were utilized here: the O'CCMoN dataset, and the Snow Telemetry (SNOTEL) dataset. Two datasets were used to provide different examples of ground-level solar energy testing for the model.

2.7.1 Modeled versus Observed Solar Angle

Penumbra's solar angle sub-model was derived from research aimed at simplifying solar azimuth and altitude calculations (*Holbert and Srinivasan, 2011*). To understand any Penumbra error due to these simplified calculations, Penumbra solar angle azimuth and altitude data for position 44.915960°N, -123.001439°W were output for every hour of June 21st, 1990 and compared against matching U.S. Navy Observatory for the same timeline and location (*Form B, 1990*) (Figure 2-6). Penumbra calculations and the U.S. Navy Observatory data for azimuth and altitude agreed well with an r^2 of 0.9923 and 0.9991, respectively.

2.7.2 Modeled versus Observed Global Irradiance

Penumbra's irradiance calculation starts as extraterrestrial irradiance derived from a global irradiance sub-model (Sun, 2015). To understand any Penumbra error due to these calculations, Penumbra TSI_{Cos} (Equation 12) was tested against the Department of Energy (DOE) NSRDB data for the Salem Oregon NSRDB station at 44.915960°N, -123.001439°W for the year 1990 (*NSRDB, 1990*). As an airport, the site had no topographic or object shadowing to interfere with the observed data. These hourly data agreed well with Penumbra hourly TSI_{Cos} with a r^2 of 0.9577 (Figure 2-7).

2.7.3 Model Calibration for Adjacent Forest and Open Sites

The O'CCMoN monitoring project provides continuous Photosynthetically Active Radiation (PAR) observations at hourly increments for eight pairs of forest and open sites extending along a 200-km transect from the crest of the Oregon Cascade Range to the

Pacific Coast. Forest sites are mature stands with well-established canopies. Open sites are former mature stands that had been clear-cut harvested shortly before installation of PAR other climate station sensors in the open site and the forest site at each transect location. The forest site versus open site installations allows a contrast between two dramatically different environment types. High resolution representation of landscape objects at these sites was required to validate Penumbra's ability to model object shadowing from individual trees. Airborne LiDAR data provided these representations, but only two of the eight O'CCMoN transect locations, Moose Mountain and Fall Creek, had existing LiDAR coverages (*Upper, 2009*). For both locations, modeled open site and forest site PAR predictions were evaluated against observed data over a four-day span at an hourly temporal grain.

Moose Mountain

The Moose Mountain Forest site is a predominantly Douglas-fir forest located in the western Oregon Cascade Range at an elevation of 658 meters above sea level on a southeasterly slope. The Moose Mountain Open site is in a clear-cut 460 meters to the southwest at an elevation of 668 meters (Figure 2-8). PAR is monitored with a LI-COR LI-190SL instrument with the Forest site sensor height being 297 centimeters (cm) and the Open site sensor height being 282 cm from ground level (*Waschmann, 2016*). Hourly uncalibrated and calibrated results demonstrate Penumbra's ability to simulate varying environments and fine detail (Figures 2-9 and 2-10).

The initial, uncalibrated Moose Mountain simulation yielded moderate agreement for the open site with a percent error of 0.511 and an RSME of 506.0 (µmoles/m^2/s) (Table 2-4). The overall simulation error over four days revealed that Penumbra on average was off by 286.1 (µmoles/m^2/s) in this environment. The initial, uncalibrated performance for the forest site was poor due to no calibration being applied, and heavily overestimated terrain-level solar energy. Simulated vs. observed PAR percent error was 19.2, and RSME was 515.7 (µmoles/m^2/s).

Calibration of Penumbra greatly improved PAR predictions for both the Open site and Forest site (Table 2-4). The Moose Mountain Open site final calibration provided an excellent observed versus simulated PAR agreement with a percent error of 1.029 and a

RSME of 224.5 (μmoles/m^2/s). The overall simulation error for the four days revealed that Penumbra on average was off by only -17.27 (μmoles/m^2/s). The Moose Mountain Forest final calibration provided a fair agreement with a percent error of 1.84 and a greatly reduced RSME of 53.78 (μmoles/m^2/s). The overall simulation error for the Forest site over four days was on average off by -15.57 (μmoles/m^2/s) (Figures 2-9, 2-10, and Table 2-4). The VISTAS static frame shoots represent the Moose Mountain calibration run portrays (Figure 2-11). Sub-frame A represent the net solar energy as PAR (μmoles/m^2/s). This data is what most researchers and stakeholders are interested in, yet most irradiance models do not spatially simulate. Sub-frame B is the Total shade reduction (0.0 – 1.0), which is the spatial variable multiplied against the global irradiance per time step. Sub-frame C is the shade reduction (0.0 – 1.0) from landscape objects only, and sub-frame B is the shade reduction (0.0 – 1.0) from topographic features only. For all (0.0 – 1.0) shade reductions 1.0 is no reduction and 0.0 is full reduction. See appendix for the VISTAS movies demonstrating these simulation results.

Falls Creek

The Falls Creek Forest site is a predominantly Douglas-fir forest. The PAR sensor location is at an elevation of 528 meters on a slightly northern slope (Figure 2-12). The Falls Creek Open site is in a recovering clear-cut 328 meters to the west at an elevation of 534 meters. PAR is monitored with a LI-COR LI-190SL instrument with the Forest site sensor height being 334 cm and the Open site sensor height being 353 cm from ground level (*Waschmann, 2016*). Hourly uncalibrated and calibrated results demonstrate Penumbra's ability to simulate varying environments and fine detail (Figures 2-13 and 2-14).

The initial, uncalibrated Falls Creek Penumbra simulation yielded an excellent Open site agreement with a percent error of 1.09 and RSME of 252.6 (μmoles/m^2/s) (Table 2-5). The overall simulation error for the four days revealed that Penumbra on average was off by -59.96 (μmoles/m^2/s). The initial, uncalibrated performance at the Forest site had poor agreement with the observed PAR data, with a percent error of 19.2 and the RSME of 515.7 (μmoles/m^2/s). We show these uncalibrated results to highlight how a simplified irradiance model performs when object and topographic shading are not assessed. To that

effect, this initial uncalibrated Penumbra simulation is already reducing solar energy by roughly half, seen by comparing the Open site to Forest site results (Figure 2-13, 2-14; note figure scales differ).

The Falls Creek Open site final calibration yielded a good observed versus simulated PAR agreement with a percent error of 0.77 and the RSME of 296.8 (µmoles/m^2/s) (Table 2-5). Initial run agreement was higher than the final calibration run due to mid-afternoon PAR reductions. The reduced agreement was the result of calibration compromises made to improve the Forest site performance. The overall simulation error for the four days revealed that Penumbra on average was off by 148.1 (µmoles/m^2/s).

The calibration compromises greatly improved the Forest site PAR. The Falls Creek Forest final calibration provided good agreement with a percent error of 1.51 and a low RSME of 34.2 (µmoles/m^2/s) (Table 2-5). The overall simulation error for the Forest site four days was on average off by -10.2 (µmoles/m^2/s). A VISTAS static frame represents the Falls Creek calibration run (Figure 2-15). See appendix for the VISTAS movies demonstrating these simulation results.

2.7.4 SNOTEL Site Calibrations

The SNOTEL Network of sites monitor and record an assortment of meteorological data in mountainous snow-zone locations in the western United States and Canada (*NRCS, 2016*). SNOTEL sites are maintained by the U.S. Department of Agriculture Natural Resources Conservation Service (NRCS) to ensure the highest practicable data quality and continuity (*Schaefer et al., 2000*). NRCS has added pyrometers to select SNOTEL sites through third party interests (*National, 2010*). These sites are potentially influenced by local and distant topographic shading and by object shading from surrounding forest vegetation. Like the O'CCMoN dataset, which specifically provides monitored forest sites, there is no guarantee all SNOTEL site irradiance data captures object shadowing. SNOTEL sites are still of value for Penumbra calibration because each site's pyrometer captures the region's atmospheric irradiance reduction and any topographic shadowing. SNOTEL data sites are also distributed throughout the Pacific Northwest, which provides testing data over a larger geographic extent than the O'CCMoN data alone.

We identified two SNOTEL sites that had appropriate pyrometer data and publicly available LiDAR data needed to represent landscape objects for calibration and testing. These sites are Meadows Pass and Mount Gardner. The high resolution spatial inputs were derived from LiDAR project bare earth and highest hit gridded data (*Cedar, 2014*). We aggregated these data to 3-meter cell resolution. Each site was compared to SNOTEL observations for four clear sky days. Penumbra temporal grain was set to 10 minutes with output aggregations set to 60 minutes to match SNOTEL irradiance data. The data from the grid cell matching the SNOTEL site latitude and longitude coordinates was queried per time step. Penumbra had a pseudo-height elevation option built-in to adjust Penumbra's queried cell data height to match the SNOTEL sensor's true height.

SNOTEL observed data was suitable for a partial calibration of Penumbra. Sites are not guaranteed to represent tree shadowing due to SNOTEL site installations being in cleared areas to capture unobstructed snow fall. Meadows Pass site observed versus simulated data showed an 22% increase in percent agreement, a RMSE drop from 288 to 34.2 (Watts/m^2). The calibrated results also reduced the four day mean error from 174.67 to 66.46 (Watts/m2) (Table 2-6). Mount Gardner site observed versus simulated data showed an 10% decrease in percent agreement, though a RMSE drop from 411.2 to 265.2 (Watts/m^2). The calibrated results also reduced the four day mean error from 292.5 to 158.0 (Watts/m2) (Table 2-6). Mount Gardner is a clear example why Penumbra is calibrated off multiple statistics. A single statistic is only capturing one factor sub-daily irradiance readings; the improvement of that one factor through calibration may negatively impact a different statistic. Find name for movie simulation of Mount Gardner site in Appendix.

2.8 Landscape Scale Simulations

We demonstrate a case study within the Mashel River Watershed, which is located west-southwest of Mount Rainer, Washington. This watershed provides a prototypical Penumbra application due to the spatially diverse topography, land management practices and stakeholder interests within the watershed.

The Mashel River Watershed area is 209 km^2. Penumbra input data and parameters are listed in Table 2-7. Gridded, the Mashel River Watershed at 30-meter resolution is 455 rows by 923 columns (419,965 total cells). Penumbra's spatial mask

option was utilized, which restricted the cells assessed to the eastern watershed delineated bounds. The mask was generated at a cell delineation position of X-366: Y-112 using a watershed delineation tool called Java Processing DEM (JPDEM) (*Pan et al., 2012*). The resulting Penumbra mask reduced the assessed cells to 149,277. This Penumbra option is rather useful for watershed simulations due to significant improvements in runtime requirements.

The nDSM (surface objects) were derived from a Douglas-fir biomass-to-height relationship (*Means and Sabin, 1989*). The watershed scale biomass values were obtained from the LandTrendr model for the year 1990 (*Kennedy et al., 2012*). The objects light transmittance was provided as a uniform grid matching the O'CCMoN Falls Creek site TR_{CALI} value, while the TI_{CALI} was obtained from the nearby Meadows Pass SNOTEL calibration (Table 2-6).

Penumbra simulation of ground surface irradiance (Watts/m^2) for the 209 km^2 Mashel River Watershed in the state of Washington, USA during 1991 on the (a) winter solstice, (b) spring equinox, (c) summer solstice, and (d) fall equinox (Figures 2-18, 2-19, 2-20, 2-21). See appendix for the movie demonstrating this simulation at a daily time step for two full years. This Mashel Watershed simulation reveals the Penumbra's ecological modeling purpose. This landscapes solar energy at any moment in time is the result of the time of year, topographic shading due to the sun's altitude, and object shading from the dominant Douglas-fir forests that grow over much of this watershed's landscape. Ignoring any component that influences the final net irradiance across any landscape is an incomplete representation of solar energy.

Spatially-distributed landscape scale representations of solar energy allow for the development and improvement of ecological processes that are driven by solar energies magnitude. Considering a watershed as an example, solar energy directly drives air temperature and provides energy for leaf photosynthesis; both variables that drive evapotranspiration rates. Solar energy directly warms surface soil and surrounding air temperature. That surface energy transfers down into subsurface soils. The quantity of solar energy available to warm subsurface soils is dependent on the landscape coverage that blocks the direct solar radiation. During rain events surface water runoff temperatures are

indirectly increased due to the available solar energy being in the surface soils. The subsurface water is indirectly warmed as it migrations through the soil column due to solar energy that attenuated from the surface. All these energy storage mechanisms indirectly impact stream water temperatures, plus the solar energy directly impacting the stream surface increases water temperatures.

2.9 Discussion

Penumbra can be used as a standalone model to create irradiance and/or shade percentage maps at varying spatial and temporal resolutions, or Penumbra can be integrated with dynamic environmental models to inform a wide variety of important sub-models including snow, forest and agricultural crop photosynthesis, soil temperature, and stream temperature.

Penumbra can simulate spatially explicit radiation and shade using standard inputs commonly used in landscape-scale analyses. Penumbra is not the first model to simulate environmental solar energy. Simplistic solar energy models provide computationally effortless irradiance at the loss of spatial heterogeneity. These models are ideal when solar energy is not a significant variable in the larger context of the research. Ray-tracing models have tackled the complexity of light interaction within detailed landscape representations, but still today are burdened by computing limitations, especially for large spatial extents. Penumbra provides a landscape perspective and modeling approach that fills the current niche existing between the simplistic to complex irradiance modeling approaches available.

Penumbra allows users to estimate spatially-distributed shading and net irradiance resulting from topography and objects. Penumbra's flexible temporal parameters allow for landscape assessments to be performed from one minute to full day aggregations. Penumbra's ability to simulate Sun position at one temporal grain, yet aggregate those time steps to a greater temporal grain allows for flexible irradiance simulations. This flexible aggregation allows for model use within many research projects involving riparian shading, forest disturbances, photosynthesis, or any other biological process where irradiance has an influence.

Penumbra is subject to the same limitations as most process based models (*Fatichi et al., 2016*). Penumbra can have lengthy computational runtime requirements, though at typical watershed resolutions and extents Penumbra performs reasonably well. While GPU processing enhancement and direct model integration assist in reducing this problem, further improvements are needed to do large extent assessments at high resolution (e.g., 1m). For some users, another drawback is the platform in which Penumbra was developed; Java. Though, the Java language was selected due to the "write once, read anywhere" perspective, and the language works across many operating systems.

Being a process-based model, Penumbra's testing and uncertainty is a necessity. The lack of ubiquitous observed irradiance data is a drawback. The degree to which observed irradiance data exists is a concern. We discovered only two vetted Northwest, USA datasets with adequate solar energy readings to perform Penumbra testing, EPA O'CCMoN and SNOTEL. Most field irradiance data are collected for a short period. The long-term irradiance monitoring focus on global irradiance, not ground-level irradiance.

Penumbra allows for dynamic integration with other environmental models to achieve representations of changing irradiance due to impacts from land-use through time. This can be especially useful for simulating scenarios of alternative land management practices across the world. One particularly important example is characterizing the radiative effects of existing forests and anthropogenic land-use on stream temperature. Furthermore, Penumbra can be integrated with dynamic vegetation growth models to determine the time required to increase riparian shade by some percentage. Urban models could also utilize Penumbra's object shading feature to determine the spatial impacts of urbanization on irradiance and heat loads within urban centers.

2.10 Conclusion

Penumbra provides the capability to represent spatially distributed shade and terrain level irradiance. These representations allow for improved landscape scale simulations of solar energy within a reasonable simulation timeline without sacrificing the spatial heterogeneity of environmental light. With this model, how solar energy interactions within complex and unique environments can be better understood.

Here Penumbra was vetted against three independent data sources each addressing different scales of solar energy. Penumbra's extraterrestrial irradiance has high accuracy with a r^2 of 0.9577. Penumbra's net irradiance for the high-resolution O'CCMoN sites revealed a mean error ranging from -10.4 to 148.1 (Watts/m^2), while the SNOTEL observed and from 66.46 to 158.0 (Watts/m^2) against the SNOTEL observed. This level of accuracy for a natural phenomenon that is difficult to simulate and not feasible to monitor at landscape scales makes Penumbra particularly useful.

Overall, Penumbra is a novel surface irradiance model which filled an environmental modeling niche by accounting for topographical shading, object shading, and impacts of atmospheric conditions. This information will lead to more integrated modeling systems to better inform stakeholders such as: watershed councils, tribes, local, state, and federal decision makers interested in quantifying effects of land use and impacts due to local climate shifts. Current modeling efforts account for no or partial solar radiation reaching the earth's surface. To better inform future land management decision making, the full consequential impacts of those choices on human and natural systems must be foreshadowed to the best of our abilities.

2.11 References

Abdelnour, A., Stieglitz, M., Pan, F, McKane, R. (2011). "Catchment hydrological responses to forest harvest amount and spatial pattern." Water Resources Research 47(9): 1-18.

Angel, E; and Shreiner, D. (2012). “Interactive Computer Graphics: A Top-Down Approach with Shader-Based OpenGL.” 6th edition. Addison Wesley: Boston MA. pp. 264-265.

Boyd, M., and Kasper, B. (2003). “Analytical methods for dynamic open channel heat and mass transfer: Methodology for heat source model Version 7.0.”

Brown, R., Ebersole, J., Brookes, A., Boxall, G., Massie, J. (2015). “Evaluating the Simulation of Metacommunities for Riverine Fishes (SMURF).” 145th Annual Meeting, Portland, Oregon, American Fisheries Society.

Cedar River LiDAR Bare Earth DEM and nDSM (computer file). (2014). “Cedar River Watershed & Floodplain, Lake Youngs Reservoir, & SCL/Tolt Reservoir Study Areas LiDAR”. Available: Puget Sound LiDAR Consortium, Seattle, WA http://pugetsoundlidar.ess.washington.edu/index.htm (January 13th, 2016).

Cushing, J.B., Winters, K.M., Lach, D., (2015), May. “Software for scientists facing wicked problems lessons from the VISTAS project.” In Proceedings of the 16th Annual International Conference on Digital Government Research (pp. 61-70). ACM.

Detenbeck, N. E., A. C. Morrison, R. W. Abele, and D. A. Kopp (2016), “Spatial statistical network models for stream and river temperature in New England, USA.” Water Resource., 52, pp. 6018–6040, doi:10.1002/2015WR018349.

Fatichi, S., Vivoni, E. R., Ogden, F.L., Ivanov, V. Y., Mirus, B., Gochis, D., Downer, C. W., Camporese, M., Davidson, J. H., Ebel, B., Jones, N., Kim, J., Mascaro, G., Niswonger, R., Restrepo, P., Rigon, R., Shen, C., Sulis, M., Tarboton, D. (2016), “An overview of current applications, challenges, and future trends in distributed process-based models in hydrology.” USA, Journal of Hydrology, 537, pp. 45–60, doi:10.1016/j.jhydrol.2016.03.026.

Form B - Locations Worldwide: 44.915960°, -123.001439° (computer file). (1990). “Complete Sun and Moon Data for One Day.” Available: Astronomical Applications Department U.S. Naval Observatory (USNO), Washington, D.C. http://aa.usno.navy.mil/data/docs/RS_OneDay.php (October 28th, 2016).

Glassner, A. S. (1989). “An Introduction to Ray Tracing.” Academic Press pp.10-19, ISBN 0-12-286160-4.

Hartmann, D. L., Ockert-Bell, M.E., Michelsen, M.L. (1992). "The Effect of Cloud Type on Earth's Energy Balance: Global Analysis." Journal of Climate 5: pp. 1281-1304.

Heckbert, P. S. (1987). "Ray Tracing JELL-O Brand® Gelatin." Computer Graphics 21(4): pp. 73-74.

Holbert, K. E. and Srinivasan D. "Solar Energy Calculations," Handbook of Renewable Energy Technology, *edited* by A. F. Zobaa and R. C. Bansal, World Scientific Publishing Co., (2011), Chapter 8, pp. 189-204, ISBN *978*-981-4289-06-1.

Johnson, S. L. (2003). "Stream temperature: scaling of observations and issues for modelling." Hydrological Processes 17(2): pp. 497-499.

Kennedy, R.E., Yang, Z., Cohen, W.B., Pfaff, E., Braaten, J. and Nelson, P., (2012). "Spatial and temporal patterns of forest disturbance and regrowth within the area of the Northwest Forest Plan." Remote Sensing of Environment, 122, pp.117-133.

Learning OpenGL. "Shadow-Mapping." www.learnopengl.com. Patreon, Web. October 02nd, 2016.

Li, G., Jackson C. R., Kraseski, K. A. (2012). "Modeled riparian stream shading: Agreement with field measurements and sensitivity to riparian conditions." Journal of Hydrology 428-429: pp. 142-151.

Lorensen, W. E. and H. E. Cline (1987). "Marching Cubes: A High Resolution 3D Surface Construction Algorithm." Computer Graphics 21(4): pp. 163-169.

Means, J. E. and T. E. Sabin (1989). "Height Growth and Site Index Curves for Douglas fir in the Suislaw National Forest Oregon." Western Journal of Applied Forestry 4(4): pp. 136-142.

Neitsch, S. L., Arnold, J. G., Kiniry, J. R., Williams, J. R. (2011). "Soil and Water Assessment Tool Theoretical Documentation Version 2009." T. W. R. Institute. College Station, Texas, USA, AgriLIFE Research & Extension pp. 32-38.

NRCS: National Water & Climate Center. (2016). "Snow Telemetry (SNOTEL) Data Collection Network." Online. U. S. D. o. Agriculture. Portland OR, NRCS National Water & Climate Center.

NSRDB Hourly Data 24232 Salem, OR (computer file). (1990). "NSRDB 1961-1990: Hourly Data Files." Available: National Renewable Energy Laboratory (NREL), Washington, D.C. http://rredc.nrel.gov/solar/old_data/nsrdb/1961-1990/hourly/1990/ (October 28th, 2016).

Pan, F., Stieglitz, M. and McKane, R.B., (2012). “An algorithm for treating flat areas and depressions in digital elevation models using linear interpolation.” Water Resources Research, 48(6).

Rost, Randi J., Bill Licea-Kane. OpenGL Shading Language. 3rd Edition. (2010). Pierson Education Inc. Boston,MA pp. 385-386.

Rost, Randi J., Bill Licea-Kane. OpenGL Shading Language. 3rd Edition. (2010). Pierson Education Inc. Boston,MA pp. 698.

Seidl, R., Rammer, W., Scheller, R. M., Spies, T. A. (2012). "An individual-based process model to simulate landscape-scale forest ecosystem dynamics." Ecological Modelling 231: pp. 87-100.

Sun as A Source of Energy. (2015) “Part 4: Irradiation Calculations” www.itacanet.org/the-sun-as-a-source-of-energy/part-4-irradiation-calculations. ITACA, Web. June 15, 2015.

Trenberth, K. E. (2002). “Earths Energy Balance.” The National Center for Atmospheric Research. Boulder, Colorado, USA pp. 5-7.

Upper Soda LiDAR Bare Earth DEM and nDSM (computer file). (2009). “Calapooia/South Santiam Study Areas LiDAR.” Available: Oregon Department of Geology and Mineral Industries, Portland, OR http://www.oregongeology.org/dogamilidarviewer (October 15th, 2016).

Ver Hoef, J.M., Peterson E.E., Clifford D., and Shah R. (2014) “SSN: An R package for spatial statistical modeling on stream networks.” Journal of Statistical Software, 56(3).

Waschmann, Ronald S., U.S. Environmental Protection Agency - Western Ecology Division. "Oregon Crest-to-Coast Climate Observations". NOAA National Centers for Environmental Information. doi:10.7289/V5TT4NWV. (15Jun2016).

2.12 Figures

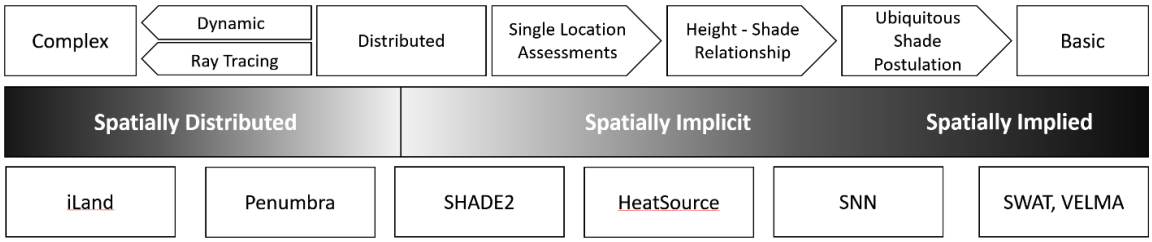

Figure 2-1: Shade modeling approach continuum.

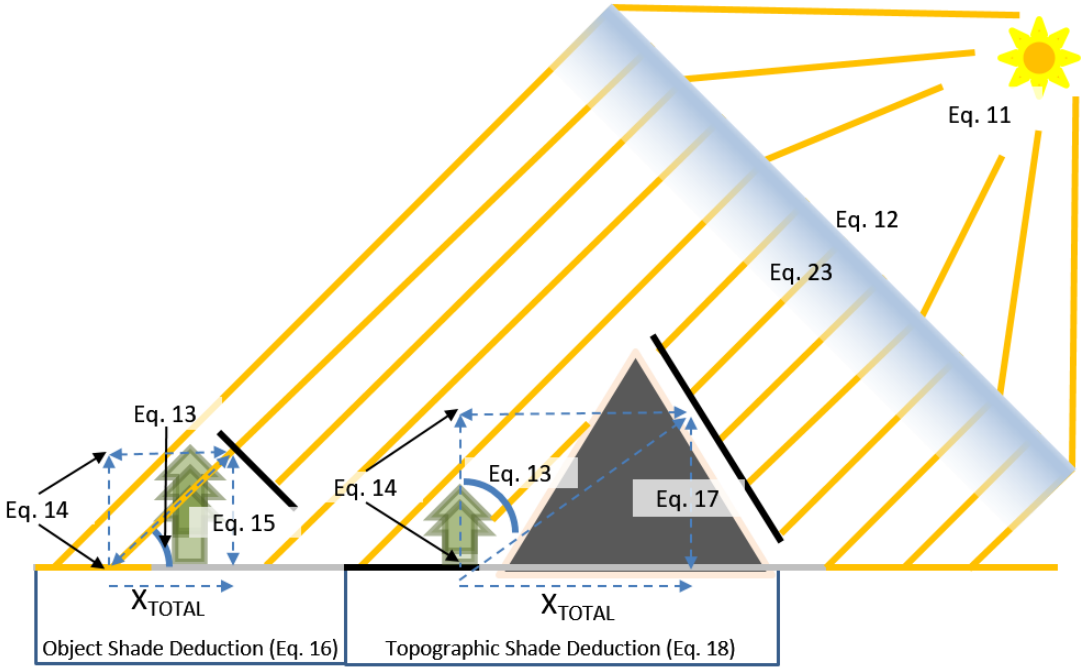

Figure 2-2: Penumbra's solar ray approach to shade modeling.

Equations defined in Section 2: Model Processing.

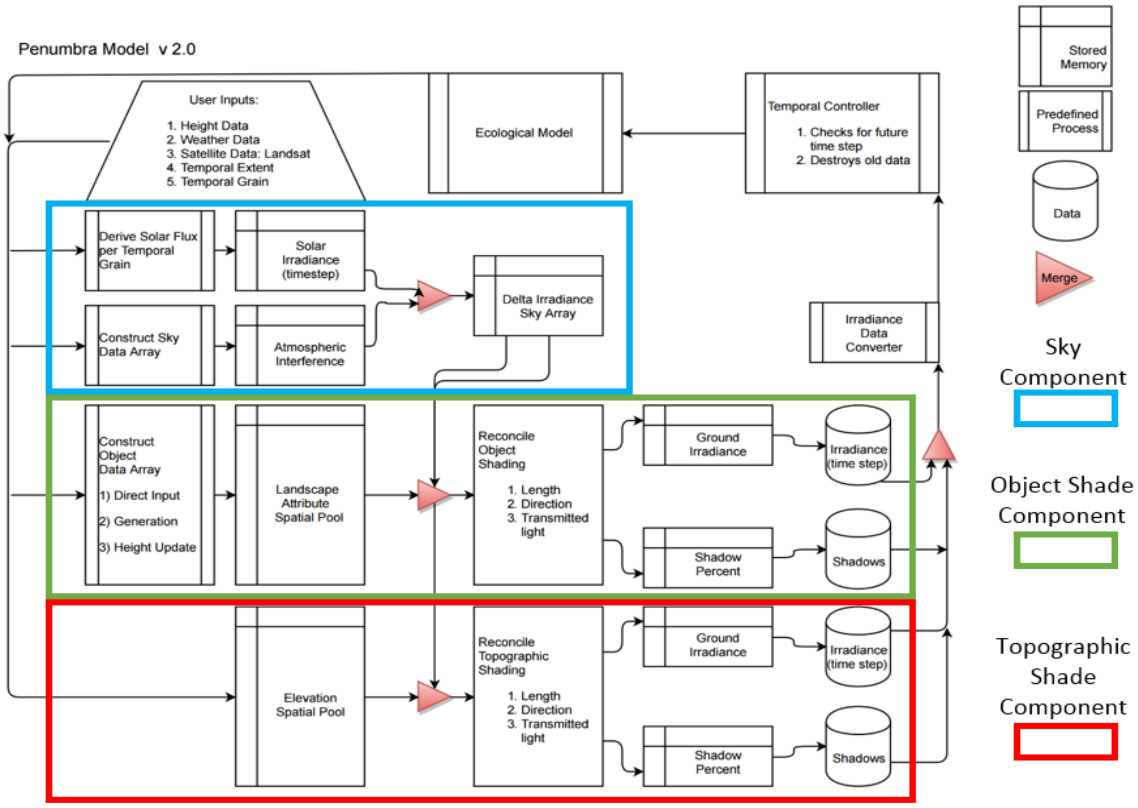

Figure 2-3: Penumbra model framework.

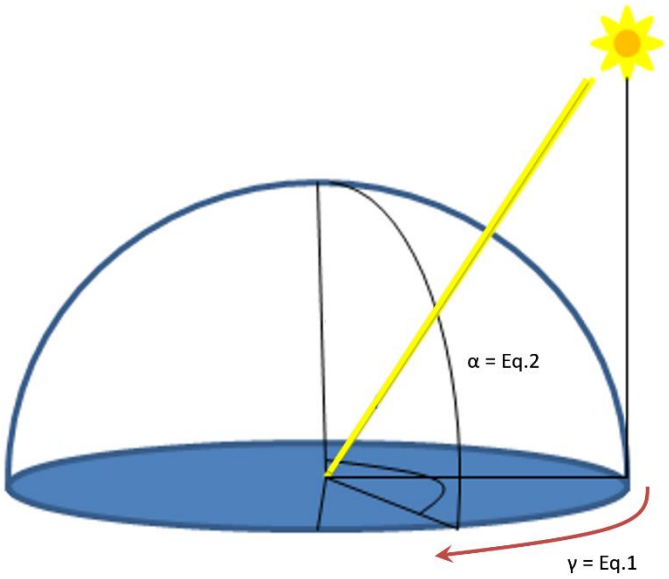

Figure 2-4: Solar azimuth (α) and altitude (γ).

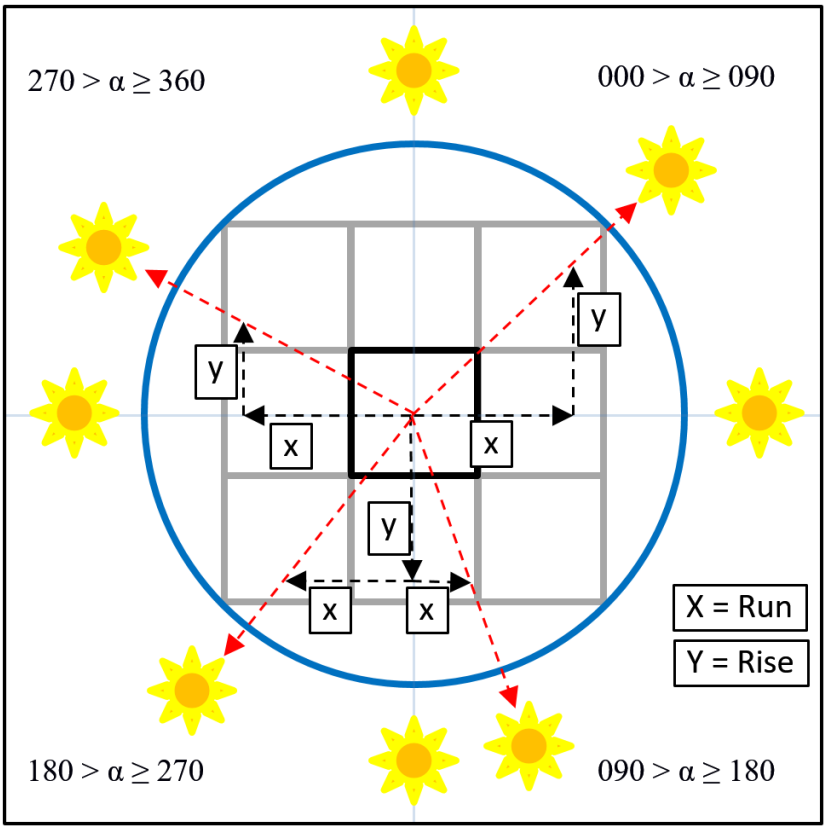

Figure 2-5: Walking Algorithm azimuth rise|run conversions.

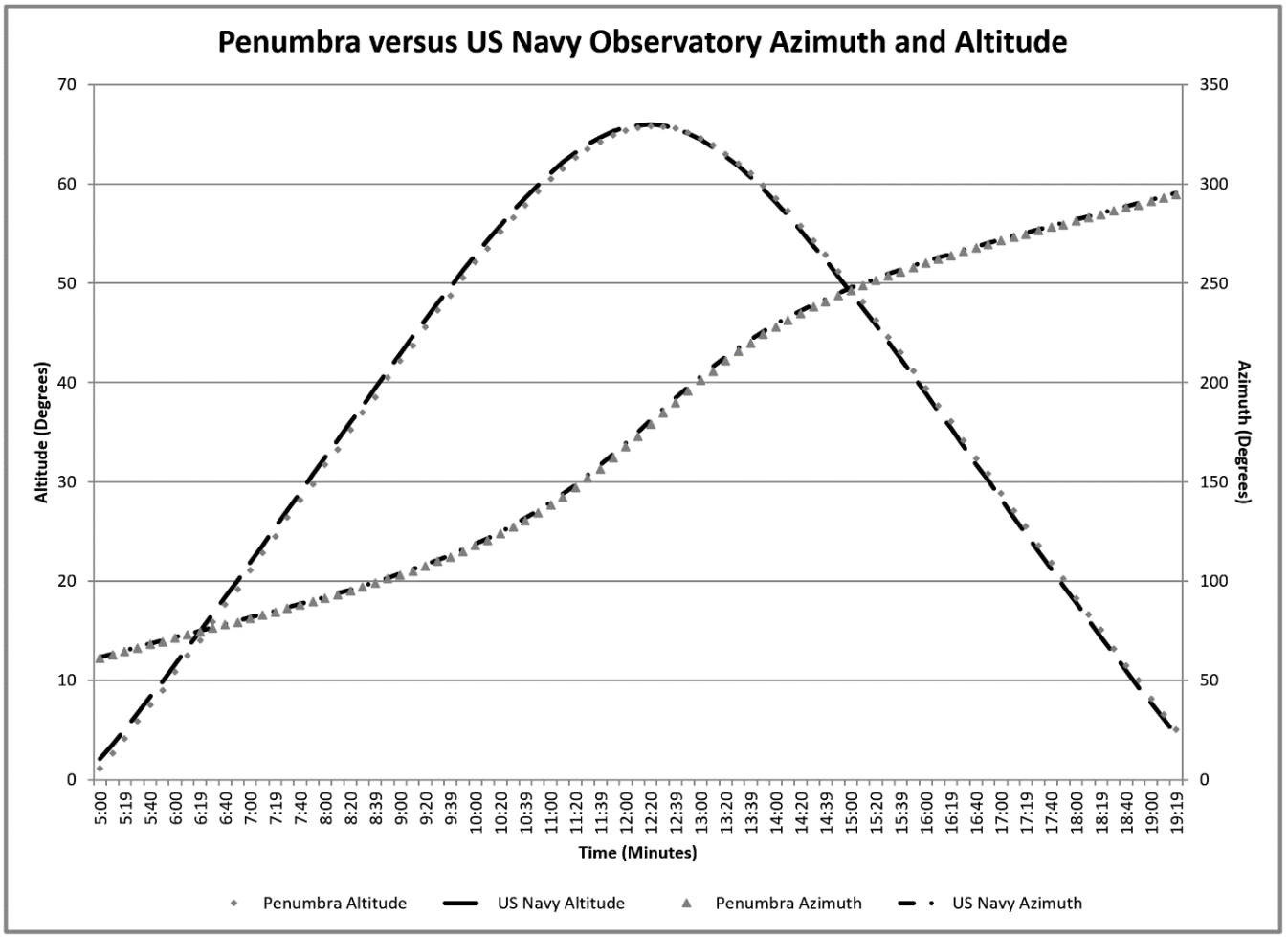

Figure 2-6: Validation of Penumbra simulated azimuth and altitude angles.

Estimations compared against the U.S. Navy Observatory for June 21st, 1990. Azimuth agreed with an r^2 of 0.9923. Altitude agreed with an r^2 of 0.9991.

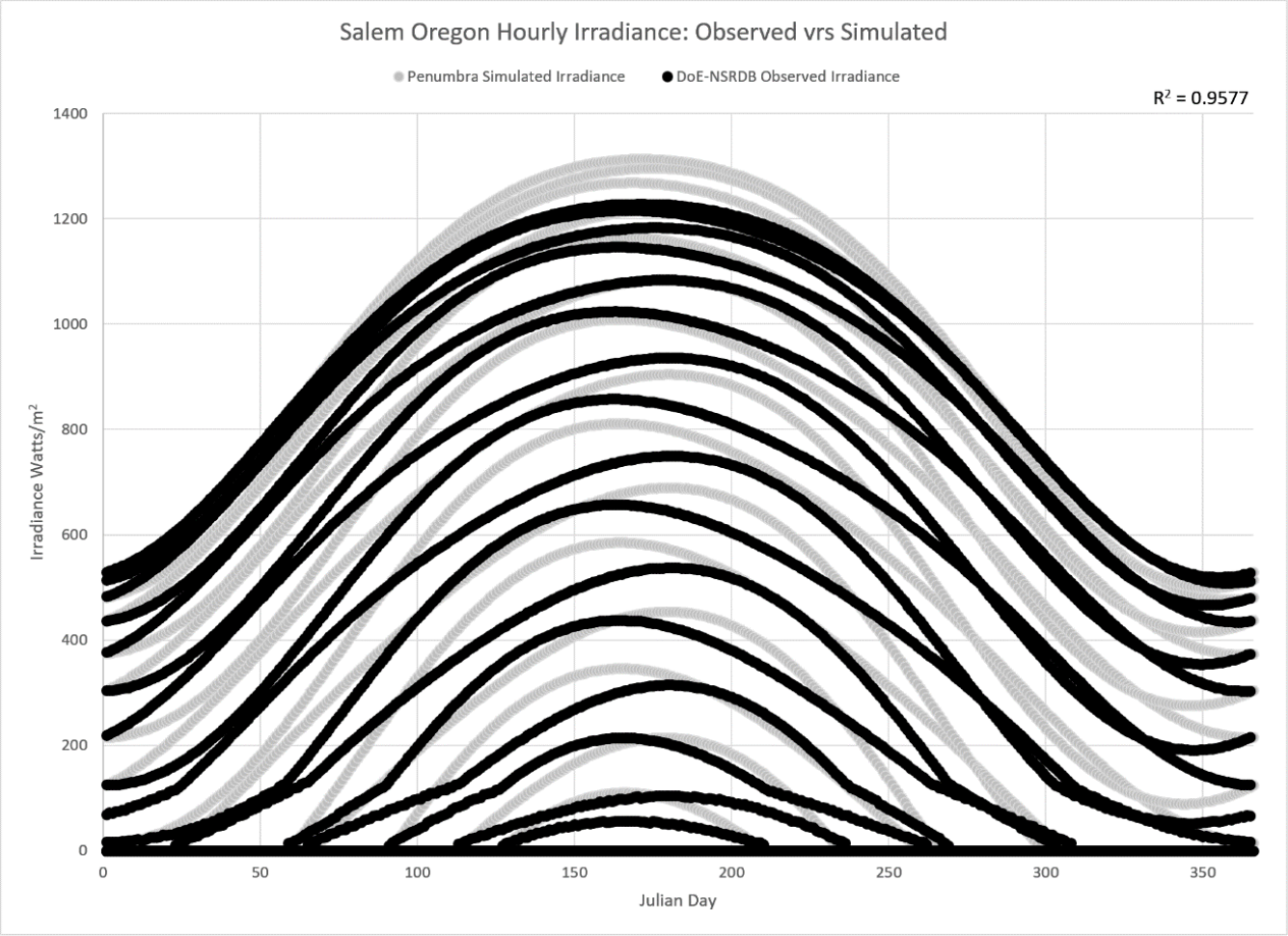

Figure 2-7: Validation of Penumbra simulated extraterrestrial irradiance.

Estimations compared against monitored DOE-NSRDB data for Salem, Oregon, USA (44.915960°N, -123.001439°W). Data represents every hour of the year 1990.

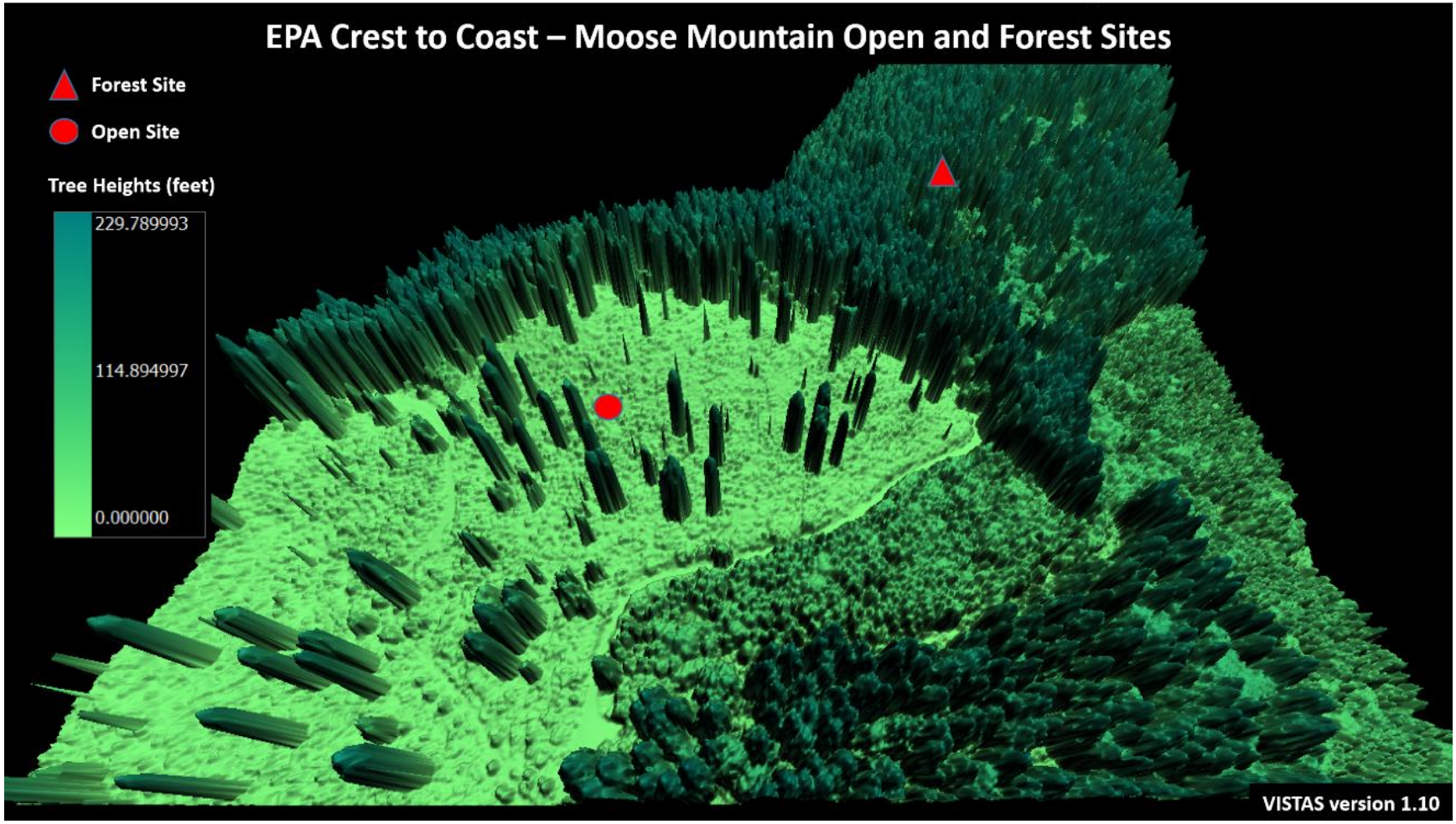

Figure 2-8: Moose Mountain Open site and Forest site.

Sites are part of the Oregon Crest-to-Coast Environmental Monitoring transect (O'CCMoN) dataset.

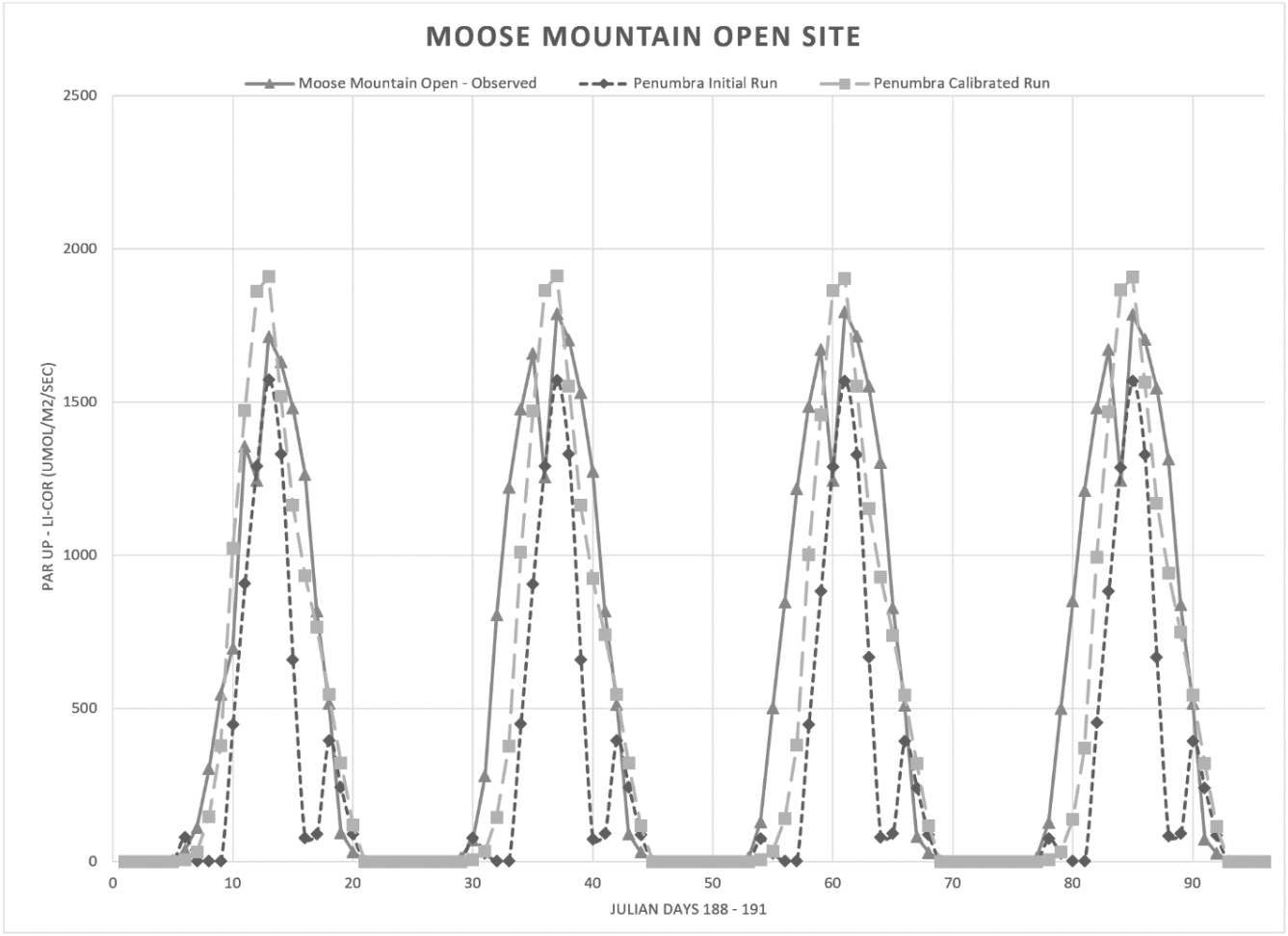

Figure 2-9: Simulated versus observed PAR for Moose Mtn. Open site.

PAR units are µmoles/m^2/s.

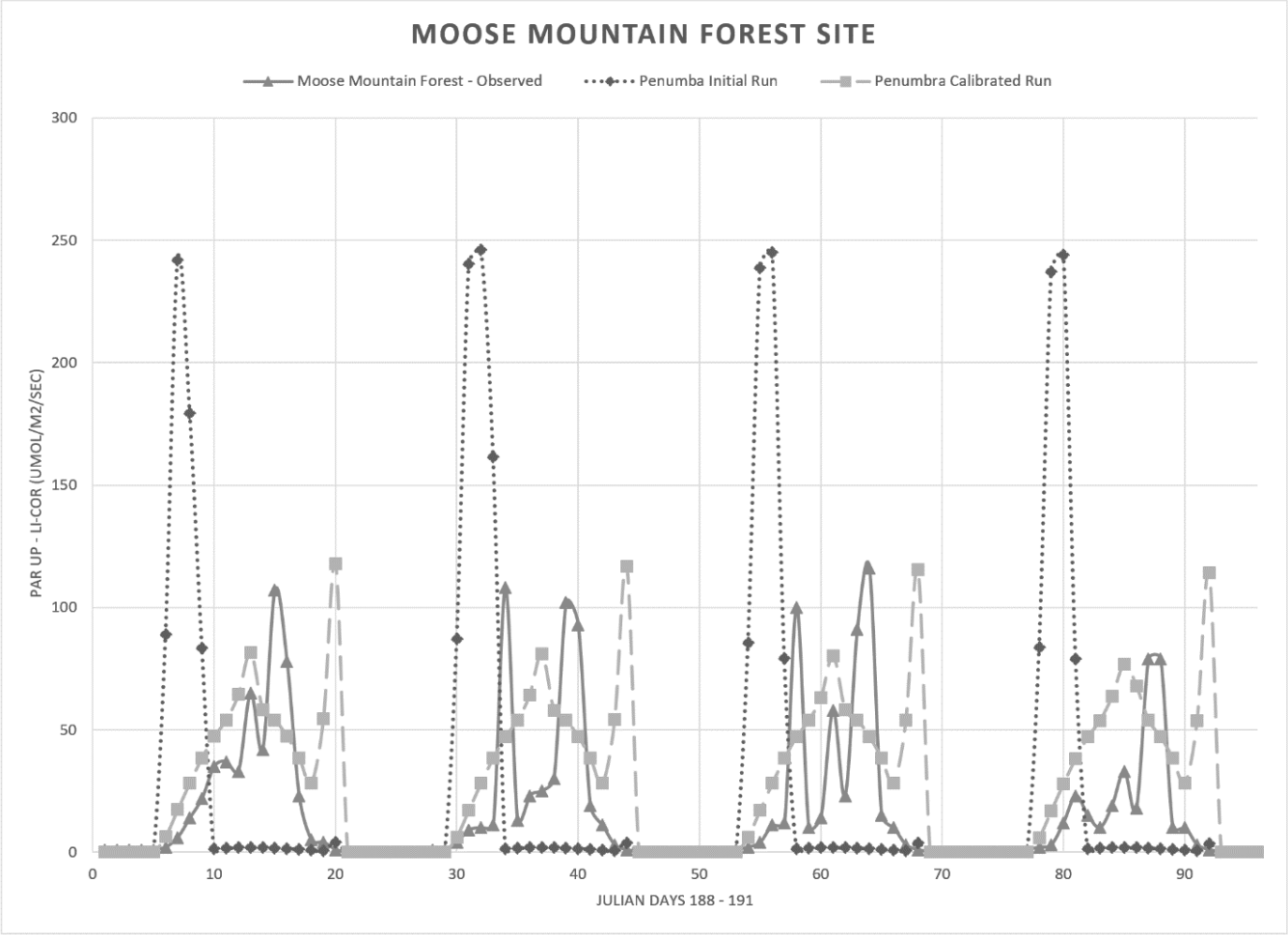

Figure 2-10: Simulated versus observed PAR for Moose Mtn. Forest site.

PAR units are µmoles/m^2/s.

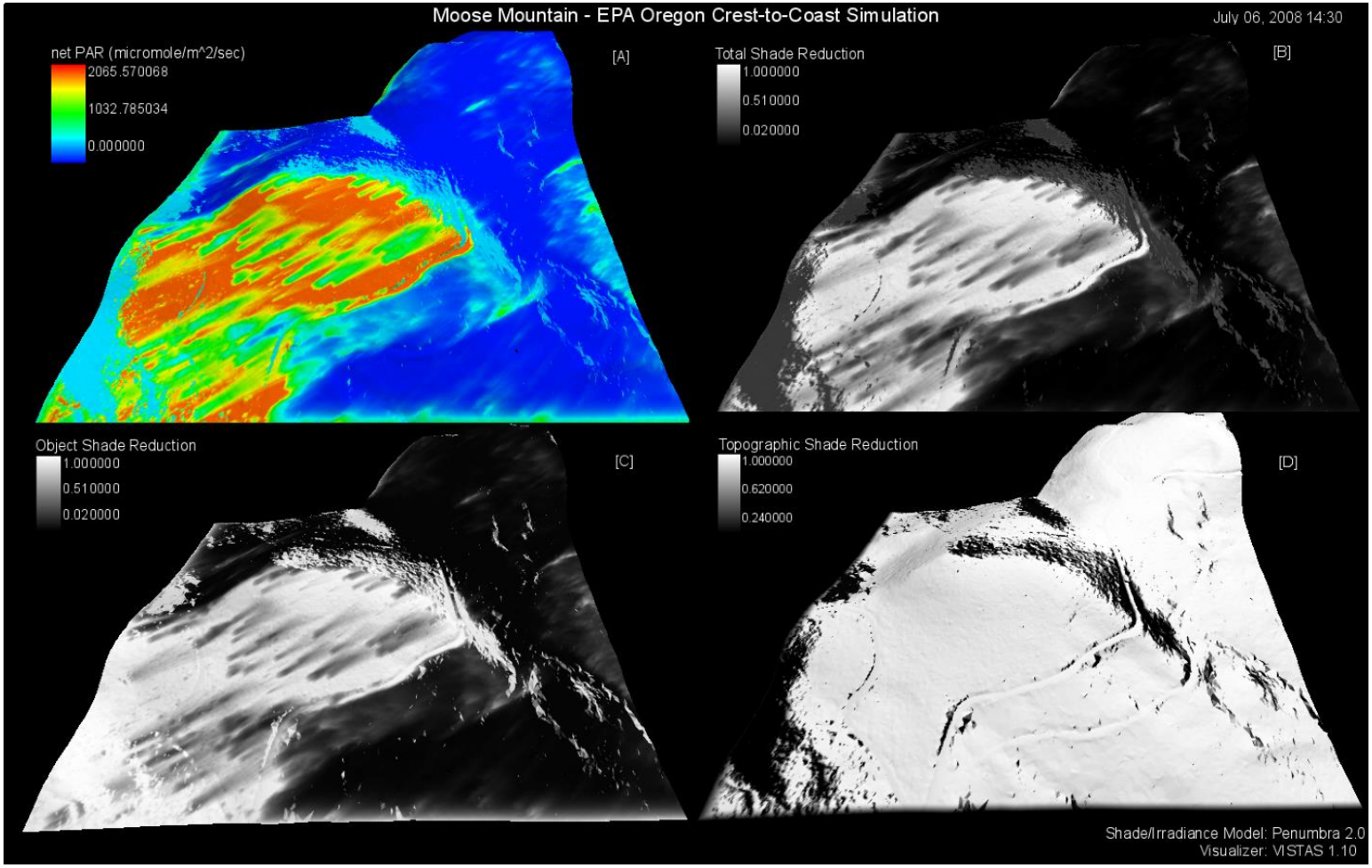

Figure 2-11: Static results for Moose Mountain Open and Forest sites.

Static simulation shot on July 06th, 2008 at 2:30pm. (A) net solar energy as PAR (µmoles/m^2/s), (B) Total shade reduction (0.0 – 1.0), (C) Object shade reduction (0.0– 1.0), (D) Topographic shade reduction (0.0 – 1.0). For all (0.0 – 1.0) shade reductions 1.0 is no reduction and 0.0 is full reduction. See appendix for the movie demonstrating this simulation.

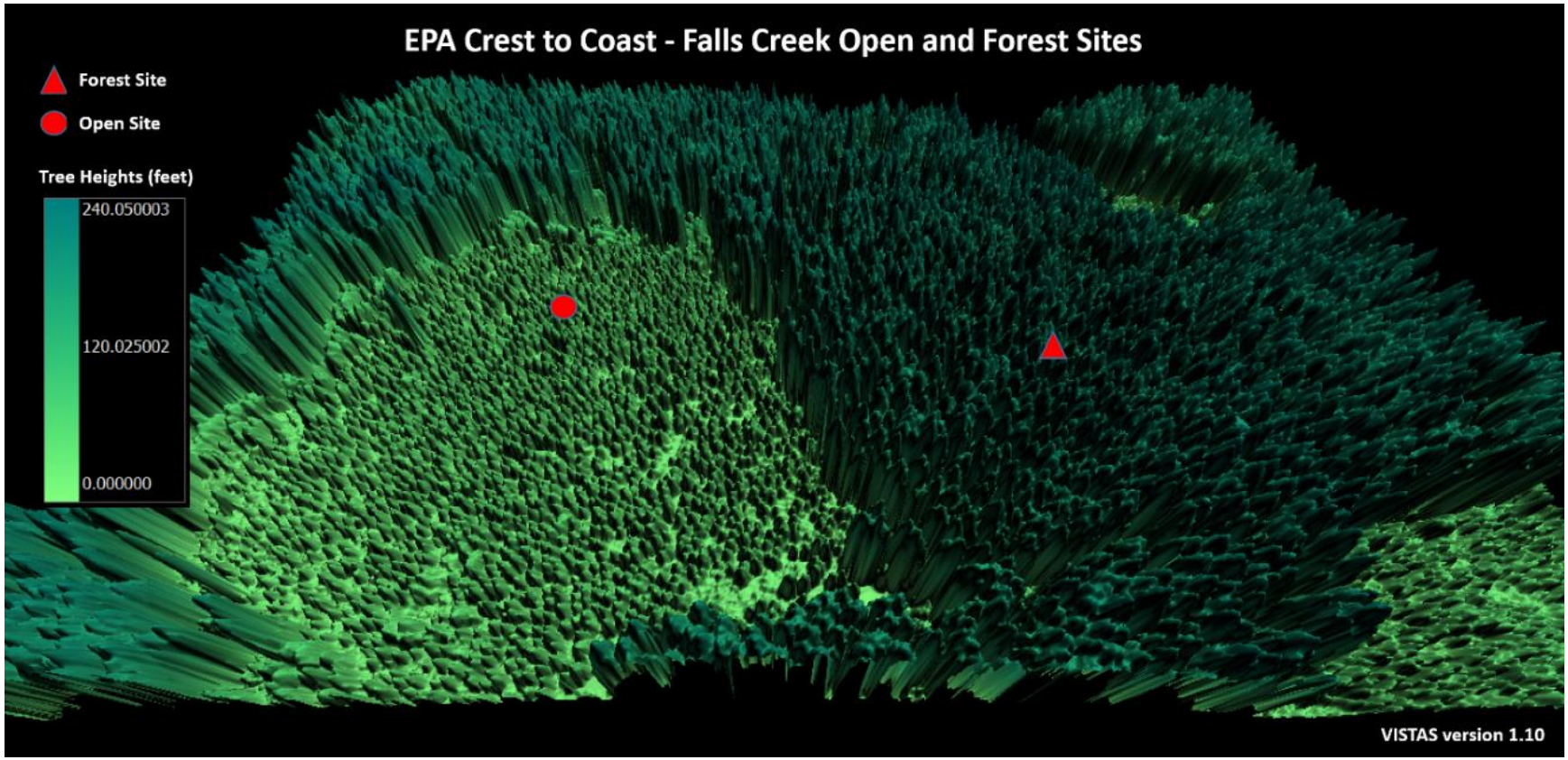

Figure 2-12: Falls Creek EPA Crest to Coast Open and Forested Sites.

Sites are part of the Oregon Crest-to-Coast Environmental Monitoring transect (O'CCMoN) dataset.

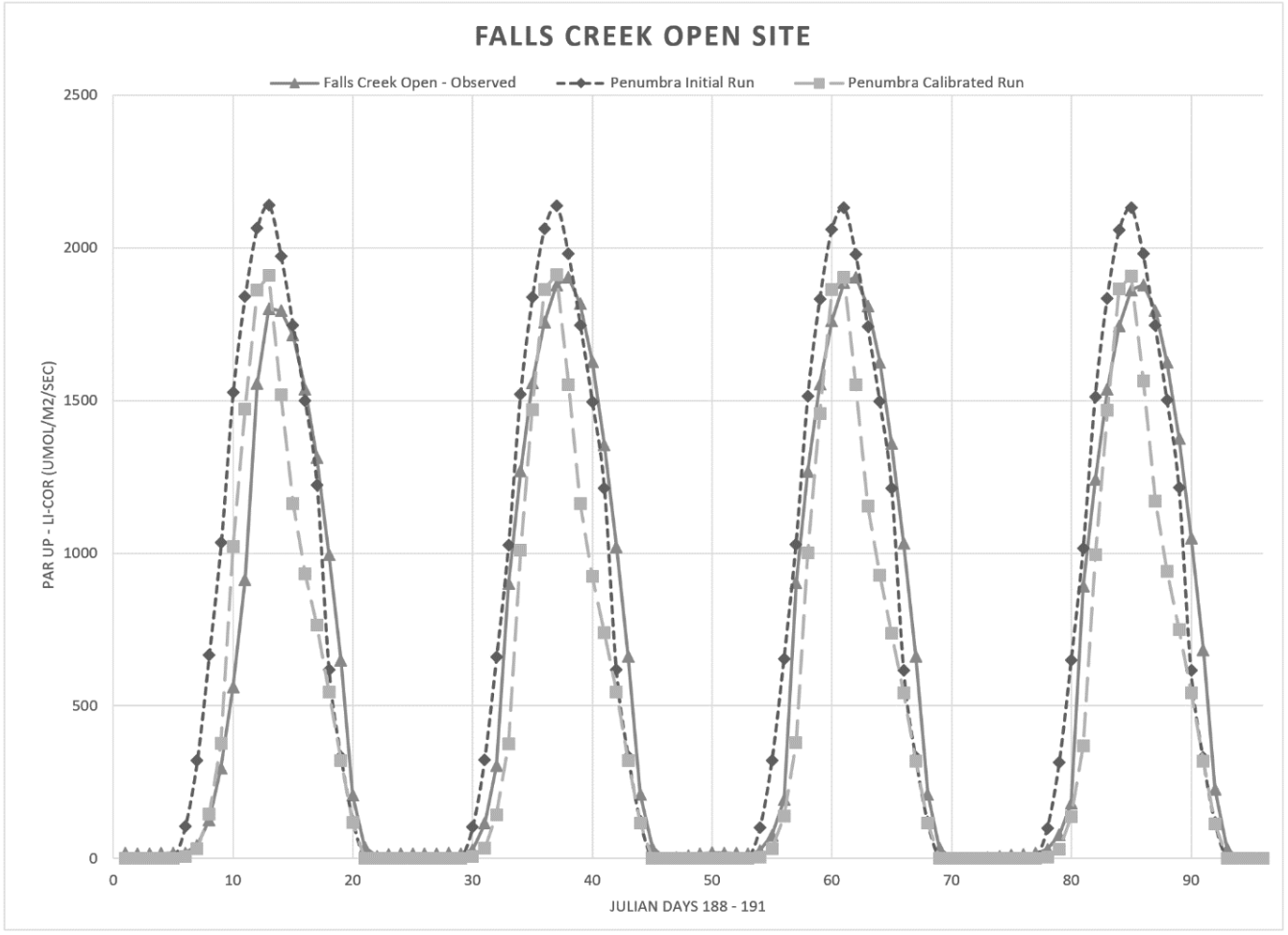

Figure 2-13: Simulated versus observed agreement for Falls Creek Open site.

PAR units are µmoles/m^2/s. *Note Figure 2-14 y-axis scale is about 0.5x

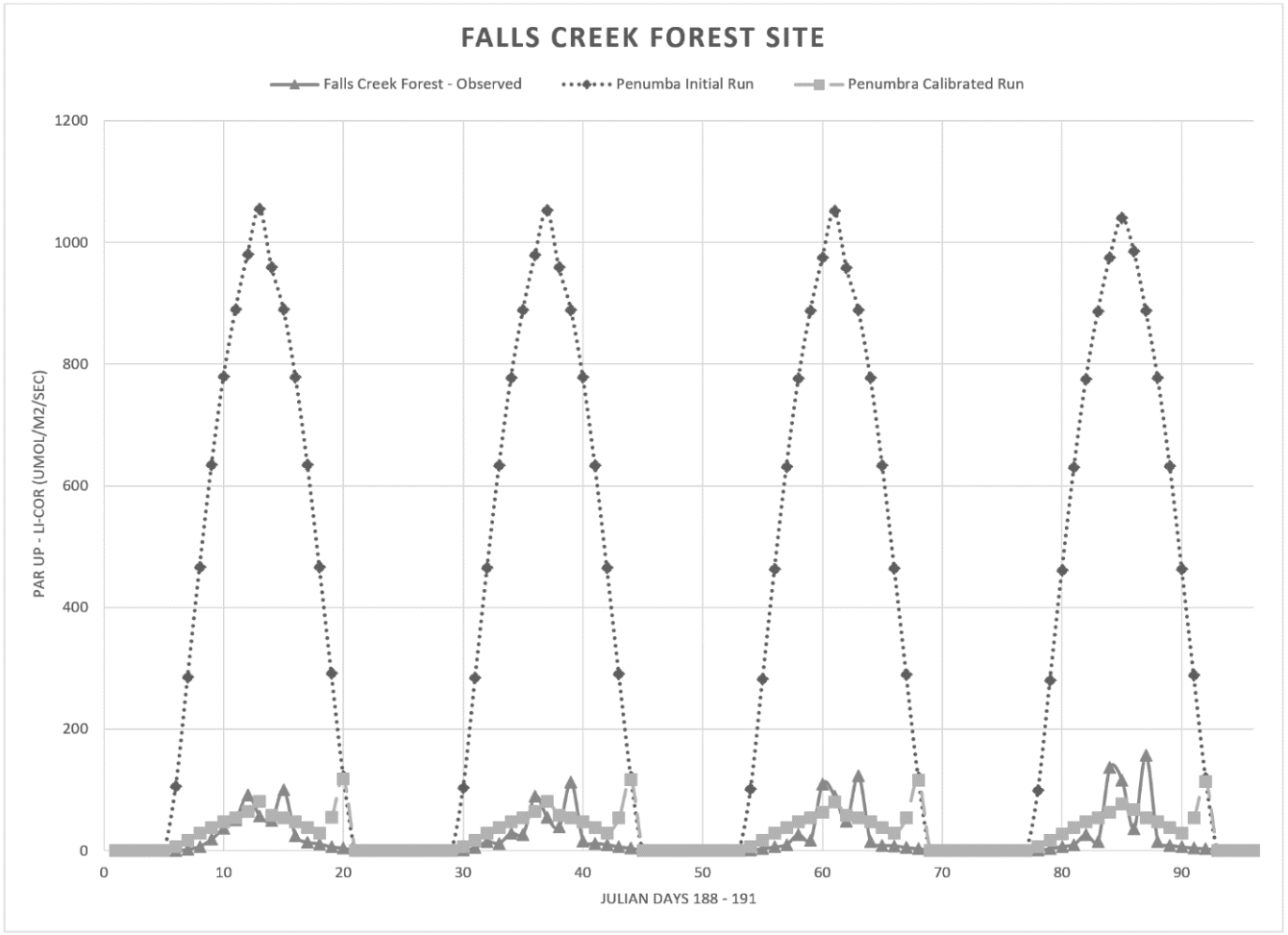

Figure 2-14: Simulated versus observed agreement for Falls Creek Forest site.

PAR units are µmoles/m^2/s. *Note Figure 2-13 y-axis scale is about 2x

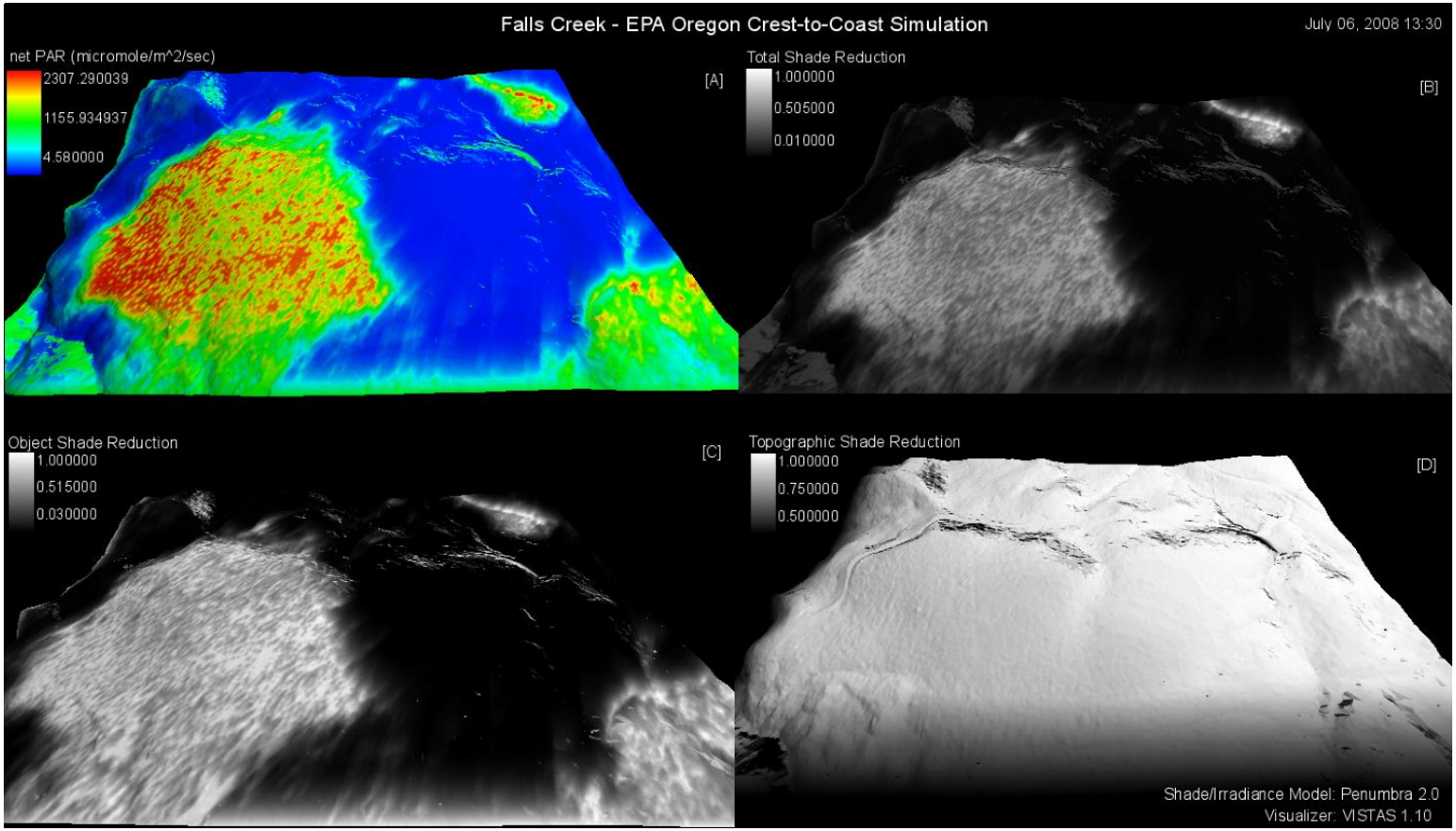

Figure 2-15: Static results for Falls Creek Open and Forest sites.

Static simulation shot on July 06th, 2008 at 2:30pm. (A) net solar energy as PAR (µmoles/m^2/s), (B) Total shade reduction (0.0 – 1.0), (C) Object shade reduction (0.0– 1.0), (D) Topographic shade reduction (0.0 – 1.0). For all (0.0 – 1.0) shade reductions 1.0 is no reduction and 0.0 is full reduction. See appendix for the movie demonstrating this simulation.

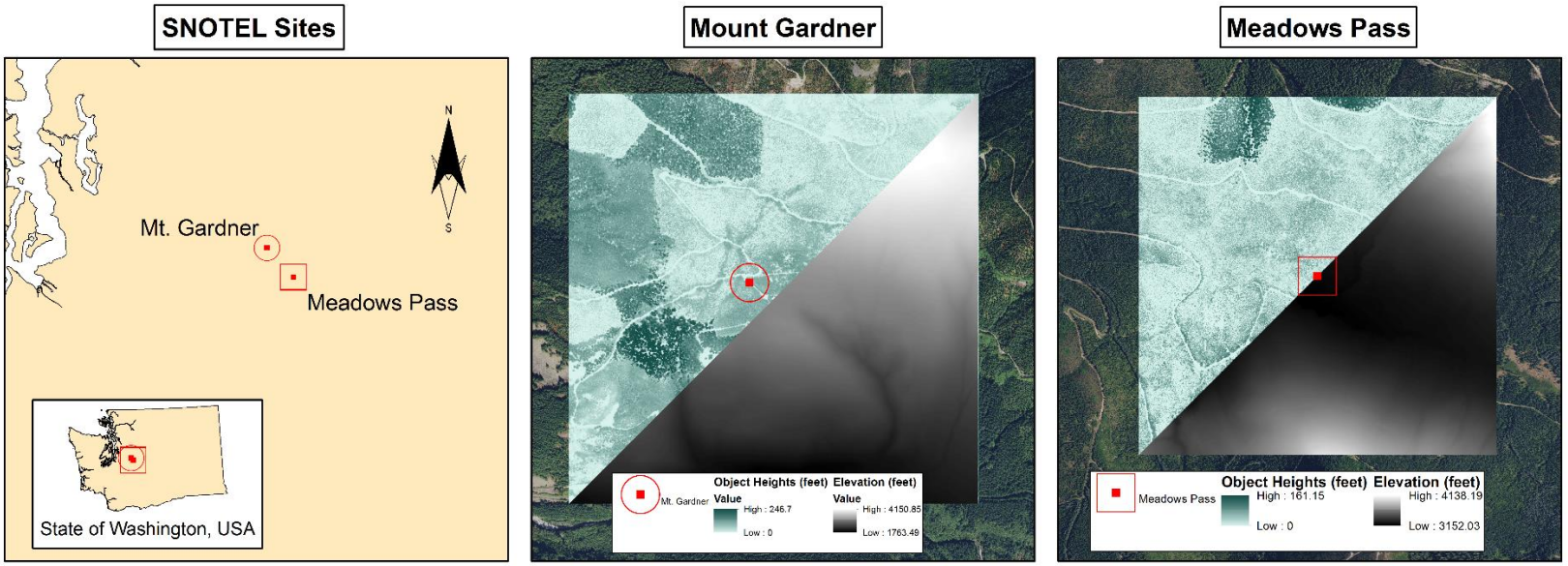

Figure 2-16: SNOTEL sites: Meadows Pass and Mount Gardner.

See appendix for the movie demonstrating the Mount Gardner site simulation.

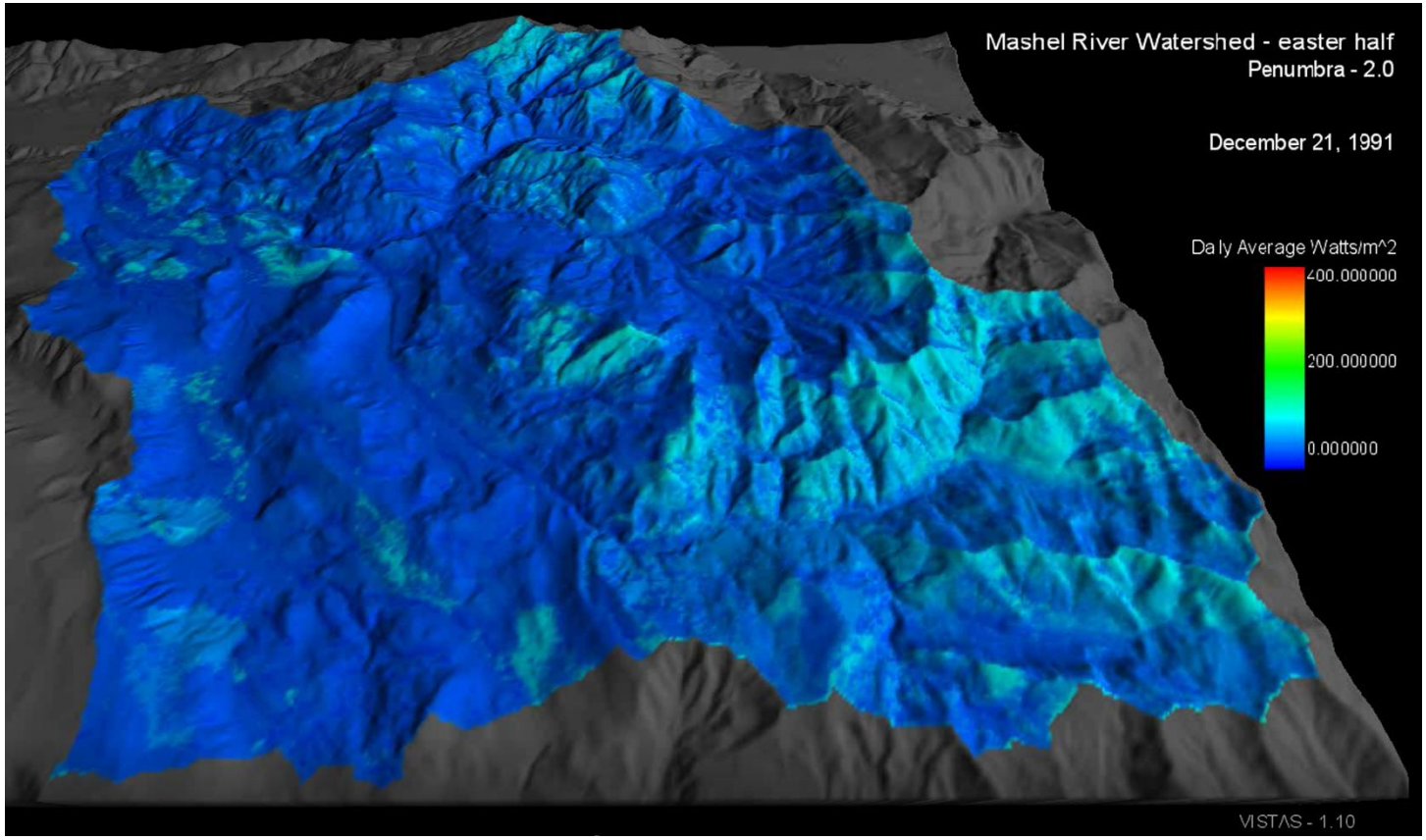

Figure 2-17: Winter solstice irradiance across eastern Mashel River Watershed.

See Appendix for movie name for full 2-year simulation of the eastern portion of the Mashel River Watershed.

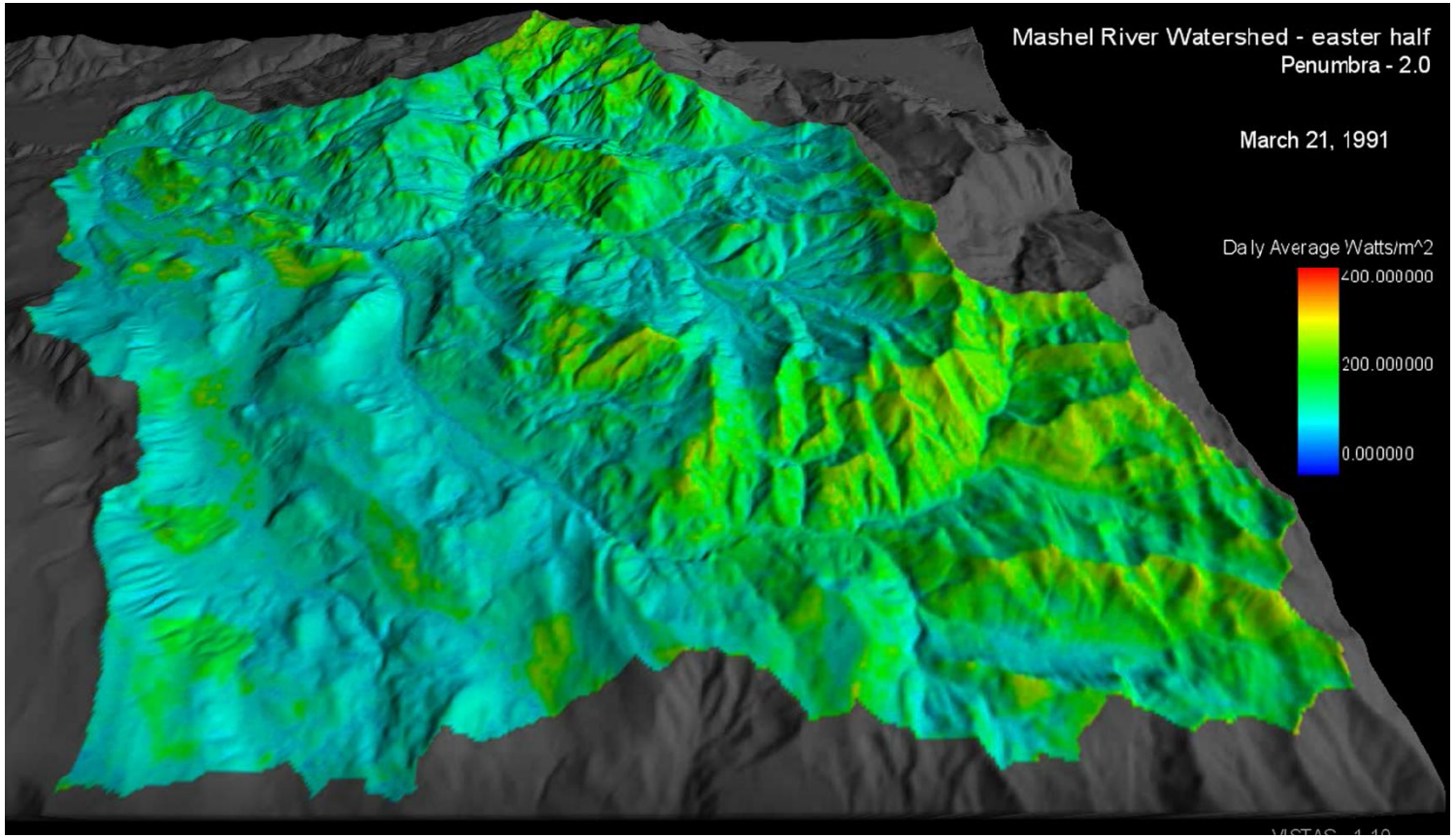

Figure 2-18: Spring equinox irradiance across eastern Mashel River Watershed.

See Appendix for movie name for full 2-year simulation of the eastern portion of the Mashel River Watershed.

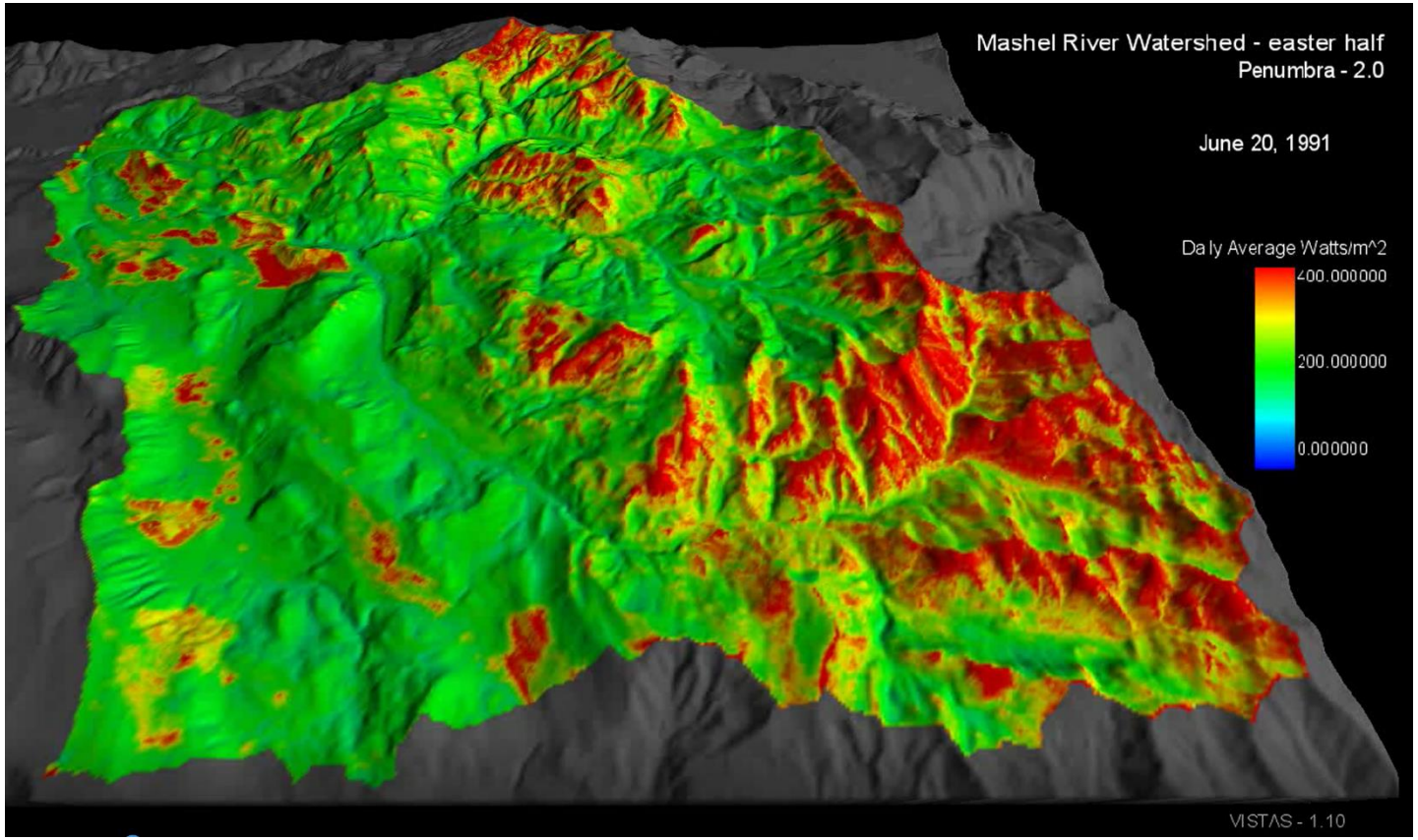

Figure 2-19: Summer solstice irradiance across eastern Mashel River Watershed.

See Appendix for movie name for full 2-year simulation of the eastern portion of the Mashel River Watershed.

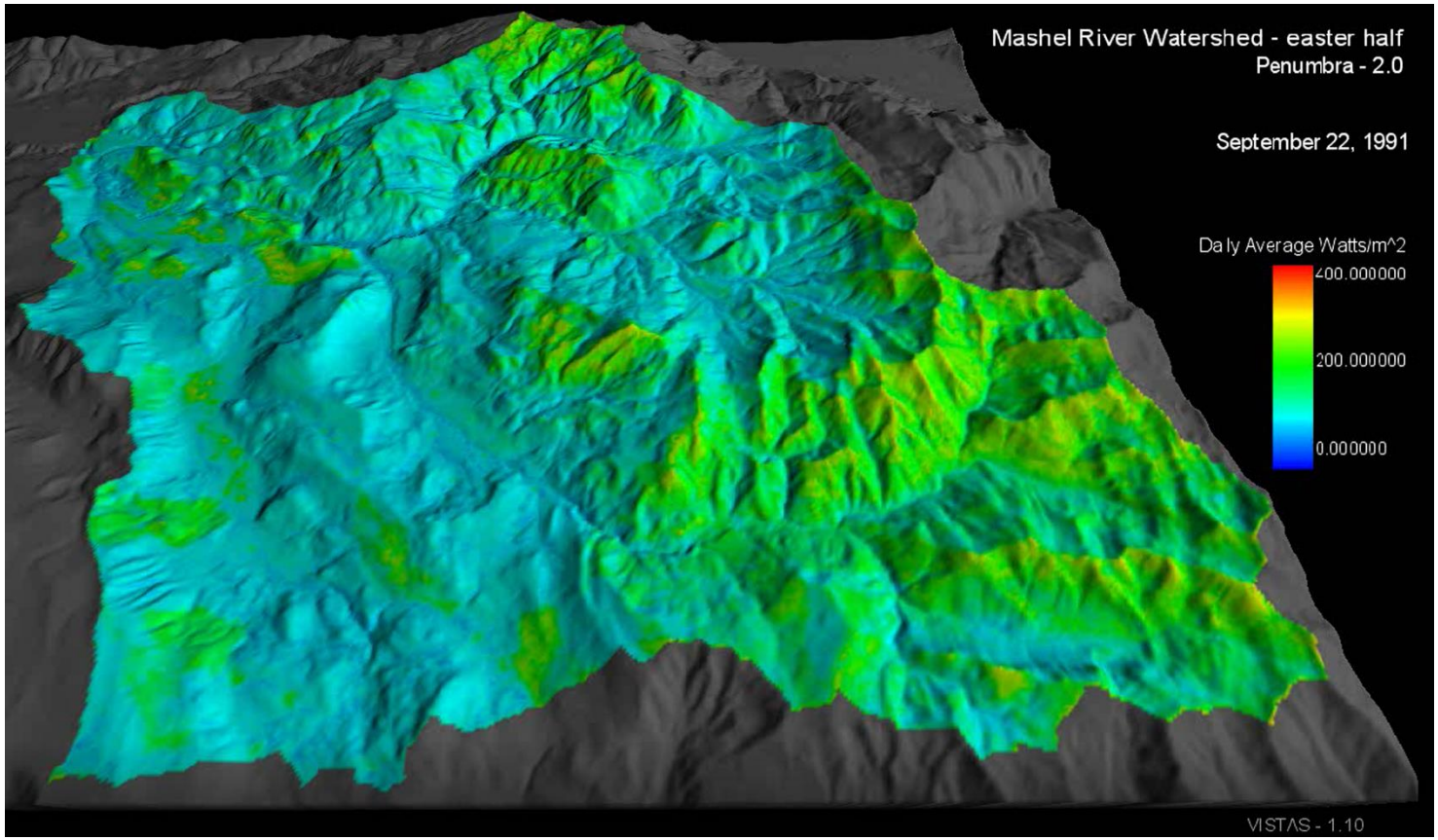

Figure 2-20: Fall equinox irradiance across eastern Mashel River Watershed.

See Appendix for movie name for full 2-year simulation of the eastern portion of the Mashel River Watershed.

2.13 Tables

Table 2-1: List of Penumbra inputs, parameters, and outputs.

Required Inputs	**Optional Inputs**	**Outputs**
Start/Stop Julian Day and Year	Forced Daily Start/Stop Times	Ground-level Irradiance Map
Temporal Grain	Daily Transmittance Map	Total Shade % Map
Temporal Aggregation	Daily Percent Cloud Coverage	Object Shade % Map
Digital Elevation Model (DEM)*	Area of Interest Mask Model	Topographic Shade % Map
Normalized Digital Surface Model (nDSM)*	Cell Data Writer X-Y Position	Specific Cell Data Values
nDSM-Object Transmittance Model (nDSM-OTM)*	Pseudo Height Adjustment	

* Technically optional: Penumbra can simulate only terrain or only object shading. If the DEM or nDSM are excluded, any shadowing that would occur is being excluded. DEM and nDSM are required for complete (topographic and object) shading to be simulated.

Table 2-2: List of Penumbra calibration parameters.

Calibration Parameter	**Range**	**Data Influence**
Total Irradiance (TI_{CALI})	0.0 – 1.0	Adjustment on extraterrestrial irradiance.
Transmittance (TR_{CALI})	0.0 – 1.0	Uniform shift on the nDSM-OTM.
Ground Effect (GR_{CALI})	0.0 – 1.0	Adjustment on topographic shade influence.
Cloud Effect (CE_{CALI})	0.0 – 1.0	Adjustment on cloud data influence.

Table 2-3: Converting azimuth and altitude angles to conform within Cartesian coordinate system.

(Conditional Equations 3 – 10)	
If azimuth is: $0 > \alpha \geq 90$: (Eq. 3) Run = X = $\lvert (\sin \alpha * v) \rvert$ (Eq. 4) Rise = $-1 * \lvert (\cos \alpha * v) \rvert$	If azimuth is: $180 > \alpha \geq 270$: (Eq. 7) Run = X = $-1 * \lvert (\sin \alpha * v) \rvert$ (Eq. 8) Rise = $\lvert (\cos \alpha * v) \rvert$
If azimuth is: $90 > \alpha \geq 180$: (Eq. 5) Run = $\lvert (\cos \alpha * v) \rvert$ (Eq. 6) Rise = $\lvert (\sin \alpha * v) \rvert$	If azimuth is: $270 > \alpha \geq 360$: (Eq. 9) Run = X = $-1 * \lvert (\cos \alpha * v) \rvert$ (Eq. 10) Rise = $-1 * \lvert (\sin \alpha * v) \rvert$

Table 2-4: Moose Mountain parameters, initial results, and calibrated results.

Open Site	*Initial Run*	*Calibrated Run*	*Calibration Parameters*	*Initial Settings*	*Calibrated Settings*
Percent Agreement	0.52	1.03	*Irradiance*	1.0	0.94
RMSE	506.0	224.6	*Transmittance*	1.0	0.945
Mean Error	286.1	-17.3	*Topographic*	0.5	0.2
Sensor ht. (cm)	282.5		*Clouds*	1.0	1.0
Forest Site					
Percent Agreement	1.55	1.86	*Irradiance*	1.0	0.94
RMSE	77.8	53.8	*Transmittance*	1.0	0.945
Mean Error	-10.0	-15.6	*Topographic*	0.5	0.2
Sensor ht. (cm)	297.2		*Clouds*	1.0	1.0

Table 2-5: Falls Creek parameters, initial results, and calibrated results.

Open Site	*Initial Run*	*Calibrated Run*	*Calibration Parameters*	*Initial Settings*	*Calibrated Settings*
Percent Agreement	1.09	0.77	*Irradiance*	1.0	1.0
RMSE	252.6	296.8	*Transmittance*	1.0	0.965
Mean Error	-59.96	148.1	*Topographic*	0.5	0.25
Sensor ht. (cm)	353		*Clouds*	1.0	1.0
Forest Site					
Percent Agreement	19.2	1.51	*Irradiance*	1.0	1.0
RMSE	515.7	34.2	*Transmittance*	1.0	0.965
Mean Error	-59.9	-10.4	*Topographic*	0.5	0.25
Sensor ht. (cm)	334		*Clouds*	1.0	1.0

Table 2-6: SNOTEL 3-Meter results for four-day site calibration sequence.

	Initial Run	*Calibrated Run*	*Calibration Parameters*	*Initial Settings*	*Calibrated Settings*
		Meadows Pass Site			
Percent Agreement	0.4657	0.6854	*Irradiance*	1.0	0.766
RMSE (Watts/m²)	288.66	34.2	*Transmittance*	1.0	1.0
Mean Error (Watts/m²)	174.67	66.46	*Topographic*	0.25	0.25
Sensor ht. (m)	5.48		*Clouds*	1.0	1.0
		Mount Gardner Site			
Percent Agreement	0.7754	0.6743	*Irradiance*	1.0	0.7335
RMSE (Watts/m²)	411.2	265.2	*Transmittance*	1.0	1.0
Mean Error (Watts/m²)	292.5	158.0	*Topographic*	0.25	0.25
Sensor ht. (m)	5.48		*Clouds*	1.0	1.0

Table 2-7: Penumbra setup for Mashel River Watershed.

Temporal Parameters		Spatial Input Data	
Temporal Grain	10 minutes	DEM	Mashel_30m_DEM.asc
Temporal Aggregation	Daily	nDSM	Mashel_30m_Objects.asc
Start_Year	1990	Transmittance	Mashel_30m_Object_Transmittance.asc
Start_Julian_Day	001	Center_Latitude	46.501747
End_Year	1990	Center_Longitude	-122.060215
End_Julian_Day	365	GPU	false
Calibration Parameters			
TI_{CALI}	0.766	TR_{CALI}	0.965
CE_{CALI}	1.0	GR_{CALI}	0.25

2.14 Appendix

1. MountGardner_15min_Jday100_300_60seconds.wmv
2. MountGardner_10min_GPU_Jday100_300_280seconds.wmv
3. PenumbraCalibration_MooseMountain2008FourDaySimulation.wmv
4. PenumbraCalibration_FallsCreek2008FourDaySimulation.wmv
5. MashelRiverWatershed-EasterHalf_Irradiance_1991_1992_71seconds.wmv

3. Improved Soil Temperature Modeling using Spatially-distributed Irradiance

3.1 Abstract

Soil temperature modeling is complicated due to the spatial and temporal variability of several influential environmental variables, including soil moisture, air temperature, and solar energy. Landscape incident solar radiation is a significant environmental driver that effects air temperature and terrain-level soil energy loading, and is therefore extremely important for accurate simulations of soil temperature. Here, we improve a soil temperature sub-model within a spatially explicit watershed ecohydrological model by including spatially explicit solar irradiance data as input. The improved sub-model can capture the resulting solar energy due to forest canopy shadowing and can therefore better represent spatiotemporal patterns of surface-level irradiance that ultimately affects soil temperature. We test the improved model at the HJ Andrews Long-term Experimental Research site, as well as using the Environmental Protection Agency (EPA) Oregon Crest-to-Coast Environmental Monitoring transect (O'CCMoN), a dataset consisting of several paired forested and open landscapes. Results demonstrate that a spatially explicit model for solar irradiance dramatically improves spatial and temporal simulations of soil temperature within a watershed-scale ecohydrological model.

3.2 Introduction

Ground soil temperature affects several key ecosystem properties. Through surface runoff and subsurface ground water transport (*Mayer, 2012*), it can lead to increased stream temperatures, which in turn have direct impact on salmonids and other fish. Soil temperature also has a direct effect on biomass accumulation. Lower soil temperatures cause a reduction of detritus decomposition and reduced root member permeability and water uptake due to increased water viscosity (*Reich et al., 2014*). Also, seasonal soil temperature trends can shift photosynthetic recovery timing, and therefore impact overall net primary production (NPP) (*Mellander et al., 2006*).

Several variables are required to mechanistically calculate ground soil temperatures at various depths. Required variables include air temperature, soil moisture, soil depth, and incoming solar energy. Air temperature and precipitation are well monitored, and several modeling products represent these data at various spatial scales (e.g., PRISM and DayMet)

(*PRISM, 2016; Thornton, 1997*). Solar energy is an environmental variable that usually is represented either via a proxy variable (i.e. canopy coverage or air temperature), or implicitly represented as global irradiance without a spatial distribution.

Many current environmental mechanistic models, such as Visualizing Ecosystem Land Management Assessments (VELMA; *Abdelnour et al., 2011*), Soil and Water Assessment Tool (SWAT; *Neitsch et al., 2011*), Regional Hydro-Ecologic Simulation System (RHESSys; *Tague and Band, 2004*), Distributed Hydrology Soil Vegetation Model (DHSVM; *Wigmosta et al.,2002*), and Hydrologic Simulation Program – Fortran (HSPF; *Bicknell et al., 1997*) use a global solar irradiance sub-model to calculate spatially implied solar energy at a watershed scale. Due to this simple representation of ground surface solar energy, these models can capture the seasonal pattern of irradiance, yet they lack a spatially heterogeneous representation of topographic and landscape object shading that affects terrain level solar energy.

There do exist models that sufficiently account for solar energy inputs into stream reaches, but they operate at local scales. SHADE2 (*Li et al., 2012*), the HeatSource Shade-a-lator (*Boyd and Kasper, 2003*), and iLand (*Seidl et al., 2012*) are all good examples of this implementation of small-area representation of solar irradiance. However, spatial heterogeneity of shade and ground-surface irradiance are rarely accounted for within large-area watershed environmental models. Penumbra (chapter 2) is a model designed to provide heterogenous shade and ground-surface irradiance at large-landscape scales. Therefore, we seek to evaluate how a spatially heterogeneous solar energy from Penumbra can improve simulations of soil temperature at multiple depths. This advancement will broaden the applicability of environmental watershed-scale mechanistic models and will allow more realistic simulations of a variety of environmental processes. These model simulations will provide improved land use decision management support tools relied upon for making policies that effect on the amount of solar energy reaching landscape terrain, streams, and critical habitat.

Ecosystem models that characterize hydrologic dynamics usually account for soil moisture by tracking the rate of soil moisture transfer based on soil porosity, soil depth, and the available precipitation per time step. VELMA, SWAT, RHESSys, and HSPF are

such mechanistic model that simulate hydrodynamics throughout a watershed using daily or sub-daily time steps. These models typically utilize uniform or homogenous input of solar energy over the entire landscape; therefore, resulting soil temperature—and subsequently water temperature—simulations do not capture the spatial heterogeneity caused by spatial distribution of irradiance at the surface. This type of irradiance reduction results from topographic shading and object shading (e.g., tree canopy) of incoming solar irradiance.

Here we advance soil modeling using a spatially-distributed solar energy model. To simulate heterogeneous solar energy reaching the earth's surface, we use Penumbra—a spatiotemporal landscape-scale solar energy model that calculates the net ground-level incident solar irradiance resulting from object and topographic shade (*Chapter 2*). Penumbra functions at a fixed extent and grid cell size and therefore is compatible with watershed-scale models such as VELMA and RHESSys. Other sub-catchment scale models can also utilize spatially heterogeneous solar energy simulations, albeit broader averaged scales. Penumbra can function at sub-daily timescales as small as one minute, though it can aggregate data from multiple time steps to a daily output to match the temporal grain of many environmental watershed models.

The purpose of this research is to test whether soil temperature simulations in a mechanistic environmental watershed model can be improved using a spatially-distributed solar irradiance model that accounts for topographic and object shading. We utilize VELMA, a spatially distributed hydro-biochemistry watershed model that simulates the growth of forests through a gridded framework under mechanistic cell interactions. VELMA's 3-D gridded voxel framework is comprised of a 2-D top surface, with each cell representing the ground surface, and four corresponding sub-surface voxels representing the landscape's soil strata. Each sub-surface voxel is characterized by its soil porosity and depth. Daily water transfers through VELMA's voxel framework, transporting nutrients and thermal energy via mechanistic rules. VELMA simulates a watershed as individual pixels, rather than at sub-catchments scales.

To demonstrate the utility of linking Penumbra with an environmental model, we specifically focus on its ability to generate spatially heterogeneous solar energy that

reaches the ground and subsequently impacts soil temperature. Through this paper: (1) we discuss common solar energy and soil temperature sub-models used in common environmental models (i.e., VELMA, SWAT, HSPF, RHESSys), (2) introduce a simple soil temperature model that utilizes spatially variable inputs of ground-level irradiance, (3) test a common process-based soil temperature method against our process-based soil temperature method that includes spatially-distributed irradiance, (4) present the two soil temperature modeling method results, and (5) provide directions for future research.

3.3 Methodology

Providing a soil temperature model spatially-distributed solar energy should provide the ability to improve modeled soil temperature. To ensure improved, or otherwise, results are only due to the added spatially-distributed solar energy the soil temperature sub-model was isolated from the VELMA model. To confirm the soil temperature model functioned equivalent in isolated form as it does within VELMA, data was captured from a VELMA simulation and tested against the isolated model. The isolated soil temperature model was then utilized to develop and test the original and new soil temperature models.

3.3.1 Global Irradiance Models: Previous and Current

Environmental watershed models typically include solar energy directly or through a proxy variable to facilitate energy requirements needed within its sub-models. Plant growth models require a daily input of solar irradiance reaching the canopy to drive photosynthesis. Stream temperature models predict shifts in water temperature through variables representing landscape shading, observed water temperatures, and air temperatures, all of which are solar energy proxies. Snowmelt models require a daily input of solar energy or air temperature to drive snow melt. While many sub-models used within watershed environmental models rely on solar energy at the earth's surface, many mechanistic models fail to capture the spatiotemporal dynamics of solar irradiance reaching the ground.

The most commonly used global solar irradiance model utilizes latitude as input and calculates the resulting energy (W/m^2) that reaches the earth's surface, where R is solar irradiance, ecc is the eccentricity correction factor, w is the Earth's constant angular

velocity, T is the time frequency, dec is the solar declination, and γ is latitude (McKane, 2014).

$$R = \left(\frac{24}{\pi}\right) * 4.921 * ecc * [wT\ sin(dec)sin(\gamma) + cos(dec)sin(wT)cos(\gamma)] \quad [1]$$

This simplistic model describes the amount of solar energy reaching the troposphere. It does not account for topographical and object shading effects. A new irradiance model called Penumbra (*Chapter 2*) was developed to include irradiance reduction effects due to topographic and object (e.g., tree canopy) shading (Figure 3-1). Figure 3-1 shows a generic schematic that showcases how Penumbra provides spatially distributed ground-level irradiance while considering solar fluctuations as well as topographic and object shading. Chapter 2 contains the detailed description of Penumbra and the mechanistic equations that drive its ability to provide spatially heterogeneous ground-level irradiance.

For the purposes of model integration to achieve improved soil temperatures using Penumbra, we note that Penumbra can provide daily (or smaller) time-steps of gridded calculations of ground-level irradiance for use within environmental watershed models. Depending on whether a spatially explicit voxel model (e.g., VELMA, Rhessys) or a semi-distributed model (e.g., SWAT, HSPF) is to be used, Penumbra can provide varying degrees of aggregated irradiance data to match the input requirements of the model.

3.3.2 Soil Temperature Model: Current Model and Improvements

Current environmental watershed models, whether utilizing a gridded landscape or aggregating to sub-catchment scales, typically utilize some version of Carlsaw and Jaeger (1959) to quantify seasonal variation in soil temperature (*Carlsaw and Jaeger, 1959*):

$$T_{soil}(z, d_n) = \bar{T}_{AA} + A_{surf} e^{-z/dd} \sin(\omega d_n - z/dd). \quad [2]$$

where $T_{soil}(z,d_n)$ is the soil temperature (°C) at depth z (mm) and day of the year d_n, $\bar{T}_{AA}$ is the average annual soil temperature, A_{surf} is the amplitude of the surface fluctuations, dd is the damping depth (mm), and ω is the angular frequency of the damping oscillations by day (d_n). At z = 0, the ground surface soil temperature reduces to the following:

$$T_{soil}(0, d_n) = \bar{T}_{AA} + A_{surf} \sin(\omega d_n). \quad [3]$$

which is the average soil temperature perturbed by surface temperature fluctuations reflecting seasonal solar patterns. At infinite depth, the soil temperature becomes equal to

the annual average soil temperature. This formulation provides a relatively simple method for calculating soil temperatures at multiple depths throughout a watershed. However, the model requires specification of soil heat capacity as well as thermal conductivity to correctly specify the amplitude coefficient and the damping depth.

VELMA applies a mechanistic version of the Carlsaw and Jaeger (1959) soil temperature method by utilizing soil moisture damping and the oscillatory effects of solar energy. Seasonal solar energy variability is represented through a time phase lag modification of a locations observed air temperature combined with a temperature modified soil depth attenuation. VELMA, along with the Carlsaw and Jaeger (1959) previously presented (Eq. 2 and Eq. 3), does not account for spatial heterogeneity of irradiance reaching the ground because of topographic or object shading. VELMA's process-based soil temperature sub-model input variables (Table 3-1) directly account for the shift in soil temperature due to moisture and soil depth, but equate a proxy for solar energy through two oscillatory equations driven by the average air temperature (Eq. 5) and soil moisture damping (Eq. 7).

For each layer, VELMA calculates the soil temperature based on the thermal attenuation of average air temperature. The degree of attenuation is adjusted daily by each soil layers' depth and soil moisture, where G_{TEMP} is the resulting top layer soil temperature, $Air_{AVETEMP}$ is daily average air temperature, Air_{LAG} is a prior $Air_{AVETEMP}$ based on seasonal oscillation, SoilDamping is the influence of soil moisture based on seasonal oscillation, $Depth_{ATTENUATION}$ is the temperature adjustment based on depth and soil damping, phaseLag is the $Air_{AVETEMP}$ based on seasonal oscillation driven by LSDepth (depth to surface) and soilDamping, LTD is the temperature accumulation at depth, and $Soil_{BELOW}$ is the influencing soil temperature from the lower soil layer:

$$G_{TEMP} = Air_{AVETEMP} + (Air_{LAG} - Air_{AVETEMP} - SoilDamping) * Depth_{ATTENUATION} \quad [4]$$

$$Air_{LAG} = \text{Past Air Temperature at Julian Day(phaseLag)} \quad [5]$$

$$\text{phaseLag} = \frac{\text{LSDepth}}{\text{SoilDamping}} * \frac{365}{2 * \pi} \quad [6]$$

$$\text{SoilDamping} = \sqrt{\frac{\text{LTD} * 365}{\pi}} \quad [7]$$

$$\text{LTD} = LTD_{ACCUMULATION} / Soil_{BELOW} \quad [8]$$

$$\text{Depth}_{\text{ATTENUATION}} = e^{\left(\frac{-\text{LSDepth}}{\text{SoilDamping}}\right)} \quad [9]$$

3.3.3 Improved Soil Temperature Model

To improve upon the VELMA soil temperature sub-model, which only uses spatially homogenous irradiance, an improved air-soil-temperature model called VELMA-AST3 was created by including spatially explicit solar energy modeling via Penumbra. Through tight model coupling, Penumbra provides environmental watershed models with spatially distributed solar energy. Like all irradiance models, daily extraterrestrial solar energy is calculated for a location in relation to the Earth's rotation around the Sun. Penumbra goes further to spatially account for reductions in energy from topographic and object shadowing. Penumbra v2 cloud coverage is a simplistic daily percent cloud coverage. Due to non-spatial cloud representation, the influence of solar energy reduction is not simulated here.

VELMA-AST3 maintained the use of soil moisture and air temperature to calculate soil temperature at all layers within the soil column. Ground-level solar irradiance data was provided through the Penumbra-VELMA integration, and influenced the VELMA-AST3 model as $\text{Reducer}_{\text{SOLAR}}$. The resulting soil temperature for top soil layer ($\text{NetSoil}_{\text{TEMP1}}$) is the daily average air temperature (Air_{TEMP}) multiplied by the $\text{Reducer}_{\text{SOLAR}}$ and $\text{Damping}_{\text{SOIL}}$.

$$\text{NetSoil}_{\text{TEMP1}} = \text{Air}_{\text{TEMP}} * \text{Reducer}_{\text{SOLAR}} * \text{Damping}_{\text{SOIL}} \quad [10]$$

VELMA's original soil temperature model functioned well without the knowledge of spatially distributed solar energy, partly due to how the soil columns moisture reduced soil temperature. With the addition of spatially-distributed solar energy, soil moisture damping approach was simplified to the inversion of each layer's soil moisture:

$$\text{Damping}_{\text{SOIL}} = 1 - \text{Layer}_{\text{SM}} \quad [11]$$

where Layer_{SM} represents the soil moisture at each soil layer (mm/meter^2).

The spatially explicit solar energy per cell and the watershed's maximum solar energy are both used to calculate the solar energy "reducer" per cell. This "reducer" represents the local reduction in soil temperature due to the lack of solar energy relative to local region's potential maximum solar energy. This approach provides a ratio in solar energy in relation to the observed air temperature driver.

Solar energy was built into the VELMA-AST modeling methodology by accounting for the proportional relationship between a cell's solar energy to the watershed's maximum solar energy. The reduction of solar energy is calculated as follows:

$$Reducer_{SOLAR} = 1 - \alpha * (1 - (Cell_{SOLAR} / Max_{SOLAR})) \quad [12]$$

where α is a calibration factor, $Cell_{SOLAR}$ is each cell of interest within the VELMA framework, and Max_{SOLAR} is watersheds maximum solar energy value amongst all watershed cells per time step. The assumption made here is the weather station providing the air temperature data is in an open environment. The temperature sensors are monitoring air that is directly influenced by solar energy. The AST model spatially modeled soil temperature using soil moisture, but was not spatially modeling the effects of solar energy on soil temperature. Equation 12 provided a way modify the impact of air temperature due to any objects reducing the total solar energy reaching the ground, such as trees.

Soil layers 2-4 are below the first layer and are therefore not directly affected by solar energy. For these layers, the soil temperature ($NetSoil_{TEMP2}$) is calculated using the two-day running average temperature of the soil layer above reduced by $Damping_{SOIL}$:

$$NetSoil_{TEMP2} = Soil_{AVE\_TEMP} * Damping_{SOIL} \quad [13]$$

$$Soil_{AVE\_TEMP} = (SoilTemp_{(JDay)} + SoilTemp_{(JDay-1)}) / 2 \quad [14]$$

where $SoilTemp_{(JDay)}$ is the current simulation time steps current layer soil temperature, and $SoilTemp_{(JDay-1)}$ is the last time steps soil temperature for the same layer. The soil moisture is applied equivalently as the top layer using the $Damping_{SOIL}$ coefficient (Eq. 11).

3.3.4 VELMA-Mimic Model

Penumbra is a model that could provide VELMA spatially-distributed solar energy. VELMA being a mechanistic model with multiple sub-models that interact with one another, the soil temperature code needed to be isolated to ensure the spatially-distributed solar energy was the cause of soil temperature modeling improvements; not sub-model interaction. The sub-model isolation was also necessary for two VELMA model framework reasons: (1) VELMA simulations require a fully delineated watershed to function, and (2) the soil moisture from VELMA is internally simulated. The first limitation is a logistical issue due to the observed soil temperature data used to test and validate the soil temperature

models. These data were collected at sites outside well-monitored watersheds (e.g., H.J. Andrews), which means the VELMA model would require calibration using additional data that was not available. The second limitation is related to the uncertainty of a VELMA simulation. Soil moisture has a significant influence on the original and new VELMA soil temperature sub-models. Even a small error in VELMA's internal soil moisture calculations would impact the comparison of the soil temperature models against the observed soil temperature data. VELMA being developed using the computer language Java made isolation of soil temperature code easily feasible.

To isolate the soil temperature sub-models, we developed a VELMA-Mimic model to represent an equivalent representation of VELMA's soil temperature sub-model. The VELMA-AST Java class was replicated as a stand-alone Java model we call the VELMA-Mimic model. Precise replication of VELMA-AST was crucial to ensure the testing of the original soil temperature was an accurate evaluation. The VELMA-AST vertical soil column and daily temporal structure were replicated with no functional changes to the original calculations. Supporting input and output code constituted most of the changes from the original VELMA-AST model to the VELMA-Mimic model. The soil moisture driver data was the most challenging VELMA-AST component due to soil moisture being VELMA derived data. The VELMA-Mimic model's spatial representation is a single X-Y cell soil column. The four vertical voxels represent the soil column. Unlike the original VELMA-AST model, in the VELMA-Mimic model soil moisture is provided as driver data to each soil column voxel per day.

3.3.5 Soil Temperature Testing Sites

H.J. Andrews (HJA) Long Term Ecological Research forest contains Watershed 10 (WS10), a 10.2-hectare catchment that was clear-cut in 1977. (Figure 3-2). The HJA-WS10 site was used to test the ability for the VELMA-Mimic model to reproduce simulation results of the soil temperature sub-model within VELMA. A standard VELMA simulation was carried out on WS10 for the year 2005. A VELMA single cell data-writer probe provided simulation output for each of the four voxels within the soil column. Soil moisture ($mm/m^2/day$) and soil temperature (Celsius) data was collected from this simulation.

The VELMA-Mimic model repeated the VELMA HJA-WS10 simulation for the single cell by being provided the probed soil moisture data and same daily air temperature driver data. The VELMA-Mimic soil temperature output data was compared to the probed VELMA HJA-WS10 soil temperature data. The two simulations matched with an r^2 of 1.0. This test confirmed the VELMA-Mimic model correctly reproduced VELMA results.

With a validated VELMA-Mimic model, the Oregon Crest-to-Coast Environmental Monitoring transect (O'CCMoN) data was utilized to evaluate both the VELMA-AST and VELMA-AST3 soil temperature performance using the VELMA-Mimic model. The O'CCMoN transect data provided air temperature, and photosynthetic active radiation (PAR), and observed soil moisture at various depths to drive the VELMA-Mimic model. Each set of paired sites contains one forested location and one open clear-cut location. Observed soil temperature at various depths was also monitored, and utilized here to test the soil temperature models. The four paired O'CCMoN sites were utilized for the VELMA-AST and VELMA-AST3 testing. These paired sites include Cascade Head, Moose Mountain, Soapgrass, and Toad Creek (Figure 3-3). These sites span the range of elevation and habitat diversity from coastal to the snow zone of the Cascades (Table 3-20).

The Cascade Head Open site was installed outside the Cascade Head Experimental Forest and Scenic Research Area-Forestry Sciences Laboratory (EFSRA-FSL) in a managed landscape at an elevation of 157 meters (Table 3-2). The Cascade Head Forest site is located 621 meters to the northeast in a predominantly Douglas fir forest at an elevation of 190 meters (Table 3-2).

The Moose Mountain, Soapgrass, and Toad Creek sites are on the western side of the Cascades Mountain Range at increasing elevations and experience moderate to extreme Cascade Mountain weather. The Moose Mountain Open site and Forest site were installed in 1998. The open site was installed within a forest clear-cut at an elevation of 668 meters, while the forest site is located 460 meters to the northeast in a predominantly Douglas fir forest at an elevation of 658 meters (Table 3-2). The Soapgrass Open site and Forest site were installed in 1998. The open site was installed within a forest clear-cut at an elevation of 1298 meters, while the forest site is located 1190 meters to the northeast in a predominantly Douglas fir forest at an elevation of 1190 meters (Table 3-2). The Toad

Creek Open site and Forest site were installed in 1997 and 1995, respectively. The open site was installed within a forest clear-cut at an elevation of 1202 meters. The forest site is located 471 meters to the east in a predominantly Douglas fir forest at an elevation of 1198 meters (Table 3-2).

3.4 Soil Temperature Model Testing

3.4.1 VELMA-Mimic Model

VELMA's AST soil temperature method was tested within the VELMA-Mimic model to establish a baseline of soil temperature simulation accuracy. This established an understanding of how well the original AST model performed. Testing the VELMA-AST model also set a precedence of soil temperature modeling performance, which any derivative soil temperature model would need surpass to be deemed a successful improvement over existing techniques.

Replicating the VELMA-AST required that the average air temperature and average soil moisture per soil column voxel be provided as driver data. The O'CCMoN data sites provided this necessary driver data for both the open and forest sites. VELMA soil column voxel depths were set to match the sensor depths of 150 mm and 300 mm (*WED-EPA, 2016*). Since the O'CCMoN data sites contained only two soil moisture probe depths, VELMA's soil temperature results below the second soil column voxel could not be evaluated.

The new VELMA-AST3 model was tested within the VELMA-Mimic model using the same O'CCMoN data sites for the same periods of time as the VELMA-AST model runs (*Oregon, 2008*). The one exception was the VELMA-AST3 employed the O'CCMoN observed solar energy data. For the open site runs, the $Cell_{SOLAR}$ and Max_{SOLAR} were provided the open sites solar energy data. For the forest site runs the, $Cell_{SOLAR}$ was provided the forest site solar data, and Max_{SOLAR} was provided the open site solar energy data.

3.5 Results

The VELMA-Mimic model revealed that the VELMA-AST methodology performed well when site specific data was provided (Table 3-3). This methodology performed less well for forest sites when the open-air temperature driver was provided. For

VELMA, this is problematic since during a standard VELMA simulation all soil temperatures would be calculated using the same single average air temperature driver, regardless of landscape cover type.

3.5.1 Penumbra Testing Using O'CCMoN Observed Data

Overall, the inclusion of spatially-distributed solar energy improved the simulated solar temperature results (Table 3-2). Both open and forested sites had gains in accuracy, though the inclusion of spatially-distributed solar energy was most beneficial for the forest sites. Through the remainder of the results' sites are referred to through their abbreviations listed under "Sites" in Table 3-2.

Cascade Head (Figure 3-4, 3-5, 3-6, 3-7, and Table 3-3)

The performance at Cascade Head increased for SL1 and SL2 for the forest site, but only improved the Open sites SL2. The Open site SL1 was the only scenario to result in a decrease in simulated versus observed agreement. Though there was a reduction in day to day simulation noise, there was also a significant separation in the simulation to observed open SL1 data trends (Figure 3-4). All CH14 simulations improved.

Moose Mountain (Figure 3-8, 3-9, 3-10, 3-11, and Table 3-3)

The performance of the AST3 model at the Moose Mountain increased for SL1 and SL2 at both Open and Forest sites, but especially for SL2. Simulated data noise was greatly reduced in the VELMA-AST3 simulations.

Soapgrass (Figures 3-12, 3-13, 3-14, 3-15, and Table 3-3)

The performance of the AST3 model for the Soapgrass site increased for SL1 and SL2 at both Open and Forest sites, but especially for SL2. Simulated data noise was greatly reduced in the VELMA-AST3 simulations. This site did result in summer simulated versus observed soil temperature data trend separation, especially in the late summer.

Toad Creek (Figures 3-16, 3-17, 3-18, 3-19, and Table 3-3)

The performance of the AST3 model for the Toad Creek increased for SL1 and SL2 at both Open and Forest sites, but especially for SL2. Simulated data noise was greatly reduced in the VELMA-AST3 simulations.

3.6 Discussion

For landscape-scale process-based models, the inclusion of spatially-distributed solar energy can provide significant improvements to ecological processes driven by solar energy. The inclusion of spatially-distributed solar energy improved VELMA's simulations of soil temperature from more than one perspective. First, the observed versus modeled comparisons for all sites (except for one) improved. The exception was the CHO site, which was an anomaly amongst the sites due to the station existing in a maintained landscape within the grassy area at the Cascade Head-EFSRA-FSL. This reduction in performance could be due to the sites soil moisture behaving different than a forest or clear cut site. In the other sites the forest floor may contain a substantial layer of detritus that would provide an insulation effect on soil temperature. The TCO site received the smallest soil temperature modeling improvement with a SL1 r^2 shifting from 0.82 to 0.83, yet the TCF site showed a significant SL1 improvement with a r^2 increase of 0.73 to 0.92. The greatest improvement was observed at the SGF site with the SL1 r^2 increasing from 0.69 to 0.92, and SGF-SL2 r^2 went from 0.57 to 0.89. The SGF site model improvement is explainable to due this sites data being utilized for the development of the VELMA-AST3 model, though not the same year of data that was tested here. The minimal increases in performance for the open sites is reasonable and understandable due to the VELMA-AST model providing open site average air temperature, which is often used as a proxy variable for solar energy. The greater improvement in forest site soil temperature is then clear due to the solar energy data reflective to the habitat differences between the open and forest sites.

Beyond the r^2 metrics, based on visual inspection of the plotted data, the daily variability in the modeled soil temperature data was reduced. The VELMA-AST model was significantly influenced by the daily average air temperature driver data, yet possessed no representation of landscape coverage or climate patterns. Therefore, the static equations that provided oscillatory proxies for solar energy did not parallel the observed air temperature. In part, this disparity explains the resulting noisy estimations of soil temperature.

The VELMA-AST approach also required a 100-day soil temperature simulation delay while the time lag built-up to a sufficient threshold for Equation 6 to function properly, which was a temporal delay observable in the data. VELMA-AST3 possesses no time lag function, so this problem was solved. Though worth noting, none of the results presented here utilized those 100 days to calculate the performance of either model.

The improvements seen here are attributed to plot level solar irradiance data driving the new soil temperature model. The prior soil temperature model predominantly utilized average air temperature as a proxy for energy. Though VELMA is a spatially-distributed model, the default weather model is driven from data representing only a single location. This setup resulted in homogeneous average air temperature. This is true for a VELMA forest cell and a VELMA bare open prairie cell. Use of this new AST3 soil temperature model within a Penumbra-VELMA integration would facilitate improved VELMA soil temperature modeling within a spatial perspective.

Even though for most sites the AST3 model performed better overall, there are moments in the data where the AST model was more accurate. This could be due to several mechanistic behaviors not being accounted for in the AST3 model. One such behavior is the soil moisture equation might be an over simplification in the AST3 model. Unique soil moisture environmental conditions may require the original AST model's soil moisture approach. Another mechanistic behavior not represented here is a detritus layer blanketing the ground. Detritus would provide an insulation effect that could buffer soil temperatures.

3.7 Conclusion

Penumbra—a spatially explicit ground-level irradiance model—was used to improve soil temperature simulations within a watershed-scale ecohydrological model. By providing the environmental model with more explicit information regarding the spatial distribution of solar energy across a landscape, the model can better capture the spatiotemporal variations of soil temperature in both forested and open sites. This model integration greatly improved the soil temperature representation within the environmental model. Therefore, researchers that utilize spatially distributed or semi-distributed mechanistic watershed-scale models should consider incorporating Penumbra or other spatially heterogeneous descriptions of ground-level irradiance to better represent surface

energy exchange at the surface, especially when modeling variable cover types such as forested, open, and agricultural cover. This is especially relevant when attempting to model the impacts of riparian shading on soil temperature and stream temperatures, which dramatically affect fish habitat.

Finally, we presented the improvement of only a soil temperature sub-model within a ecohydrological model; however, other sub-models can also benefit by the inclusion of spatiotemporal representations of ground-level irradiance. The integration of Penumbra with environmental models could potentially benefit several processes, such as soil temperature, snow melt, water temperature, and plant growth via photosynthesis. Integration with environmental models can provide dynamic feedbacks between other environmental processes, such as tree growth and shade (irradiance reduction). As tree growth is simulated within watershed models, their heights could be transferred back to Penumbra, which then alter the amount of solar energy that is intercepted by the canopy and does not reach the ground. This dynamic integrated modeling approach could be extremely beneficial for looking at the long-term effects of planting riparian buffers and determining how many years it takes before stream temperatures are reduced by some threshold. Therefore, future studies should investigate the incorporation of spatially explicit ground-level irradiance on the simulations of these quantities.

3.8 References

Abdelnour, A., Stieglitz, M., Pan, F, McKane, R. (2011). "Catchment hydrological responses to forest harvest amount and spatial pattern." Water Resources Research 47(9): 1-18.

Bicknell, B.R., Imhoff, J.C., Kittle, J.L., Jr., Donigian, A.S., Jr., and Johanson, R.C., (1997), "Hydrological Simulation Program--Fortran: User's manual for version 11": U.S. Environmental Protection Agency, National Exposure Research Laboratory, Athens, Ga., EPA/600/R-97/080, p. 755.

Boyd, M., and Kasper, B. (2003). "Analytical methods for dynamic open channel heat and mass transfer: Methodology for heat source model Version 7.0."

Carlson, H.S., and Jaeger, J.C. (1959). "Conduction of Heat in Solids." 2nd edition. Clarendon Press, Oxford.

Li, G., Jackson C. R., Kraseski, K. A. (2012). "Modeled riparian stream shading: Agreement with field measurements and sensitivity to riparian conditions." Journal of Hydrology 428-429: pp. 142-151.

Mayer, T. D. (2012). "Controls of summer stream temperature in the Pacific Northwest." Journal of Hydrology 475: pp. 323-335.

McKane, R.B., Brookes, A., Djang, K., Stieglitz, M., Abdelnour, A. G., Pan, F., Halama, J. J., Pettus, P. B., Phillips, D. L. (2014) "VELMA Version 2.0 – User Manual and Technical Documentation." U.S. Environmental Protection Agency, Office of Research and Development, National Health and Environmental Effects Research Laboratory, Western Ecology Division, Corvallis, Oregon, USA: p. 60.

Mellander, P.E., Stahli, M., Gustafsson, D., and Bishop, K. (2006) "Modelling the effect of low soil temperatures on transpiration by Scots pine", Hydrological Processes., 20, pp. 1929–1944.

Neitsch, S. L., Arnold, J. G., Kiniry, J. R., Williams, J. R. (2011). "Soil and Water Assessment Tool Theoretical Documentation Version 2009." T. W. R. Institute. College Station, Texas, USA, AgriLIFE Research & Extension pp. 32-38.

Oregon Crest to Coast (computer file). (2008). "EPA Oregon Cascade Mountain Crest-to-Coast transect." Available: National Oceanic and Atmospheric Administration https://data.noaa.gov/dataset/oregon-crest-to-coast-environmental-monitoring-transect-dataset, ftp://islay.coas.oregonstate.edu/forestbiomass/mr200/ (June 15th, 2016).

PRISM Climate Group, Oregon State University, www.prism.oregonstate.edu, Accessed 16 Feb 2016.

Reich, P. B., Luo, Y., Bradford, J. B., Poorter, H., Perry, C. H., Oleksyn, J. (2014). "Temperature drives global patterns in forest biomass distribution in leaves, stems, and roots." Proceedings of the National Academy of Sciences, USA 111(38): pp. 13721-13726.

Seidl, R., Rammer, W., Scheller, R. M., Spies, T. A. (2012). "An individual-based process model to simulate landscape-scale forest ecosystem dynamics." Ecological Modelling 231: pp. 87-100.

Tague, C. L., and L. E. Band (2004), "RHESSys: Regional hydro-ecologic simulation system—An object-oriented approach to spatially distributed modeling of carbon, water, and nutrient cycling." Earth Interactions., 8(19), pp. 1–42.

Thornton, P.E., Running, S.W., White, M.A. (1997). "Generating surfaces of daily meteorological variables over large regions of complex terrain." Journal of Hydrology 190: pp. 204-251. http://dx.doi.org/10.1016/S00022-1694(96)03128-9

WED-EPA. (computer file) "Crest-to-Coast Overview." Available: National Oceanic and Atmospheric Administration https://data.noaa.gov/dataset/oregon-crest-to-coast-environmental-monitoring-transect-dataset, https://www.ncei.noaa.gov/data/epa/oc2c/docs/epa-oregon-crest-to-coast_overview_c20160616.pdf (December 21st, 2016).

3.9 Figures

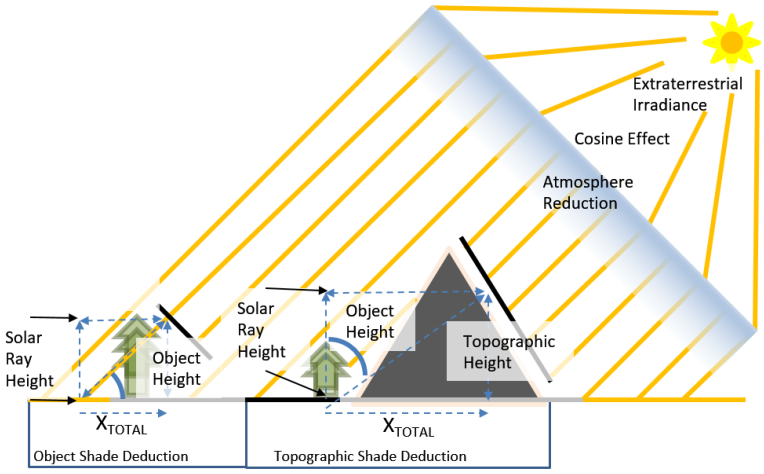

Figure 3-1: Penumbra's uniform solar ray approach to shade modeling.

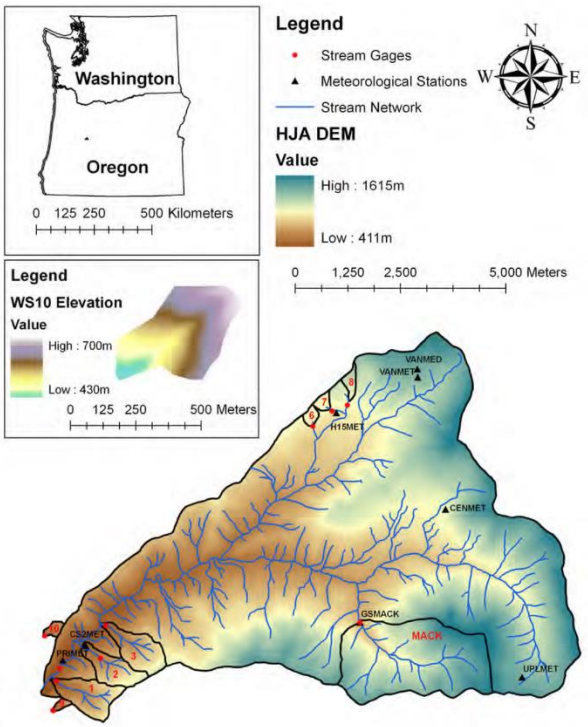

Figure 3-2: H.J.Andrews Experimental Forest Watershed-10 (WS10) site.

WS10 located in the western Cascade Range of Oregon. Image from Abdelnour et al., 2011 paper.

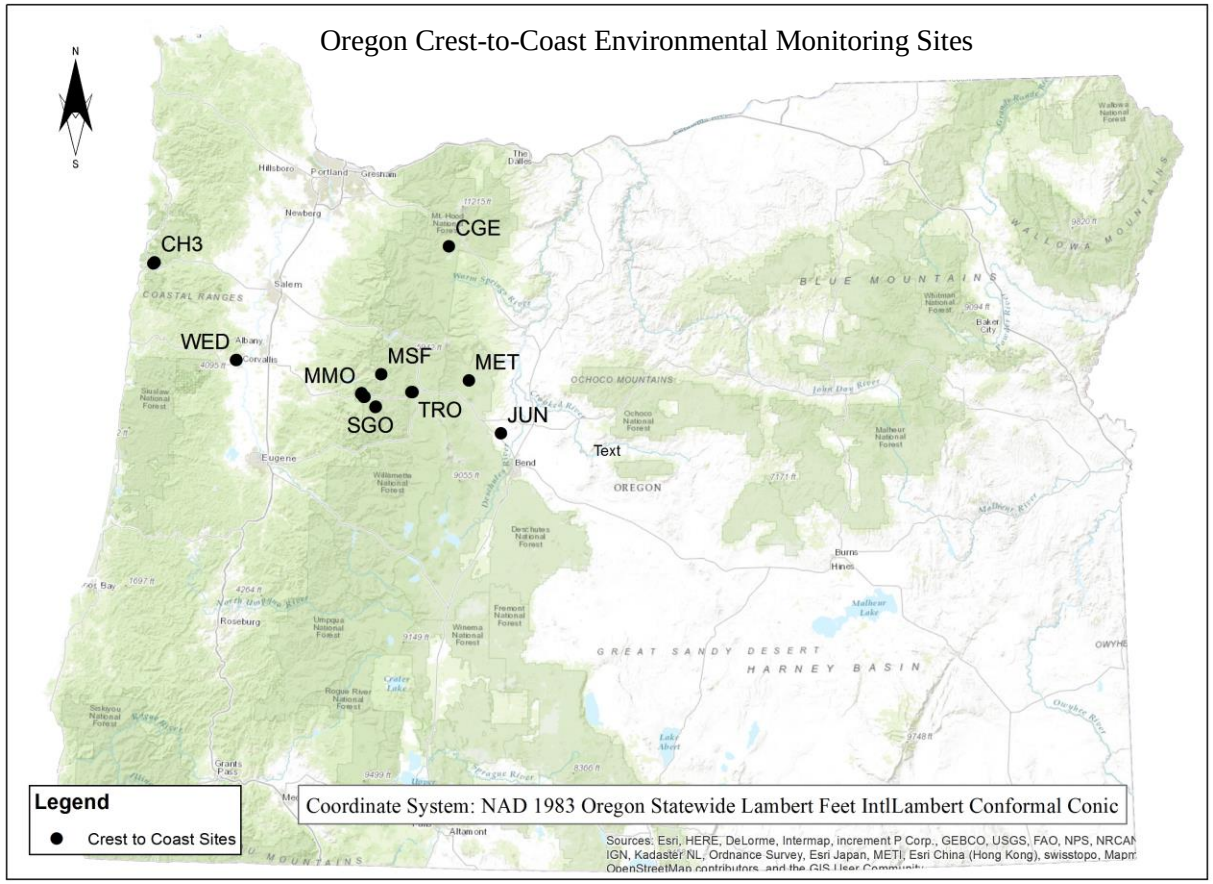

Figure 3-3: Oregon Crest-to-Coast Environmental Monitoring transect site locations.

Simulation r^2 values are calculated using Julian days 101-365. Ignoring the first 100 days prevented the AST model from being penalized for its 100-day phase lag, which only occurs during the first year of simulation. Though VELMA simulates soil moisture, these results were driven from observed soil moisture data.

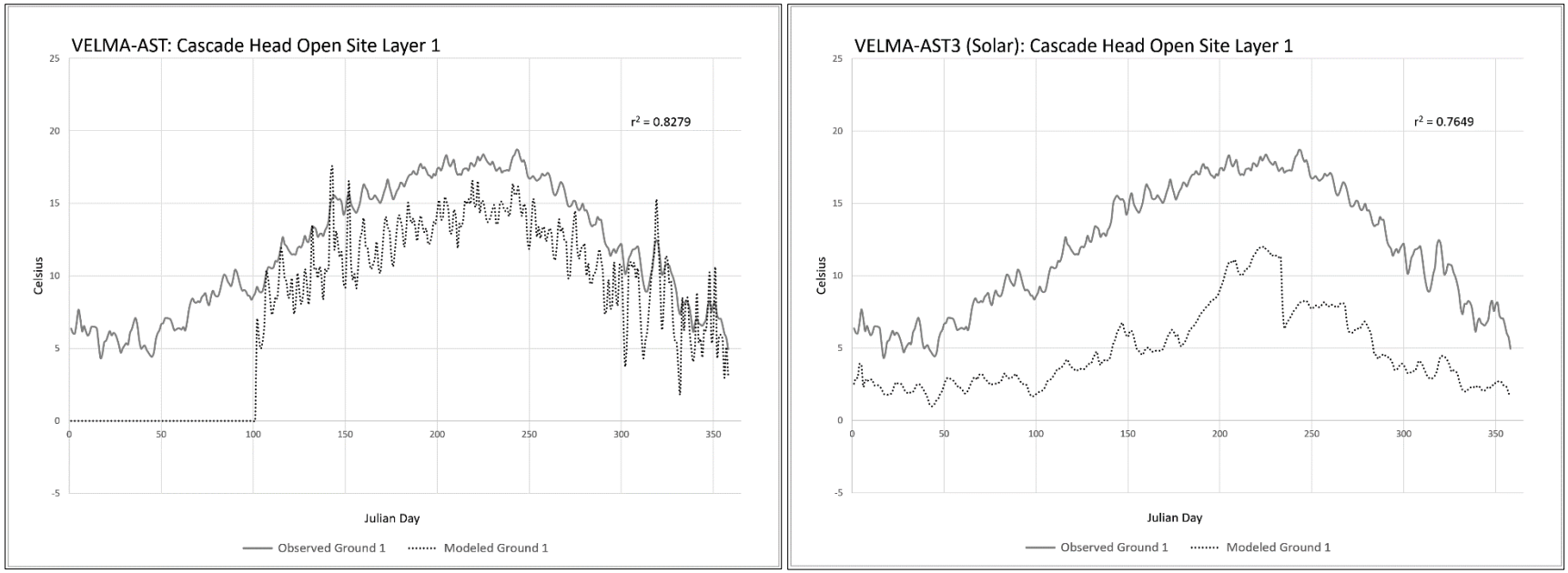

Figure 3-4: Comparison AST and AST3 for Cascade Head Open site soil layer 1.

Simulation r^2 values are calculated using Julian days 101-365. Ignoring the first 100 days prevented the AST model from being penalized for its 100-day phase lag, which only occurs during the first year of simulation. Though VELMA simulates soil moisture, these results were driven from observed soil moisture data.

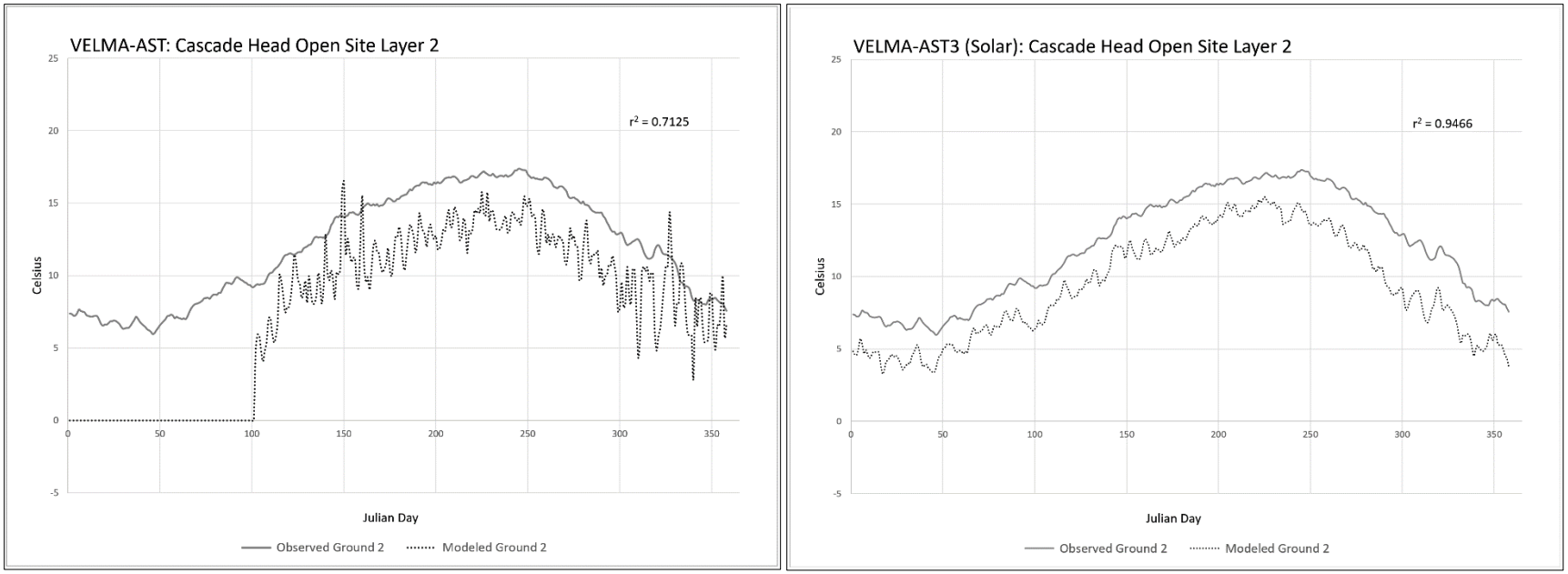

Figure 3-5: Comparison AST and AST3 for Cascade Head Open site soil layer 2.

Simulation r^2 values are calculated using Julian days 101-365. Ignoring the first 100 days prevented the AST model from being penalized for its 100-day phase lag, which only occurs during the first year of simulation. Though VELMA simulates soil moisture, these results were driven from observed soil moisture data.

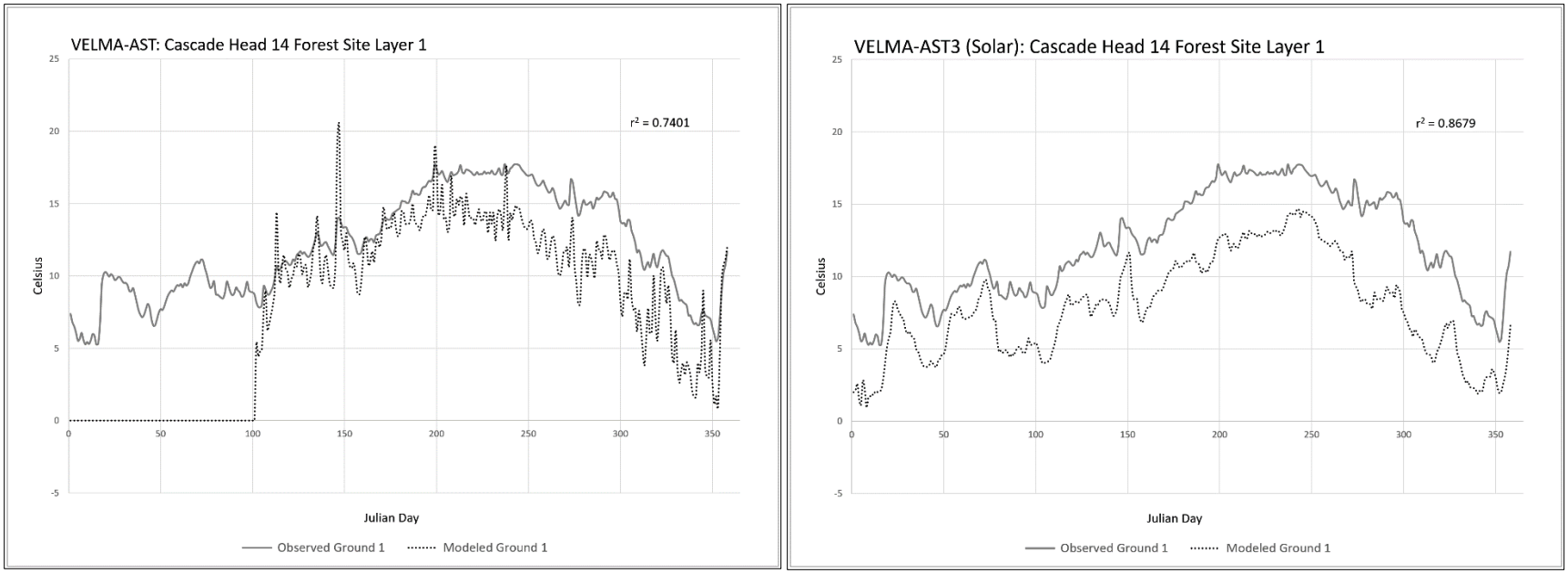

Figure 3-6: Comparison AST and AST3 for Cascade Head 14 Forest site soil layer 1.

Simulation r^2 values are calculated using Julian days 101-365. Ignoring the first 100 days prevented the AST model from being penalized for its 100-day phase lag, which only occurs during the first year of simulation. Though VELMA simulates soil moisture, these results were driven from observed soil moisture data.

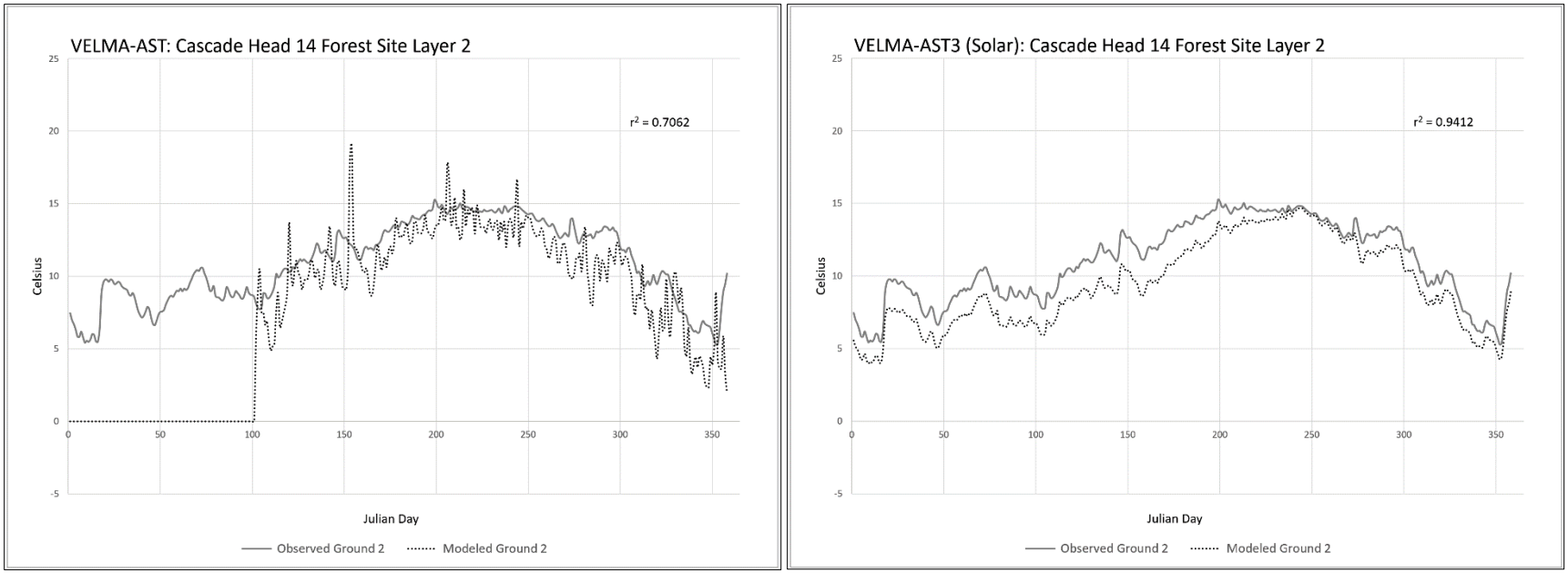

Figure 3-7: Comparison AST and AST3 for Cascade Head 14 Forest site soil layer 2.

Simulation r^2 values are calculated using Julian days 101-365. Ignoring the first 100 days prevented the AST model from being penalized for its 100-day phase lag, which only occurs during the first year of simulation. Though VELMA simulates soil moisture, these results were driven from observed soil moisture data.

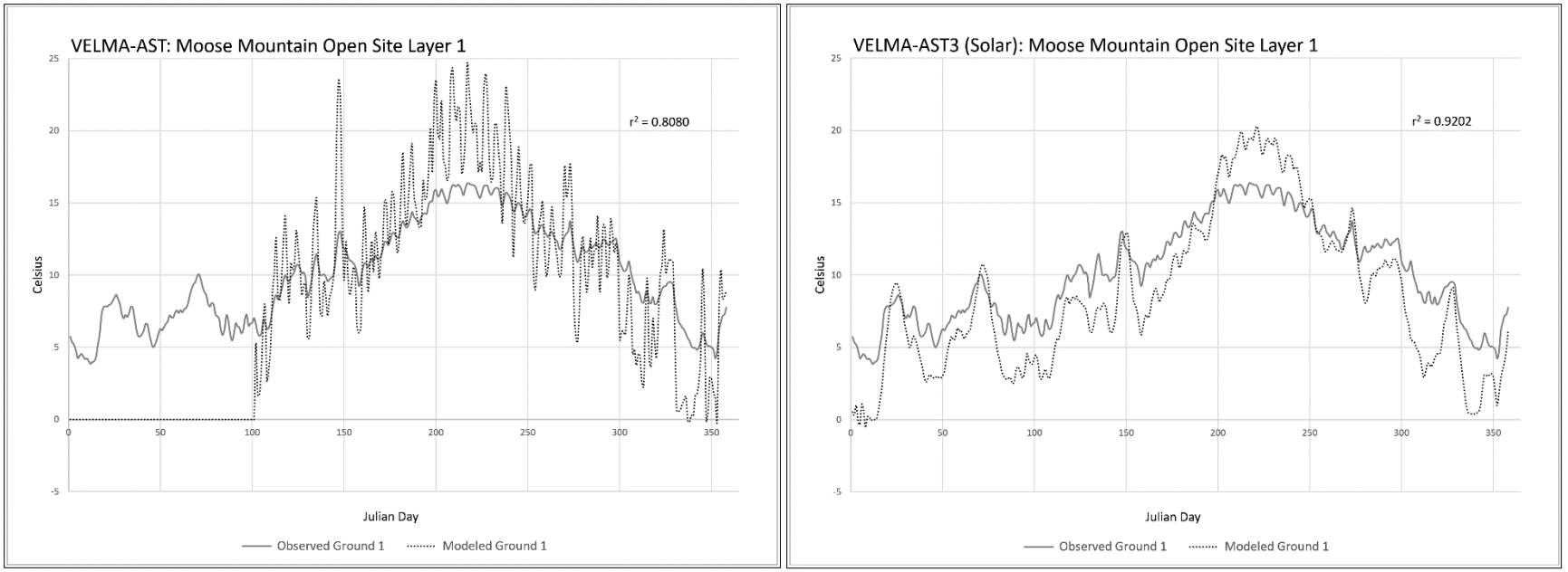

Figure 3-8: Comparison AST and AST3 for Moose Mountain Open site soil layer 1.

Simulation r^2 values are calculated using Julian days 101-365. Ignoring the first 100 days prevented the AST model from being penalized for its 100-day phase lag, which only occurs during the first year of simulation. Though VELMA simulates soil moisture, these results were driven from observed soil moisture data.

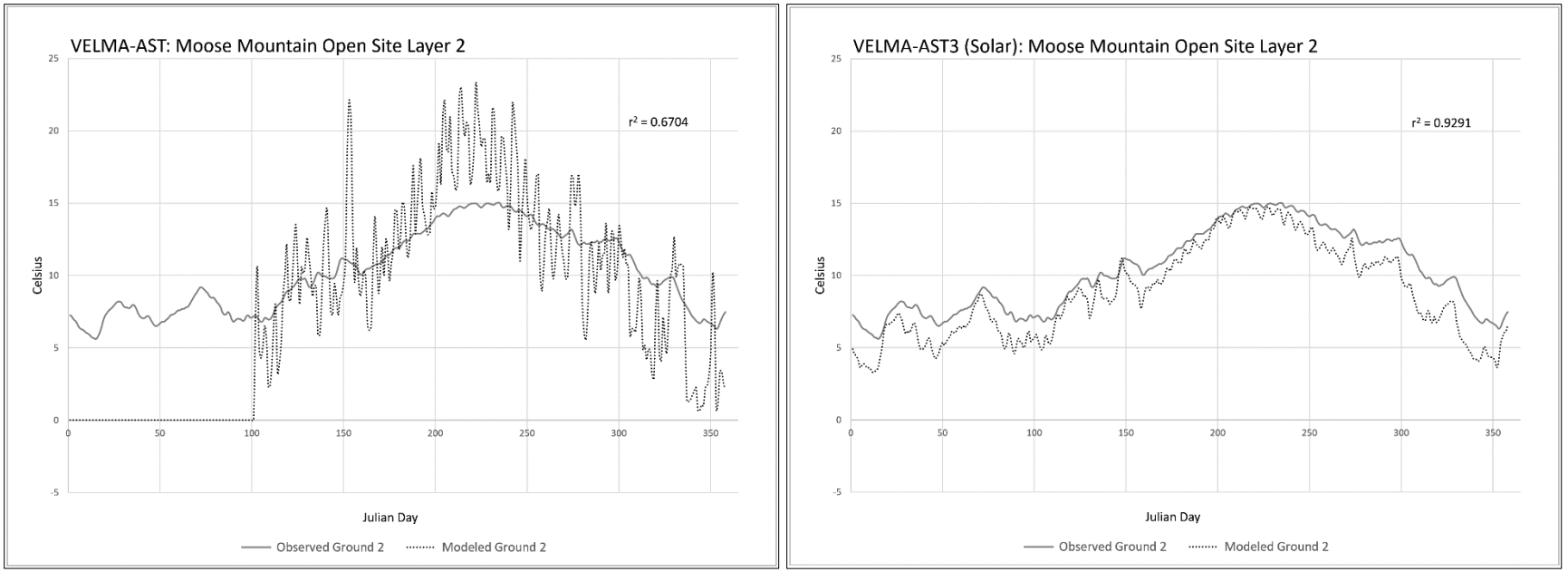

Figure 3-9: Comparison AST and AST3 for Moose Mountain Open site soil layer 2.

Simulation r^2 values are calculated using Julian days 101-365. Ignoring the first 100 days prevented the AST model from being penalized for its 100-day phase lag, which only occurs during the first year of simulation. Though VELMA simulates soil moisture, these results were driven from observed soil moisture data.

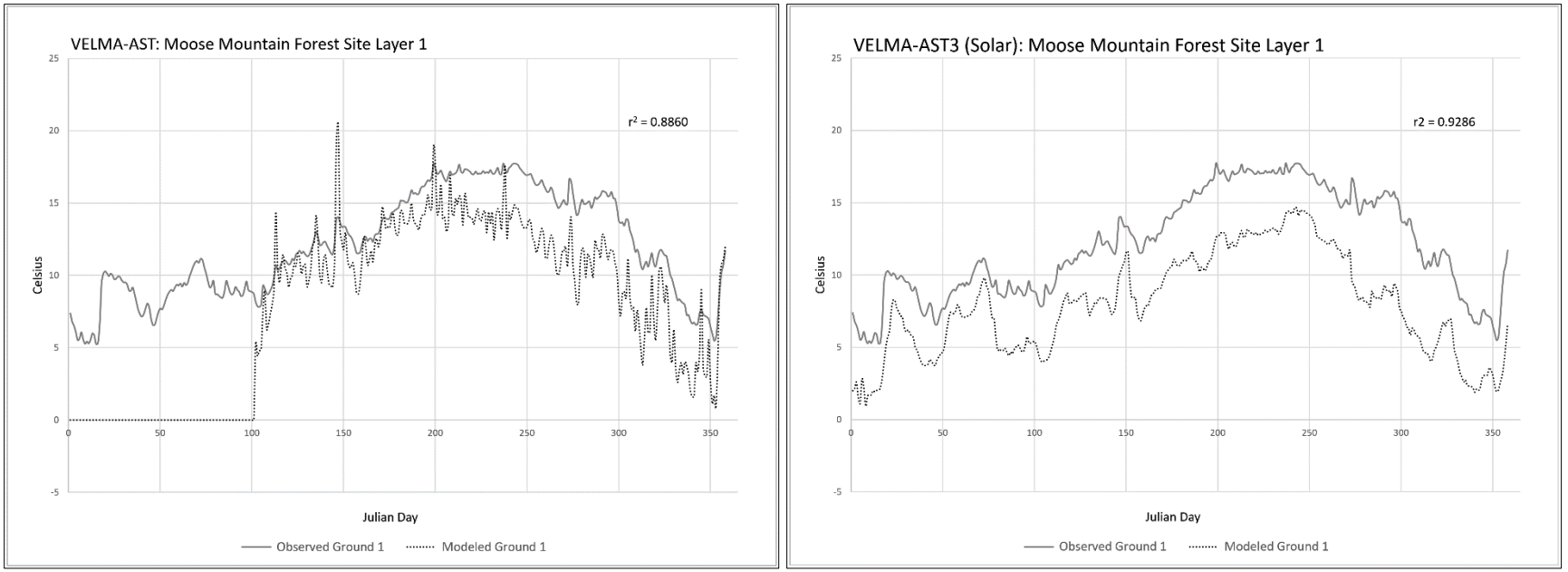

Figure 3-10: Comparison AST and AST3 for Moose Mountain Forest site soil layer 1.

Simulation r^2 values are calculated using Julian days 101-365. Ignoring the first 100 days prevented the AST model from being penalized for its 100-day phase lag, which only occurs during the first year of simulation. Though VELMA simulates soil moisture, these results were driven from observed soil moisture data.

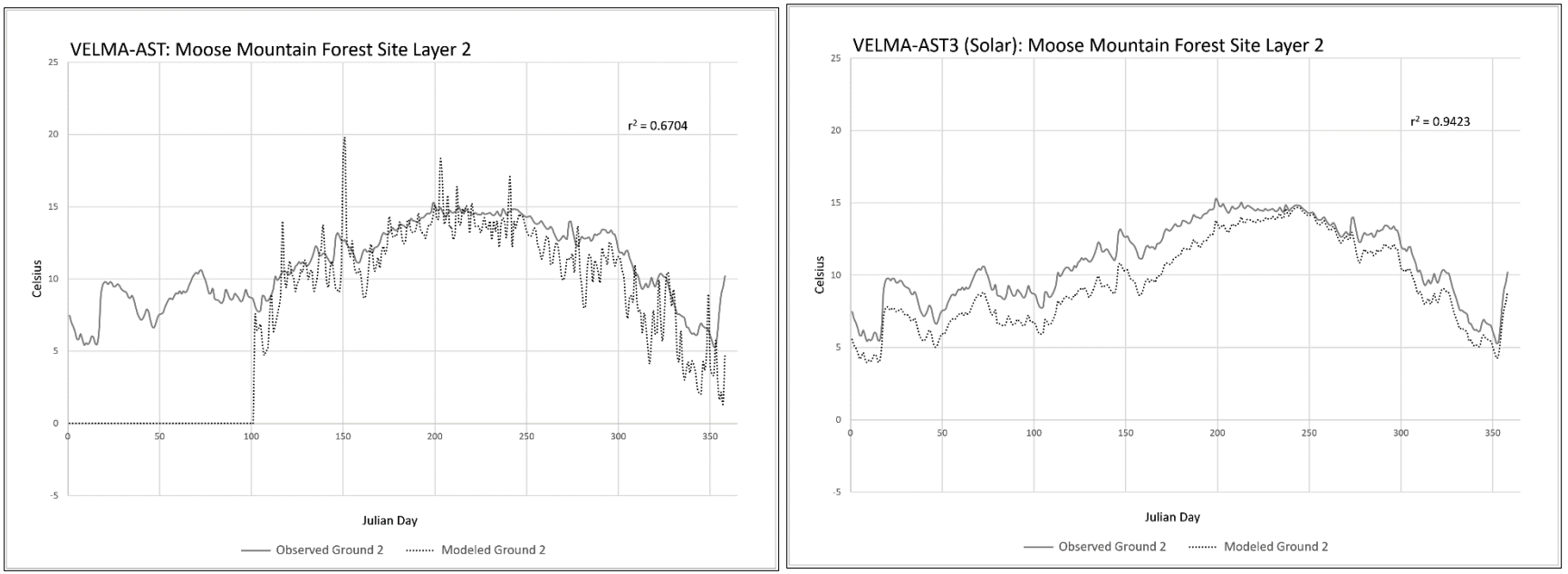

Figure 3-11: Comparison AST and AST3 for Moose Mountain Forest site soil layer 2.

Simulation r^2 values are calculated using Julian days 101-365. Ignoring the first 100 days prevented the AST model from being penalized for its 100-day phase lag, which only occurs during the first year of simulation. Though VELMA simulates soil moisture, these results were driven from observed soil moisture data.

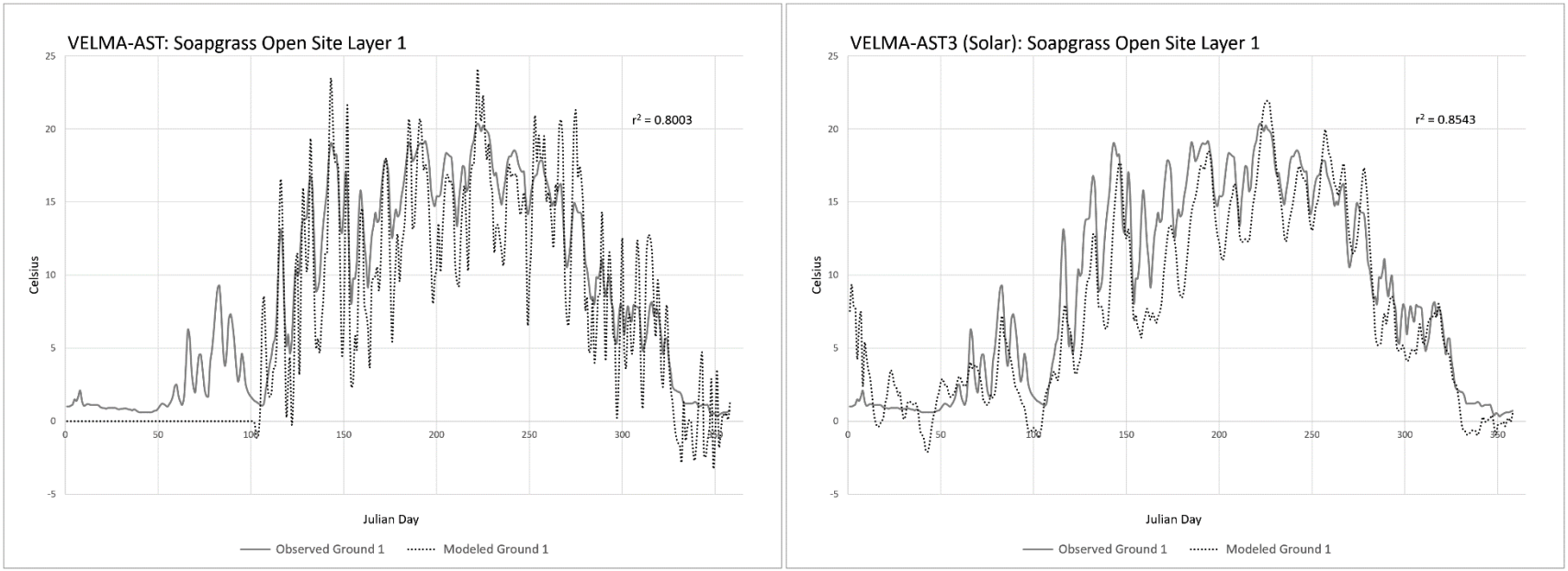

Figure 3-12: Comparison AST and AST3 for Soapgrass Open site soil layer 1.

Simulation r^2 values are calculated using Julian days 101-365. Ignoring the first 100 days prevented the AST model from being penalized for its 100-day phase lag, which only occurs during the first year of simulation. Though VELMA simulates soil moisture, these results were driven from observed soil moisture data.

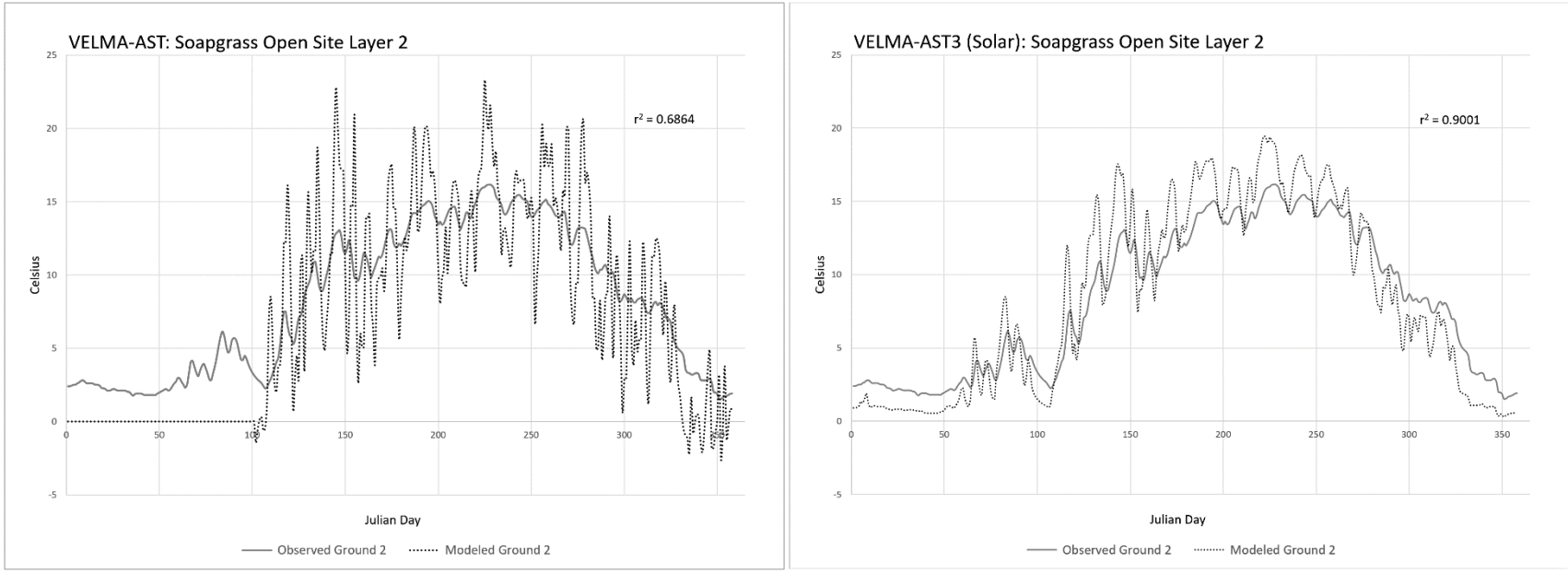

Figure 3-13: Comparison AST and AST3 for Soapgrass Open site soil layer 2.

Simulation r^2 values are calculated using Julian days 101-365. Ignoring the first 100 days prevented the AST model from being penalized for its 100-day phase lag, which only occurs during the first year of simulation. Though VELMA simulates soil moisture, these results were driven from observed soil moisture data.

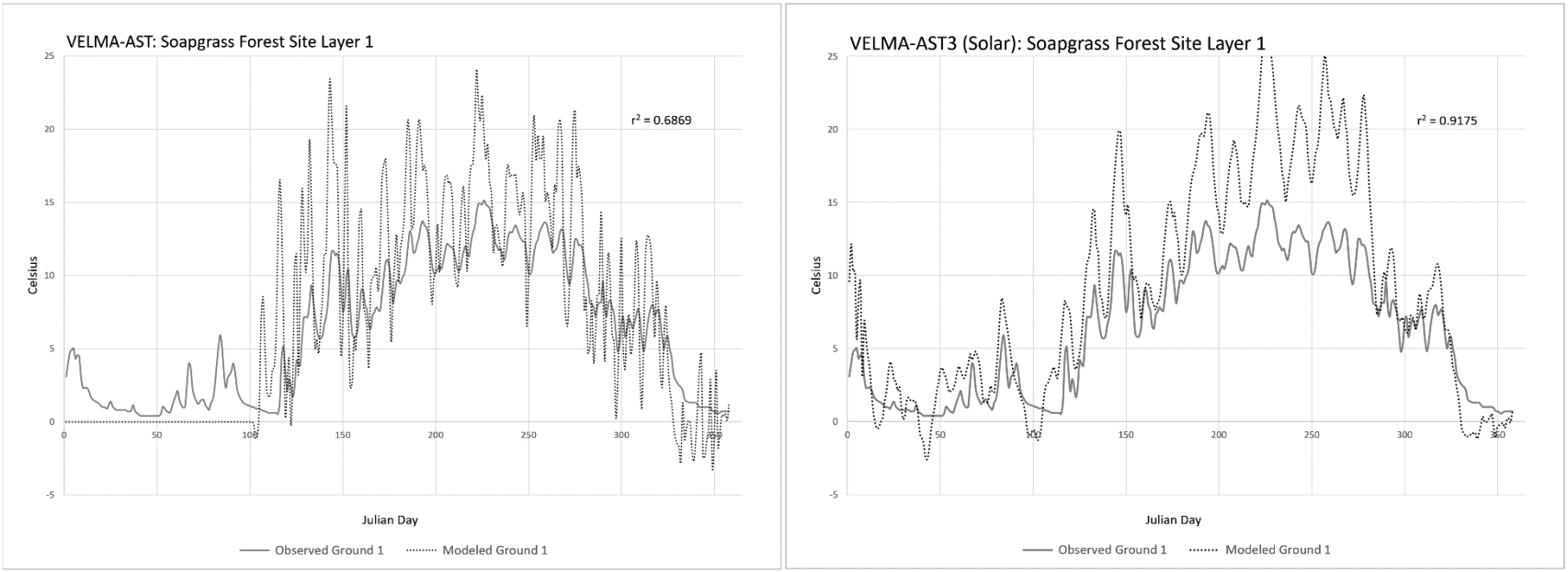

Figure 3-14: Comparison AST and AST3 for Soapgrass Forest site soil layer 1.

Simulation r^2 values are calculated using Julian days 101-365. Ignoring the first 100 days prevented the AST model from being penalized for its 100-day phase lag, which only occurs during the first year of simulation. Though VELMA simulates soil moisture, these results were driven from observed soil moisture data.

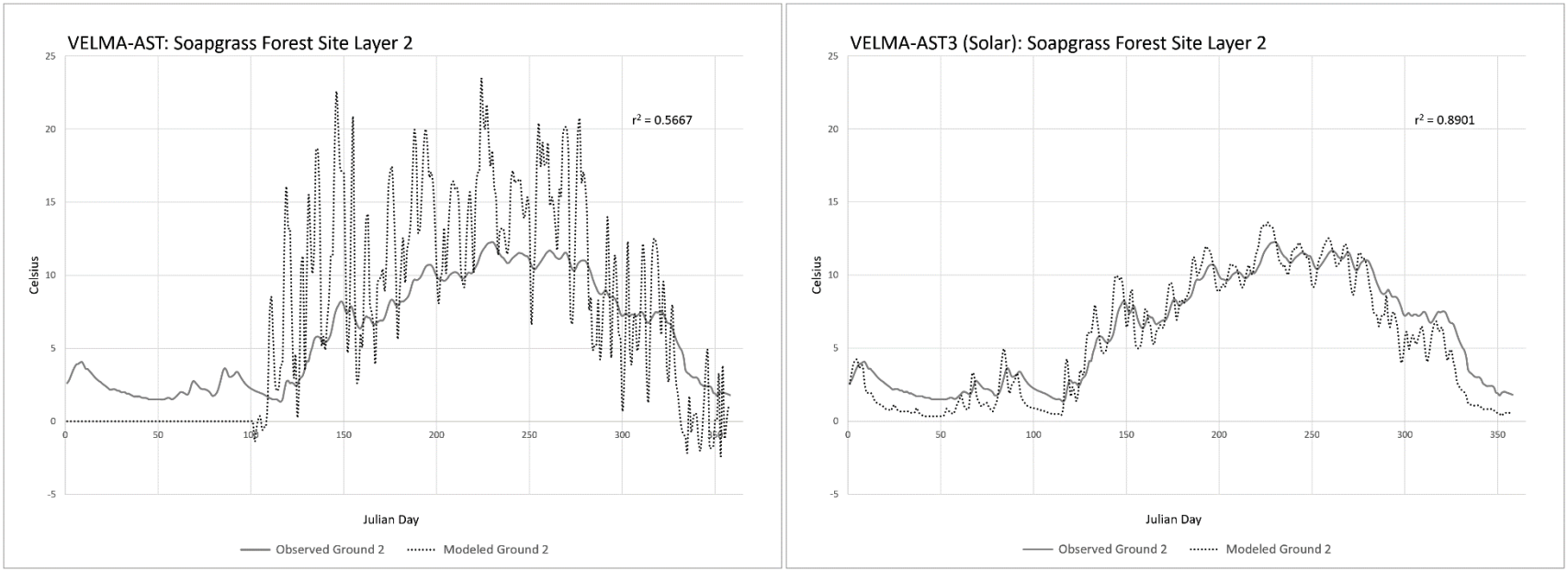

Figure 3-15: Comparison AST and AST3 for Soapgrass Forest site soil layer 2.

Simulation r^2 values are calculated using Julian days 101-365. Ignoring the first 100 days prevented the AST model from being penalized for its 100-day phase lag, which only occurs during the first year of simulation. Though VELMA simulates soil moisture, these results were driven from observed soil moisture data.

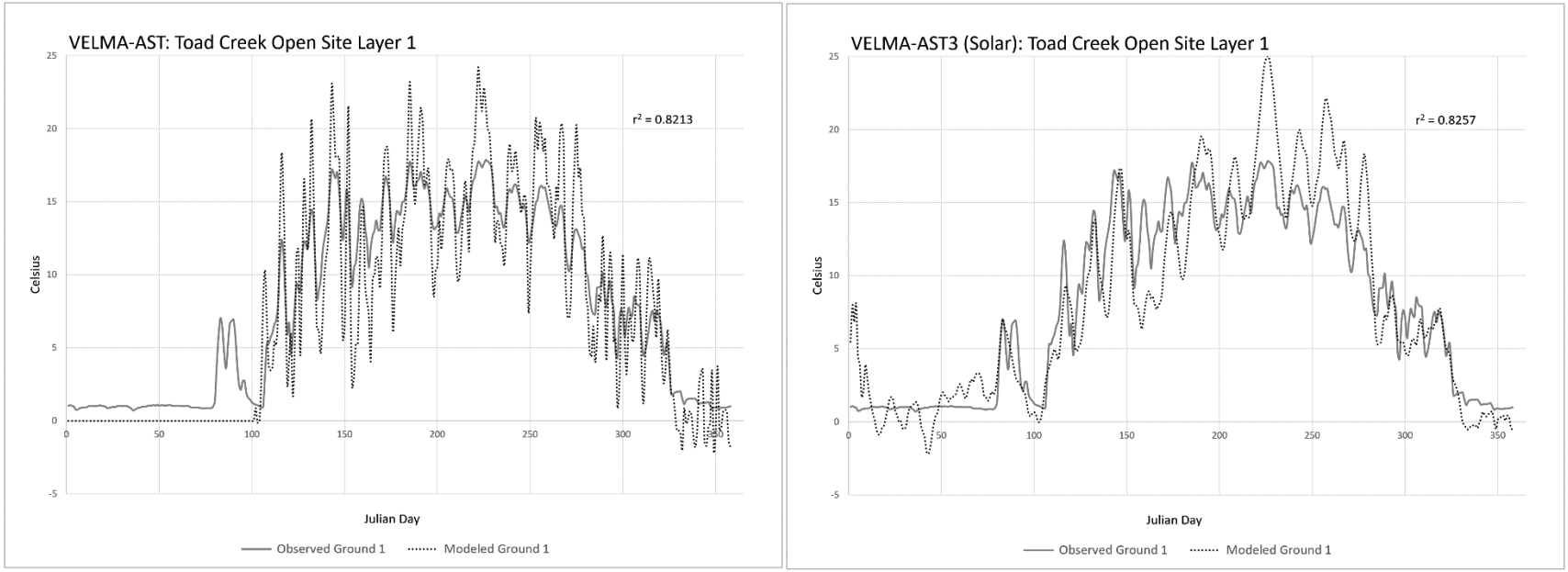

Figure 3-16: Comparison AST and AST3 for Toad Creek Open site soil layer 1.

Simulation r^2 values are calculated using Julian days 101-365. Ignoring the first 100 days prevented the AST model from being penalized for its 100-day phase lag, which only occurs during the first year of simulation. Though VELMA simulates soil moisture, these results were driven from observed soil moisture data.

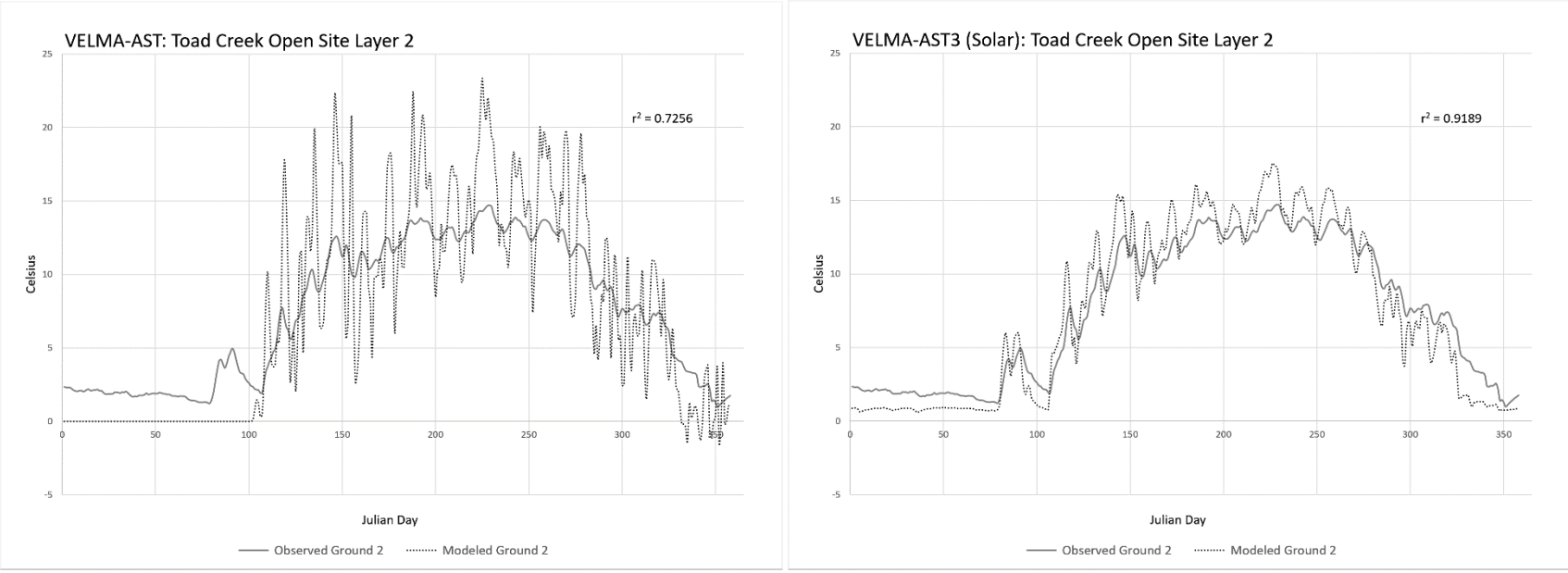

Figure 3-17: Comparison AST and AST3 for Toad Creek Open site soil layer 2.

Simulation r^2 values are calculated using Julian days 101-365. Ignoring the first 100 days prevented the AST model from being penalized for its 100-day phase lag, which only occurs during the first year of simulation. Though VELMA simulates soil moisture, these results were driven from observed soil moisture data.

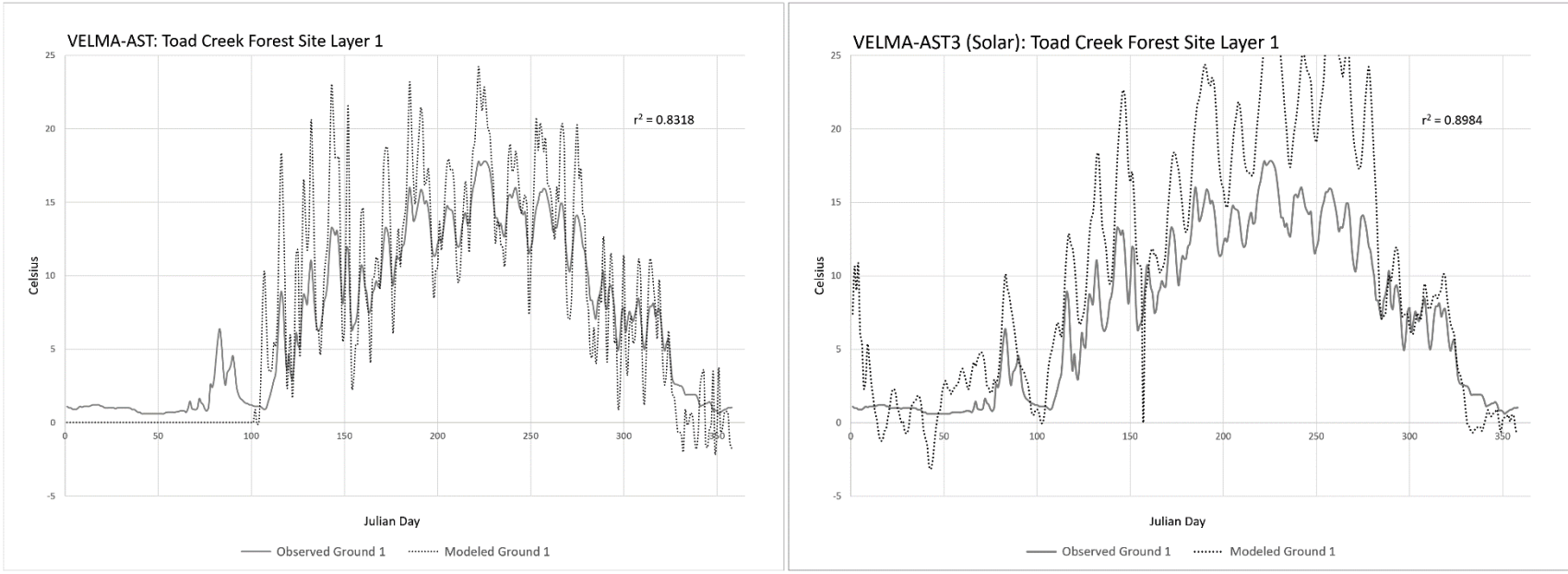

Figure 3-18: Comparison AST and AST3 for Toad Creek Forest site soil layer 1.

Simulation r^2 values are calculated using Julian days 101-365. Ignoring the first 100 days prevented the AST model from being penalized for its 100-day phase lag, which only occurs during the first year of simulation. Though VELMA simulates soil moisture, these results were driven from observed soil moisture data.

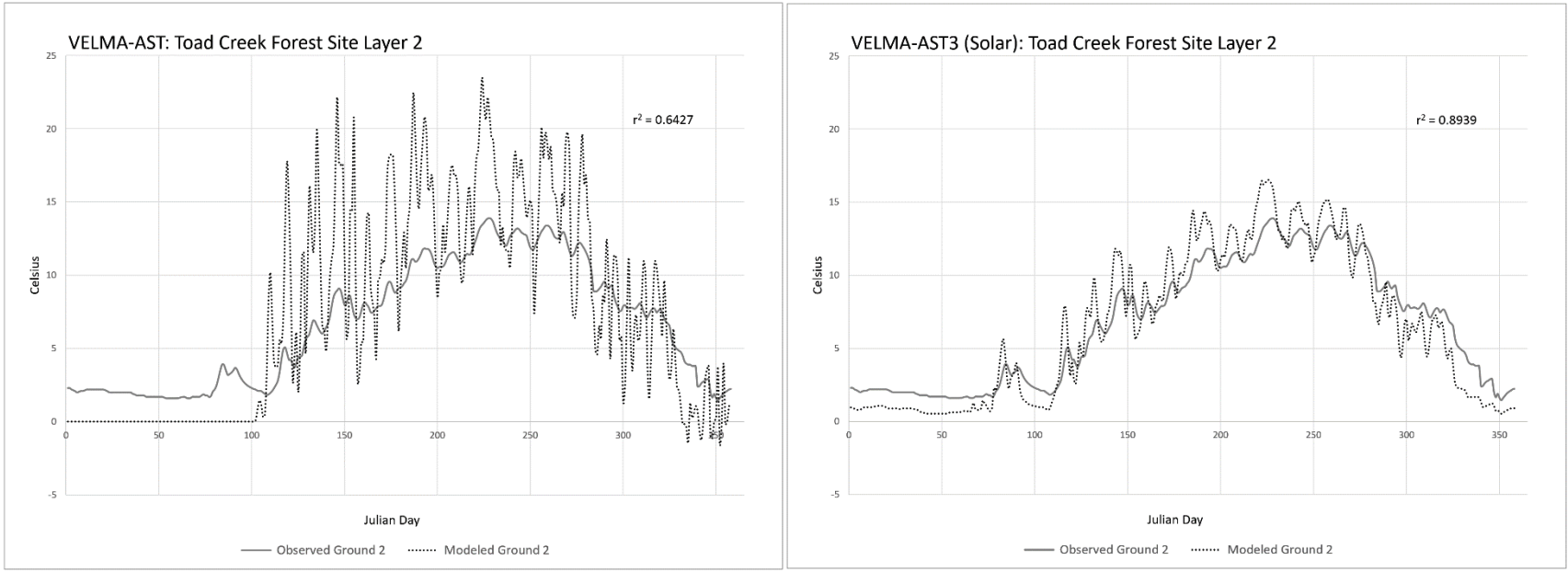

Figure 3-19: Comparison AST and AST3 for Toad Creek Forest site soil layer 2.

Simulation r^2 values are calculated using Julian days 101-365. Ignoring the first 100 days prevented the AST model from being penalized for its 100-day phase lag, which only occurs during the first year of simulation. Though VELMA simulates soil moisture, these results were driven from observed soil moisture data.

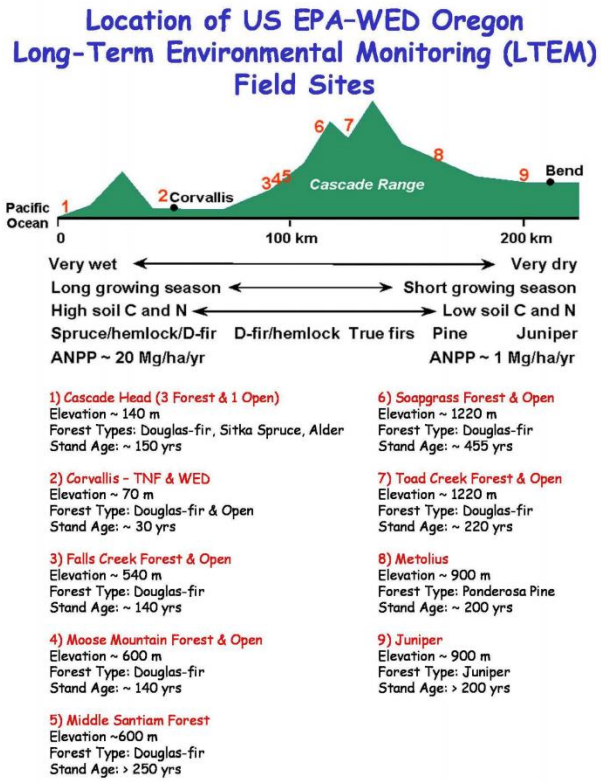

Figure 3-20: Location of field sites along stylized elevation profile, physical and biological characteristics across this transect, and names and major features of the various sites.

Image obtained from Crest-to-Coast Overview (*WED-EPA, 2016*).

3.10 Tables

Table 3-1: VELMA soil temperature sub-model inputs variables.

Variables	Variable Descriptions
$Air_{AVETEMP}$	Fixed Value of 8.2 (Celsius).
LSDepth	Soil column depth to center (mm) per layer of interest.
$LTD_{ACCUMULATION}$	Summation of thermal deltas per layer of interest.
$Soil_{BELOW}$	Soil Layer Below the layer of interest
Soil Moisture	Volume of Soil Moisture (mm/m^2)

Table 3-2: O'CCMoN paired Open and Forest sites.

Site Name	Elevation (meters)	Vegetative State
Cascade Head – Open (CHO)	157	Lawn
Cascade Head – Forest (CH14)	190	Douglas-fir
Moose Mountain – Open (MMO)	668	Clear-cut
Moose Mountain – Forest (MMF)	658	Douglas-fir
Soapgrass – Open (SGO)	1298	Clear-cut
Soapgrass – Forest (SGF)	1190	Douglas-fir
Toad Creek – Open (TCO)	1202	Clear-cut
Toad Creek – Forest (TCF)	1198	Douglas-fir

Table 3-3: VELMA-AST and VELMA-AST3 O'CCMoN results.

O'CCMoN Paired Site Locations	Sites	Soil Layer 1		Soil Layer 2	
		AST (r^2)	AST3 (r^2)	AST (r^2)	AST3 (r^2)
Cascade Head	Open Site (CHO)	0.8279	0.7649	0.7125	0.9466
	Forest Site (CH14)	0.7401	0.8679	0.7062	0.9412
Moose Mountain	Open Site (MMO)	0.8080	0.9202	0.6704	0.9291
	Forest Site (MMF)	0.8860	0.9286	0.6981	0.9423
Soapgrass	Open Site (SGO)	0.8003	0.8543	0.6864	0.9001
	Forest Site (SGF)	0.6869	0.9175	0.5667	0.8901
Toad Creek	Open Site (TCO)	0.8213	0.8257	0.7256	0.9189
	Forest Site (TCF)	0.8318	0.8984	0.6427	0.8939

4. Dynamic landscape irradiance influenced by dynamic forest growth and disturbance

4.1 Abstract

Solar radiation is a significant environmental driver that impacts the quality and resilience of terrestrial and aquatic habitats, yet its spatiotemporal variations are difficult to model accurately at high resolution over large, complex watersheds. Forest disturbance regimes (e.g., fire, harvest) greatly impact the amount of solar radiation that reaches the earth's surface, and while these impacts have been studied extensively at small extents, few studies have accurately modeled these impacts across watershed scales. To model a dynamic representation of solar energy reaching the earth's surface amidst changing land cover, an environmental model must simulate both forest growth and disturbance, along with the interception of light due to these dynamic shifts upon forest landscapes. To accomplish this task, we integrate a landscape-scale ecohydrology model that simulates forest growth and disturbance with a landscape-scale solar energy model that models the ground-level incident solar irradiance resulting from object and topographic shade. This model integration is tested in the Mashel River Watershed, a 20,948-hectare area located west of Mount Rainer Washington, USA, to produce spatially explicit dynamic representations of surface energy radiant flux (Kilowatts/m^2/month) amidst different disturbance (i.e., harvest) regimes, including suspended harvest, historic harvest, and intensified harvest from the years 1990 through 2008. Results demonstrate that this integrated modeling framework is effective at simulating high-resolution representations of surface energy dynamically amidst real and theoretical management scenarios over large and complex watersheds and landscapes.

4.2 Introduction

Policy makers and landscape managers are required to generate management plans that balance a multitude of competing objectives. Some objectives involve habitat suitability, adequate water flow, or maintaining stream temperatures. Yet, policy makers and landscape managers have limited tools to answer complex questions regarding dynamic forest growth and the resulting impact of solar energy upon the landscapes under evaluation. Here the integration of Visualizing Ecosystems for Land Management

Assessment (VELMA; *Abdelnour et al., 2011*) and Penumbra (Chapter 2), two spatiotemporal large-area landscape models, is presented as a method for advancing decision support tool development for watershed modeling.

Solar radiation impacts on terrestrial and aquatic ecosystems have been well described and studied at point location and plot scales within a wide spectrum of environmental science. For example, significant soil moisture and soil temperature differences have been observed along forest and clear-cut boundaries and have been correlated to the spatial distribution of solar irradiance (*Redding, 2003*). The maximum stream temperature of a small stream system was observed to be directly impacted by the positioning the removal of shade (*Johnson, 2003*). Solar radiation has direct and indirect impacts on stream habitats; where latitude and shading conditions at plot level scales have significant impacts on a variety of fish species success of survival (*Caissie, 2006*). Within polar and alpine regions, biota Open Top Chamber studies found that the local solar irradiance was the main environmental driver for snow depth (*Bokhorst, 2013*). At a microscale, increased algal accrual due to the reduction of canopy shading reduced the diversity of an invertebrate community (*Kelly, 2003*).

Despite its importance, solar energy is difficult to model accurately at large watershed scales. Many environmental factors reduce the incident solar energy before reaching Earth's surface, including local and distant topography, canopy vegetation, and clouds (*Trenberth, 2002; Johnson 2003*). At any time, any given location might be affected by all or none of these factors. For ecological modeling the dynamics of solar energy and landscape shadowing present a difficult problem for processes impacted by solar energy. Questions regarding the impact of riparian buffer widths, shifts in forest harvest schedules, or alternative forest harvest patterns rely on accurate representations of ground-level irradiance, but they are ultimately difficult to answer due to the complexity and size of watershed ecosystems.

Accurate spatial representation of irradiance requires sub-daily simulations of solar position combined with the spatial depiction of the dynamic topographic and vegetative shading over time. This level of solar energy modeling is needed due to subtle, yet relentless, shifts to an ecological landscape causing variations to the spatial and temporal

patterns of solar energy. These patterns can accumulate into significant impacts on a landscape at both small and large scale extents over time.

The short-term impact from land coverage alterations or disturbance regimes (e.g., timber harvest, fire, land use change) have been retrospectively studied, but few ecological models possess the ability to represent such land change. Partly this is due to statistical models being favorable due to ease of use. Yet, when observed data is not available to inform statistical models, then process-based models can often provide improved simulated versus observed results (*Yearsley, 2012*). The improved performance can partly be attributed to process-based models being developed from data trends, and grid-based process-based models providing increased spatial heterogeneity (*Yearsley, 2012*). Even fewer ecological models possess the ability to simulate solar irradiance impacts to a landscape due to tree growth or disturbance over decadal timespans. A few candidate models are Hydrologic Simulation Program – Fortran (HSPF; *Bicknell et al., 1997*) and Distributed Hydrology Soil Vegetation Model (DHSVM; *Wigmosta et al., 2002*).

To dynamically simulate surface-level irradiance over large landscapes at daily to decadal timescales amidst alternative forest disturbance regimes, we integrate a landscape-scale ecohydrology model VELMA with a spatially explicit landscape-scale ground-level irradiance model called Penumbra (*Chapter 2*). This model integration will provide a decision support tool for assisting stakeholders to visualize the impacts of alternative management scenarios over watershed landscape scales and over decadal timescales. The model integration creates a dynamic feedback between VELMA and Penumbra. The forest growth and disturbance simulations of VELMA provide input to Penumbra as daily changes to forest height, which then is translated into canopy light transmittance. The resulting product is a dynamic simulation of distributed solar irradiance reaching the earth's surface overall decadal timescales due to the land management policies imparted on the watershed.

Here we describe three Mashel River Watershed forest management regimes that we simulate using the integrated Penumbra-VELMA modeling framework. The baseline scenario is a historic representation of Mashel River Watershed based on LandTrendr

biomass and landscape disturbance. An intensified scenario represents increased forest harvesting, and a suspended scenario represents a halt on all forest disturbances.

4.3 Model Integration

VELMA can dynamically model forest growth in a spatially-distributed (grid-based) manner across large, complex watersheds. VELMA requires inputs of rainfall and temperature across a watershed and mechanistically simulates the movement and spatial distribution of water, nutrients, and biomass at daily time steps. Being spatially explicit (grid-based), VELMA can temporally (i.e., daily) disturb forests with a high level of spatial control. While VELMA includes many sub-models ranging from snow dynamics to the biogeochemical cycling of carbon and nitrogen in multi-layered soils, VELMA lacks a representation of ground-level irradiance that includes shading due to topography and objects.

Penumbra can dynamically model ground-level irradiance by accounting for a watershed's topography, forest canopy structure, and solar position at sub-daily time steps. Penumbra simulates environmental light deductions from incident solar energy at the top of the atmosphere. Solar energy deductions include topographic shading, object shading (e.g., vegetative shading, buildings) and cloud coverage (*Chapter 2*).

Penumbra and VELMA were easily integrated since they shared analogous architectures: both models were developed in the computer language Java and are compatible with Java version 8.1. A depiction of the model integration is shown in Figure 4-1. Both models are grid based and functional at watershed scales. Penumbra was developed as a stand-alone model, yet it also has a Java class that acts an as entry point for external model integration. Integration of Penumbra and VELMA was achieved through a scripting method called Reflection (*Java, 2016*). Within VELMA, Penumbra replaced VELMA's simpler daily homogeneous irradiance sub-model called calSolar.

CalSolar calculated a daily global irradiance value, but applied no shadowing to reduce solar energy to a ground-level net irradiance. Therefore, it did not account for dynamic reductions or increases in irradiance due to tree growth or harvesting, respectively. To improve upon this simplified representation of irradiance, Penumbra

provided VELMA an enhanced spatially-distributed understanding of ground-level irradiance influenced by topography and object shadowing at landscape scales.

The model integration requires cross-model communication during each daily time step. VELMA performs forest biomass growth calculations and disturbances, then makes the Penumbra reflection call. When Penumbra is called, VELMA gives its current aboveground stem (AgStem) biomass and leaf (Leaf) biomass quantities as inputs into Penumbra. Penumbra incorporates the AgStem biomass to update its internal object height array, and Leaf biomass to update its internal light transmittance array (*Chapter 2*). Penumbra's enhanced understanding of daily landscape biomass change allows for sub-daily shifts in landscape shadowing. The dynamic shifts of the landscape occurring within VELMA are reflected as daily shifts in Penumbra's landscape, which then cause Penumbra's simulation of ground-level irradiance to change. Decreased ground-level irradiance occurs due to increases in canopy shadowing from tree growth in height and canopy thickening. Increased ground-level irradiance occurs through the loss of canopy, either through seasonal shifts (senescence) or disturbances such as: forest harvesting, fires, herbivory, or land use change.

Penumbra's aggregated daily irradiance data are sent back to VELMA. This model integration has been shown to be effective at improving VELMA's soil temperature sub-model (*Chapter 3*). In this study, we will show how this model integration can provide dynamic representations of surface-level irradiance at watershed-scales given different management scenarios of forest disturbance associated with intensity levels of forest harvest. The Java call itself is performed through Reflection. Future work will improve other VELMA sub-models including the mechanics of photosynthesis, stream temperature, and snow.

The VELMA model requires an understanding of the state of the landscape at initialization. The VELMA forest biomass state was initialized for 1st January, 1990. The LandTrendr model provided year 1990 biomass data for VELMA to initialize a forest state (*Kennedy et al., 2012*). All spatial input data were at 30-meter resolution.

4.4 Site Description

The Mashel River Watershed is a 20,948-hectare area located west of Mount Rainer within the State of Washington, USA (Figure 4-2). The basin elevation ranges from 200 meters to 1500 meters with slopes up to 52 degrees. 48% percent of aspects face between East and West, while the remaining 52% percent of aspects face between West and East.

4.5 Site Disturbance Scenarios

Three disturbance scenarios are used to test the model integration of VELMA and Penumbra, including a historical harvest, suspended harvest, and intensified harvest. With a mixture of forest activities occurring (growth and harvest), Penumbra dynamically simulated the potential surface-level solar irradiance across a changing Mashel River Watershed.

4.5.1 Historic Harvest

The Mashel River Watershed was selected due to the contrast of management between the minimally harvested state owned lands and moderately to intensively harvested private forest lands (Figure 4-3). The watershed is owned and utilized by several stakeholder groups including the Washington State Department of Natural Resources, the Nisqually Tribe, watershed council, forest timber management groups, private landowners, and the Town of Eatonville. Each stakeholder has deliberate land management goals, which are apparent from viewing the spatial distribution of land ownership and historical management practices (Figures 4-2 and 4-3). These management objectives center around timber production, salmonid recovery, and watershed health indices such as stream temperature and water quality. At watershed scales, the diversity of landowners and alternative land management practices create a spatially complex array of forest disturbance (Figure 4-3). This makes high-resolution, dynamic modeling across large spatial scales extremely important.

To model historical forest disturbance, we utilized LandTrendr forest disturbance data and set up VELMA to accurately simulate these different forest management regimes (*Kennedy et al., 2012*). Data from LandTrendr (Figure 4-3) show that 24.1% of the watershed area was harvested between 1990 and 2008.

4.5.2 Suspended Harvest

The suspended harvest scenario represents a hypothetical landscape where all disturbance is halted at 1990. The VELMA and Penumbra integrated modeling framework was run from 1990-2008 under the assumption that all disturbance is absent during this period. Due to no harvesting occurring, there is no figure to represent the Suspend Harvest.

4.5.3 Intensified Harvest

The intensified harvest scenario represents a hypothetical scenario where a significant increase in landscape disturbance is present between 1990-2008. To achieve this, LandTrendr forest ages between 0-99 years were categorized into five year increments. Each five-year bin was assigned a sequential forest harvest date starting at the year 1990. This resulted in VELMA harvesting any forest area with an age greater than 40 years. This resulted in a 73% increase in areal harvesting (Figure 4-4). LandTrendr forest ages between 100-358 years were categorized into 30 year increments. Each thirty-year bin was assigned a sequential forest harvest date starting at the year 1990. These disturbances increased harvesting an additional 4%.

The intensified harvest scenario is shown in Figure 4. Notice that the complexity in forest age across the landscape is maintained. We specifically chose to maintain this complexity rather than harvest the entire landscape at a single time step. This approach provided a more realistic hypothetical scenario of increased disturbance. Even though this scenario provides a spatially feasible scenario, this scenario does not perfectly match cut patterns seen within this watershed. The added forest cut patterns are less clumped; more intermittent. This forest cut pattern will affect the forest canopy light environment differently than patch cutting where one area of forest is cleared, and another area is undisturbed.

4.6 Watershed Simulations and Results

The Mashel River Watershed was simulated from 1990 through 2008 under three contrasting land-management scenarios described above: historic harvest, suspended harvest, and intensified harvest. All three scenarios started with an equivalent time-zero representation of the year 1990.

4.6.1 Historic Harvest Scenario (1990-2008)

The historic harvest scenario represented actual (LandTrendr-detected) forest change from 1990 through 2008. Though LandTrendr data specify a variety of forest disturbance types (e.g. harvesting, fire, infestation), VELMA treated all disturbances as forest harvest only. This harvest assumption is representative for the Mashel River Watershed between 1990 and 2008 due to the intense forest harvesting that took place in the region over those two decades. VELMA simulated landscape forest biomass dynamics by simulating these historical harvest events, as well as changes in forest biomass associated with daily growth and mortality. Importantly, for Penumbra's object-shading algorithm, simulated changes in forest biomass reflect changes in leaf biomass and tree height at the plot level (30-m). Simulated changes in leaf biomass are particularly dynamic, reflecting significant seasonal changes in forest canopy growth and senescence.

Figure 5 and 6 show the biomass and irradiance simulations at July 19 for years 1990 and 2008. Notice that the patches of disturbance, i.e., low biomass, in the left panels correspond to the patches of high surface-level irradiance shown in the right panels. This demonstrates the expected results that forest disturbance (in this case harvest) removes biomass and tree cover from the landscape and therefore allows more energy to reach the surface.

4.6.2 Suspended Harvest Scenario (1990-2008)

The suspended harvest scenario is a hypothetical simulation scenario where forest harvest is halted in 1990. LandTrendr data provided a realistic 1990 forest biomass state for VELMA to initialize its spatial representation of the forest across the Mashel River Watershed. After January 1990, VELMA simulated forest growth in a hypothetical scenario of no disturbance across the entire watershed. Through the Penumbra-VELMA integration, Penumbra simulated the resulting surface-level irradiance amidst a growing forest with no disturbance across the landscape from 1990-2008. With no clear-cutting, forest fires, or any other forest disturbance, Penumbra dynamically simulated the potential ground-level solar irradiance across an unmanaged Mashel River Watershed.

The resulting biomass, as simulated by VELMA, and the ground-level irradiance, as simulated by Penumbra reveal the shift in watershed solar energy through time (Figure

4-7). This effect is most striking in the movie of the simulation (Appendix). Notice that across the landscape, the forest growth fills in the disturbance patchiness that was seen in the historical simulation. This corresponds to reduced ground-level irradiance modeled by Penumbra. Large biomass values subsequently correspond to large and thick forest cover that reduce the incoming solar radiation.

4.6.3 Intensified Harvest Scenario (1990-2008)

Penumbra dynamically simulated the potential ground-level solar irradiance across an intensely harvested Mashel River Watershed (Figure 4-8), whereby simulated clear-cutting occurred in much of the 30-m cells within the Mashel River Watershed at some point between 1990-2008. As expected, biomass values for this simulation are much less than the biomass values from the historical and suspended harvest scenarios. This reduced biomass leads to less canopy coverage and tree height over the watershed, which in turn allows Penumbra to dynamically represent ground-level irradiance due to intensified forest harvesting. The resulting irradiance values show increased values compared to the historical and suspended harvest scenarios (Figure 4-8).

4.6.4 Aggregated Results

Ground-level spatial irradiance data simulated using Penumbra was obtained as spatially-distributed (grid-based) daily data for all three simulations from 1990 through 2008. This data was spatially and temporally aggregated to total ground-level radiant flux at a monthly time step (Watts/m^2/month) (Figure 4-9).

Comparison of the two decades of aggregated monthly data reveal the gain and loss of ground-level solar energy due to land use activities (Figure 4-9, 4-10). Compared to the Historic Harvest scenario, the Suspended Harvest scenario resulted in (1) a 44.3% decrease in ground level solar energy over two decades, (2) a small decrease of ground-level energy during winter months, (3) and a substantial decrease of ground-level solar energy during summer months with a maximum single month reduction of 43.4% in July 2008. Compared to the Historic Harvest scenario, the Intensified Harvest scenario resulted in (1) a 79.6% increase in total ground-level solar energy over the two decades, (2) a considerable increase in ground-level solar energy during winter months, and (3) a substantial increase of ground-

level solar energy during summer months with a maximum single month increase of 62.5% in June 1998.

4.7 Discussion

By developing an integrated modeling tool using a spatially explicit watershed-scale ecohydrology model and a spatially-distributed ground-level irradiance model, we simulated the effects of three land management scenarios in the Mashel River Watershed on resulting biomass and surface-level irradiance quantities. These scenarios included (1) historic harvest activity replication, (2) suspended forest harvest activity, and (3) intensified forest harvest activity. Two decades of modeled daily solar irradiance and aboveground total carbon show the Penumbra-VELMA integration captures daily dynamic shifts of solar irradiance due to landscape forest growth and disturbance. The Penumbra-VELMA integration has allowed for the dynamic simulation of surface-level irradiance resulting from forest growth and harvest.

Our three theoretical simulations revealed the potential increase and reduction of ground-level solar energy due to altered land management policy. The suspended scenario revealed a maximum single month reduction of 43.4% in July 2008 (Figure 4-9). The total two-decade ground-level solar energy reduction reached 2294.7 Megawatts. The intensified scenario revealed a maximum single month increase of 62.5% in June 1998 (Figure 4-9). The total two-decade ground-level solar energy increase reached 5608.0 Megawatts.

Based on each scenario harvesting pattern, these values trend in a logical direction. But, the Intensified and Suspended scenarios are hypothetical; therefore, not testable. Several sources of error could influence these results. The dynamic interaction between VELMA and Penumbra relies on plot research describing biomass to height relationships. The forest site index of 38 may not be ideal for the Mashel River Watershed (*Means and Sabin, 1989*). Cloud coverage was not utilized by Penumbra during these simulations. Accounting for clouds would reduce total available solar energy seasonally.

These historical and hypothetical forest harvest simulations demonstrate the potential benefit this model integration provides to ecological researchers. Many ecological models could improve their simulation accuracy through the inclusion of spatially-

distributed solar energy. The Penumbra-VELMA integrated model has already proven beneficial to the VELMA soil temperature sub-model (*Chapter 3*). Spatially-distributed irradiance could improve other sub-models simulating: stream temperature, micro and macroinvertebrate habitat, photosynthesis, evapotranspiration, and snow melt.

The integration of Penumbra within VELMA also demonstrates a new decision support tool that allows watershed models to assess habitat suitability, policy impacts, biochemical transport, or the mixed interactions of all aspects (*Guzy et al., 2016*). To our knowledge, these Penumbra-VELMA simulations are the first demonstration of daily to decadal estimates of land-surface solar radiation, across plot to watershed scales, for a topographically and biologically heterogeneous landscape. As such, the integration of Penumbra-VELMA represents a significant advancement toward an enhanced understanding in support of land use planning and management.

4.8 Conclusion

The integration of Penumbra and VELMA provides a theoretical representation of spatially-distributed irradiance where dynamic forest growth and disturbance dynamically affect ground level solar energy estimations. The three Mashel River Watershed scenarios presented the use of this modeling integration effort as a decision support tool aimed at providing the capability of contrasting landscape scale solar energy resulting from contrasting forest management plans. The simulations provide process-level details on solar energy response to forest growth and harvest, which could not feasibly be captured through experimentation or observation. This integration will allow for improved sub-modeling of soil temperature, stream temperature, habitat suitability, photosynthesis, snow dynamics, and any other ecological process where spatially-distributed solar energy has a significant impact on environmental process. As a decision support tool framework, Penumbra-VELMA can provide stakeholders the ability to simulate and understand a variety of landscape management plans prior to implementation of management activities that can take years to decades to come to fruition.

4.9 References

Abdelnour, A., et al., 2011. "Catchment hydrological responses to forest harvest amount and spatial pattern." Water Resources Research 47(9): 1-18.

Bicknell, B.R., Imhoff, J.C., Kittle, J.L., Jr., Donigian, A.S., Jr., and Johanson, R.C., 1997, Hydrological Simulation Program--Fortran: User's manual for version 11: U.S. Environmental Protection Agency, National Exposure Research Laboratory, Athens, Ga., EPA/600/R-97/080, p. 755.

Bokhorst, S., et al., 2013. "Variable temperature effects of Open Top Chambers at polar and alpine sites explained by irradiance and snow depth." Global Change Biology 19(1): 64-74.

Caissie D., 2006. The thermal regime of rivers: a review. Freshwater Biology 51: 1389–1406

Guzy, M. R., C. L. Smith, J. P. Bolte, D. W. Hulse and S. V. Gregory., 2008. Policy research using agent based modeling to assess future impacts of urban expansion into farmlands and forests. Ecology and Society 13(1): 37.

Java Tutorials. “Trail: The Reflection API”. *www.docs.oracle.com/javase/tutorial/reflect*. Oracle, Web. December 20th, 2016.

Johnson, S. L., 2003. "Stream temperature: scaling of observations and issues for modelling." Hydrological Processes 17(2): 497-499

Kelly, D. J., et al., 2003. "Effects of Solar Ultraviolet Radiation on Stream Benthuc Communities: An Intersite Comparison." Ecological Society of America 84(10): 2724-2740.

Kennedy, R.E., Yang, Z., Cohen, W.B., Pfaff, E., Braaten, J. and Nelson, P., 2012. Spatial and temporal patterns of forest disturbance and regrowth within the area of the Northwest Forest Plan. *Remote Sensing of Environment*, *122*, pp.117-133.

Means, J. E. and T. E. Sabin (1989). "Height Growth and Site Index Curves for Douglas fir in the Suislaw National Forest Oregon." Western Journal of Applied Forestry 4(4): 136-142.

Redding, T. E., et al., 2003. "Spatial patterns of soil temperature and moisture across subalpine forest-clearcut edges in the southern interior of British Columbia." Canadian Journal of Soil Science (83): 121–130.

Sun, N., J. Yearsley, N. Voisin, and D.P. Lettenmaier, 2013: A spatially distributed model for the assessment of land use impacts on stream temperature in small urban watersheds, Hydrological Processes.

Trenberth, K. E. (2002). Earths Energy Balance. The National Center for Atmospheric Research. Boulder, Colorado, USA pp. 5-7.

Wigmosta, M.S., B. Nijssen, P. Storck, and D.P. Lettenmaier, 2002: The Distributed Hydrology Soil Vegetation Model, In Mathematical Models of Small Watershed Hydrology and Applications, V.P. Singh, D.K. Frevert, eds., Water Resource Publications, Littleton, CO., p. 7-42.

Yearsley, J., 2012. "A grid-based approach for simulating stream temperature." Water Resources Research 48(3).

4.10 Figures

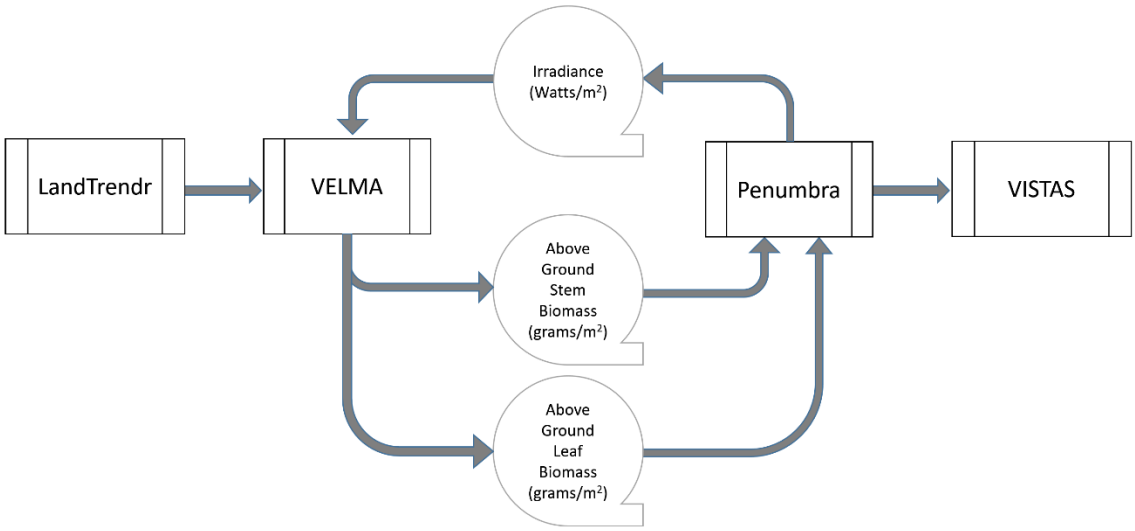

Figure 4-1: Penumbra-VELMA tightly-coupled model integration.

Presented in this research, VELMA initial 1990 biomass and 1990-2008 historic harvest patterns are defined by LandTrendr. Simulation outputs displayed by VISTAS v1.10.

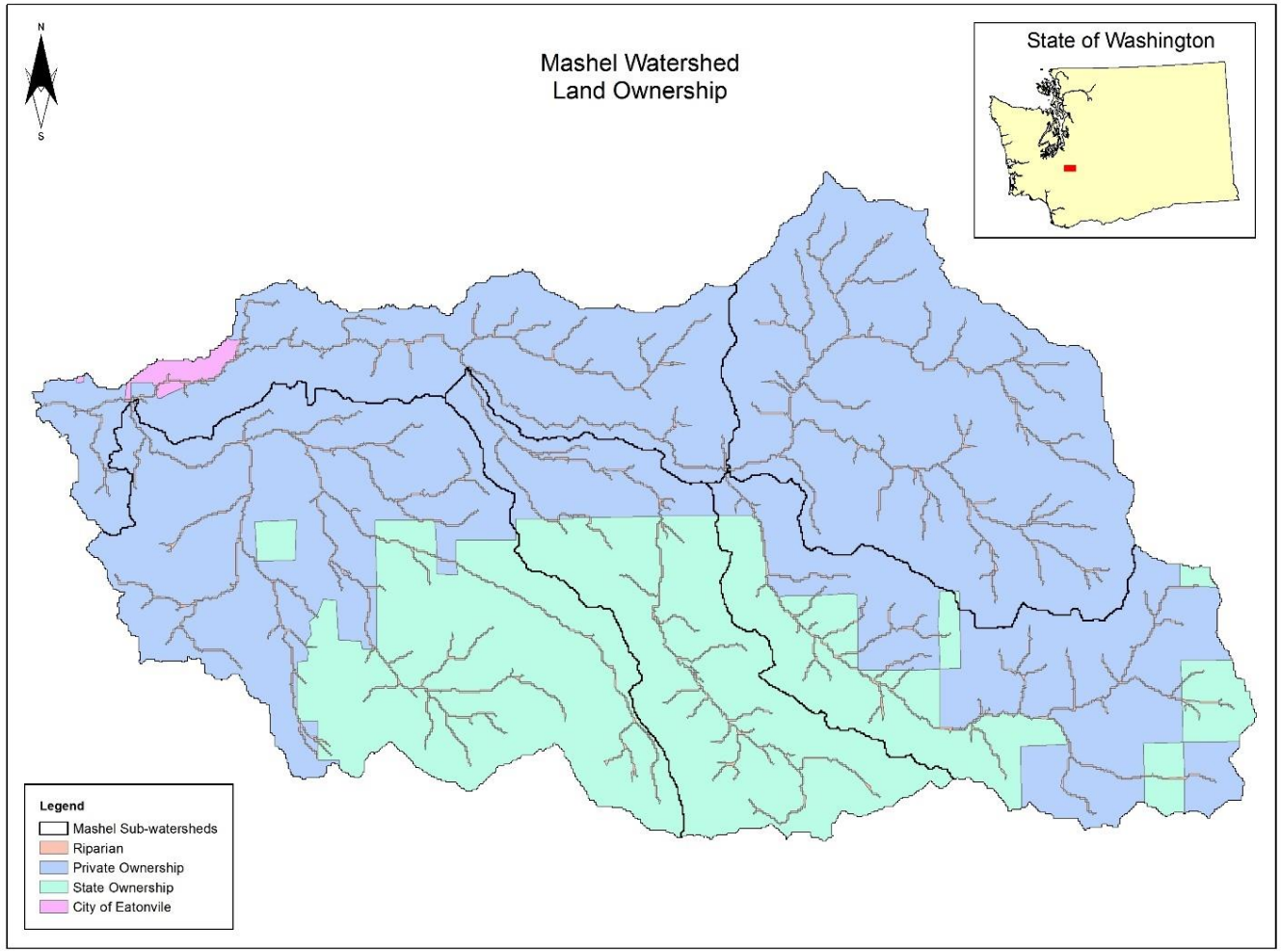

Figure 4-2: Mashel River Watershed land ownership and major sub-watersheds.

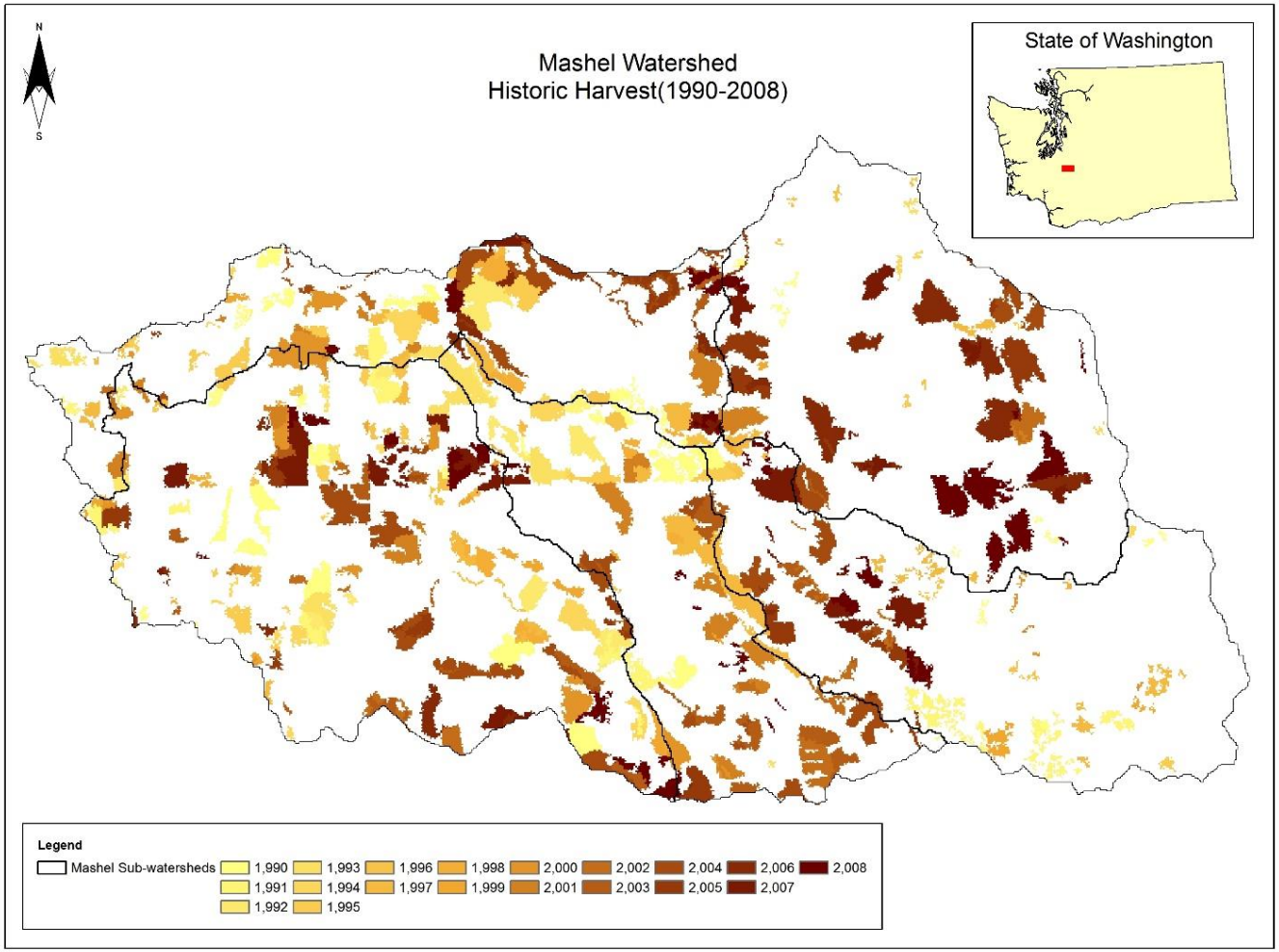

Figure 4-3: Historic forest harvest pattern of the Mashel River Watershed.

Harvest patterns derived from LandTrendr assessment for years 1990 through 2008.

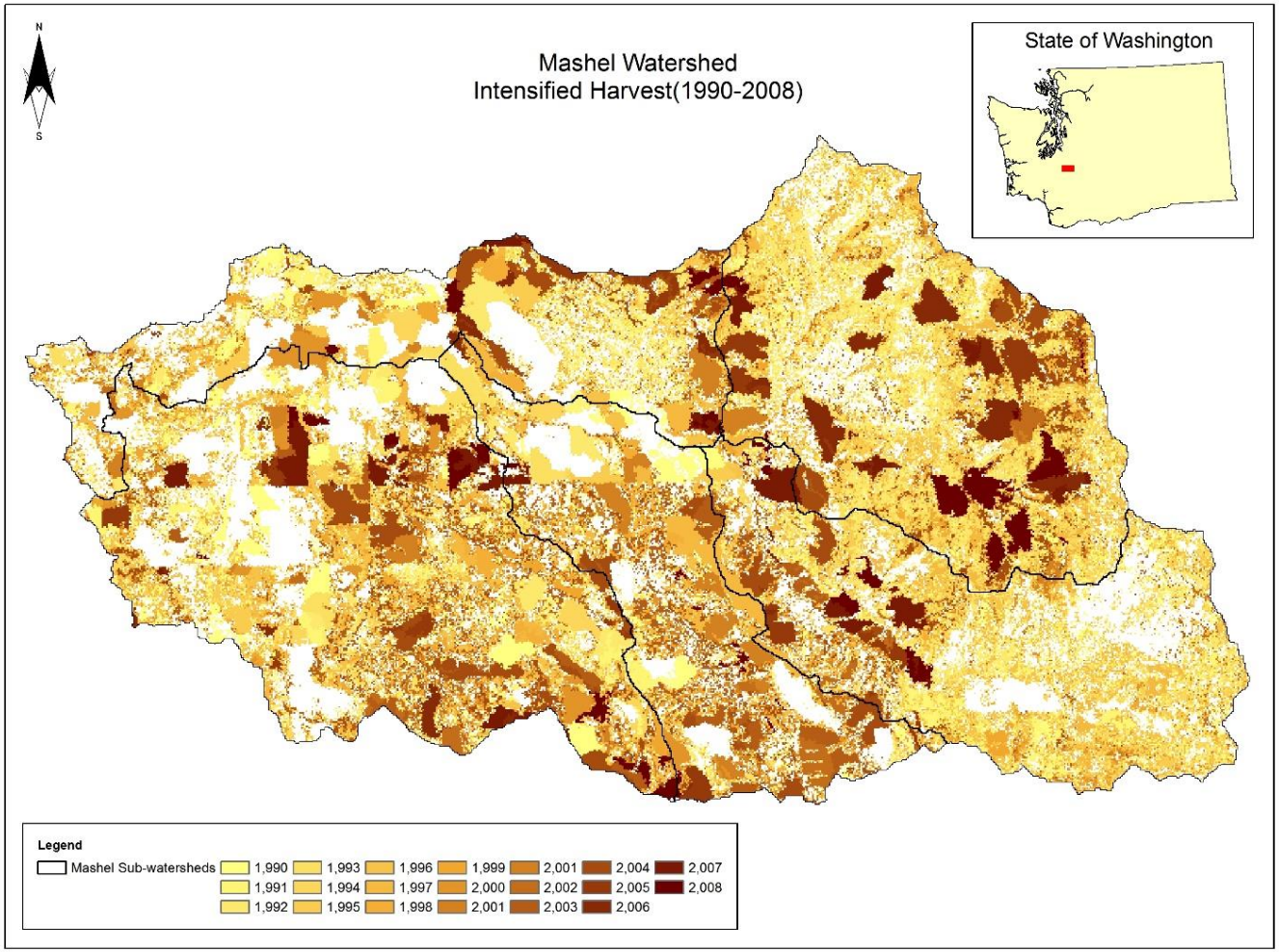

Figure 4-4: Intensified forest harvest pattern of the Mashel River Watershed scenario.

Pattern includes historical (LandTrendr-based) harvests from 1990-2008 plus a 74% percent increase in harvested area during that 19-year period. Areas shown in white were not harvested.

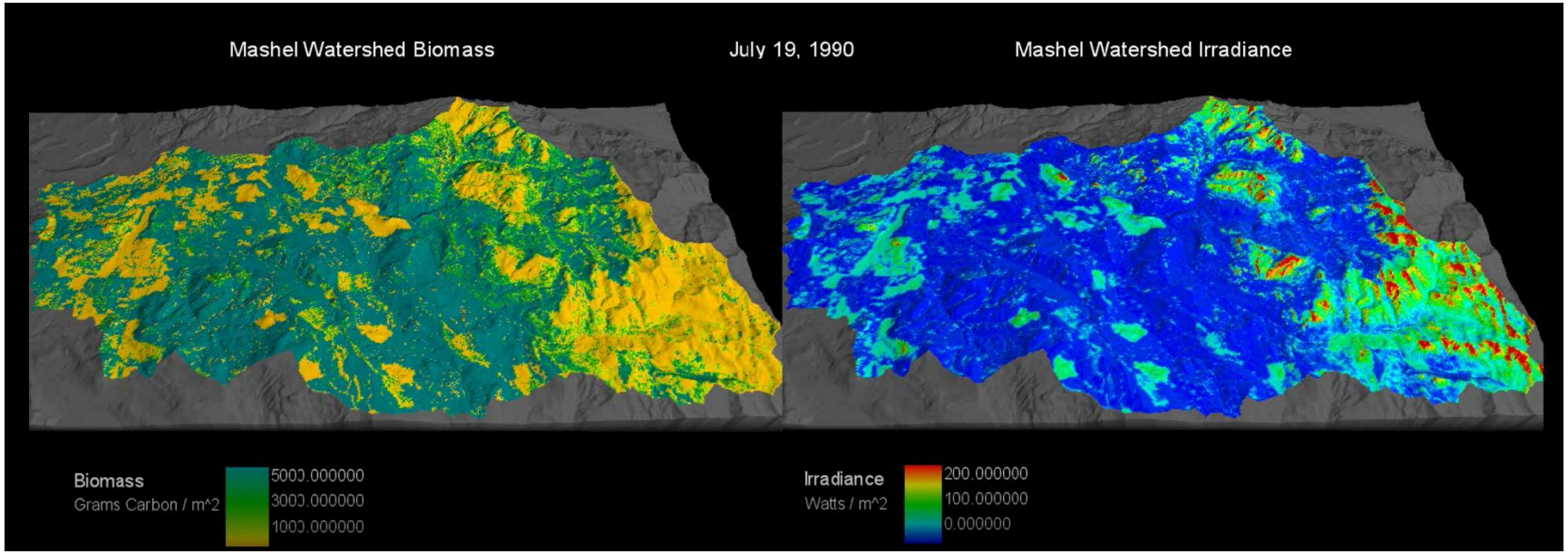

Figure 4-5: Initial 1990 state for the Penumbra-VELMA simulation.

Simulation of Mashel River Watershed on July 19th, 1990: (a) VELMA biomass (grams of carbon/meter^2) historic LandTrendr based biomass, (b) Penumbra simulated daily average ground-level irradiance (Watts/m^2) resulting from VELMA biomass growth at year time step zero.

*Note: biomass scale is restricted to differentiate disturbed low biomass regions from dominant forest regions. True biomass range is from 0 to 48360 grams of carbon/meter^2.

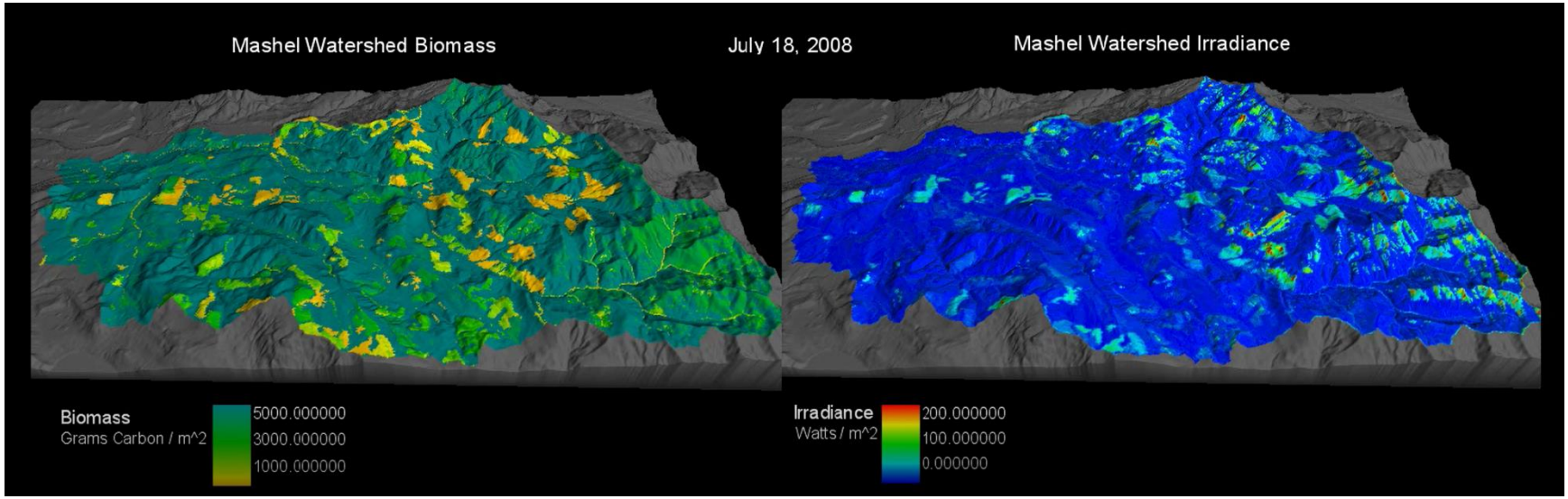

Figure 4-6: Historic scenario static result for the Penumbra-VELMA simulation.

Simulation of Mashel River Watershed on July 19th, 2008 after 19 years of dynamic Penumbra-VELMA interactions: (a) VELMA biomass (grams of carbon/meter^2) due to suspended forest harvesting, (b) Penumbra simulated daily average ground-level irradiance (Watts/m^2) resulting from VELMA biomass growth and suspended harvesting.

*Note: biomass scale is restricted to differentiate disturbed low biomass regions from dominant forest regions. True biomass range is from 0 to 48360 grams of carbon/meter^2.

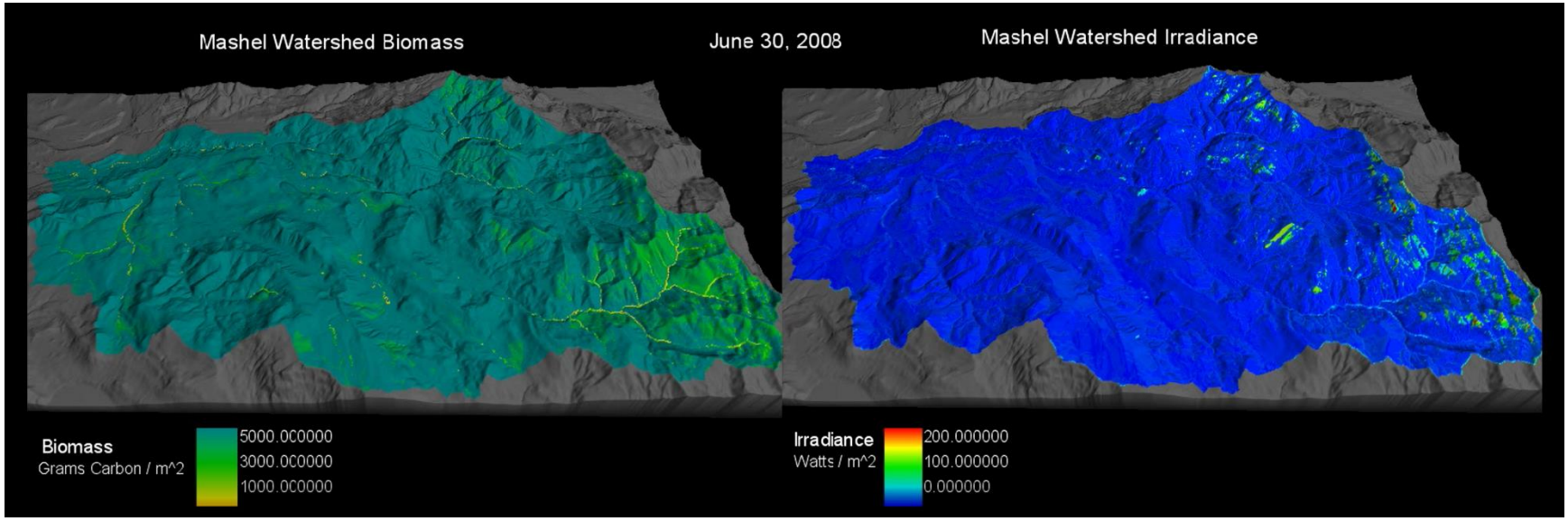

Figure 4-7: Suspended scenario static result for the Penumbra-VELMA simulation.

Simulation of Mashel River Watershed on July 19th, 2008 after 19 years of dynamic Penumbra-VELMA interactions: (a) VELMA biomass (grams of carbon/meter^2) due to suspended forest harvesting, (b) Penumbra simulated daily average ground-level irradiance (Watts/m^2) resulting from VELMA biomass growth and suspended harvesting.

*Note: biomass scale is restricted to differentiate disturbed low biomass regions from dominant forest regions. True biomass range is from 0 to 48360 grams of carbon/meter^2.

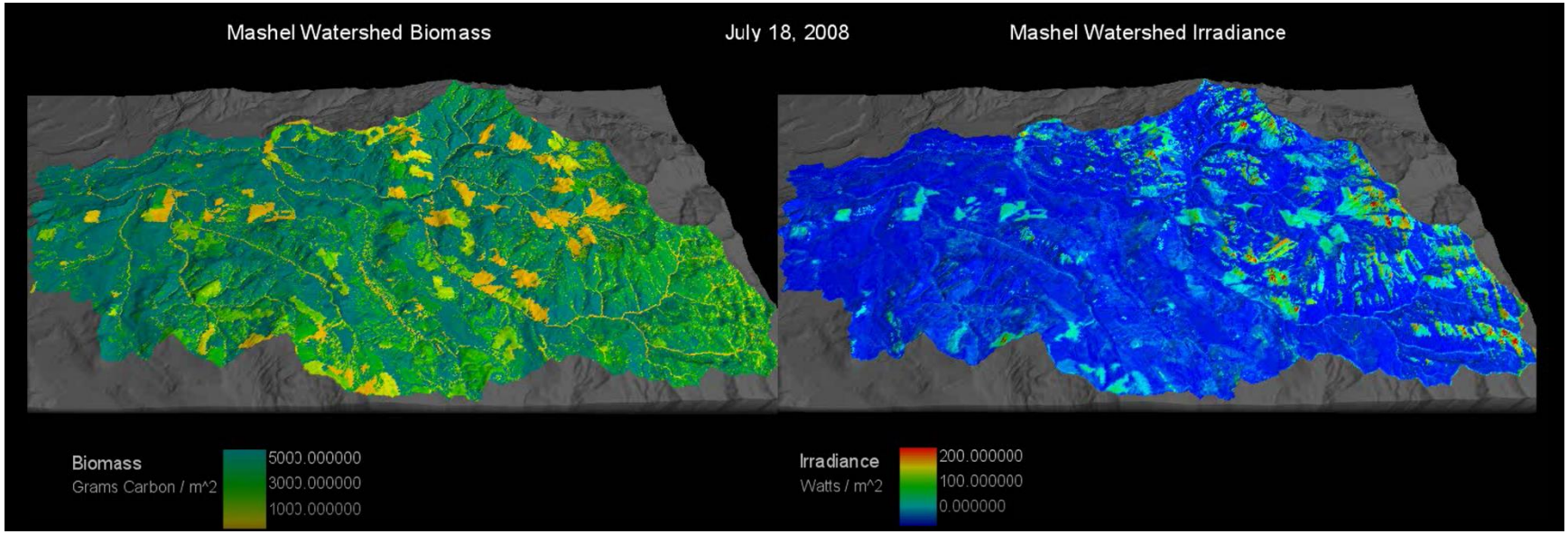

Figure 4-8: Intensified scenario static result for the Penumbra-VELMA simulation.

Simulation of Mashel River Watershed on July 19th, 2008 after 19 years of dynamic Penumbra-VELMA interactions: (a) VELMA biomass (grams of carbon/meter^2) due to intensified forest harvesting, (b) Penumbra simulated daily average ground-level irradiance (Watts/m^2) resulting from VELMA biomass growth and intensified harvesting.

*Note: biomass scale is restricted to differentiate disturbed low biomass regions from dominant forest regions. True biomass range is from 0 to 48360 grams of carbon/meter^2.

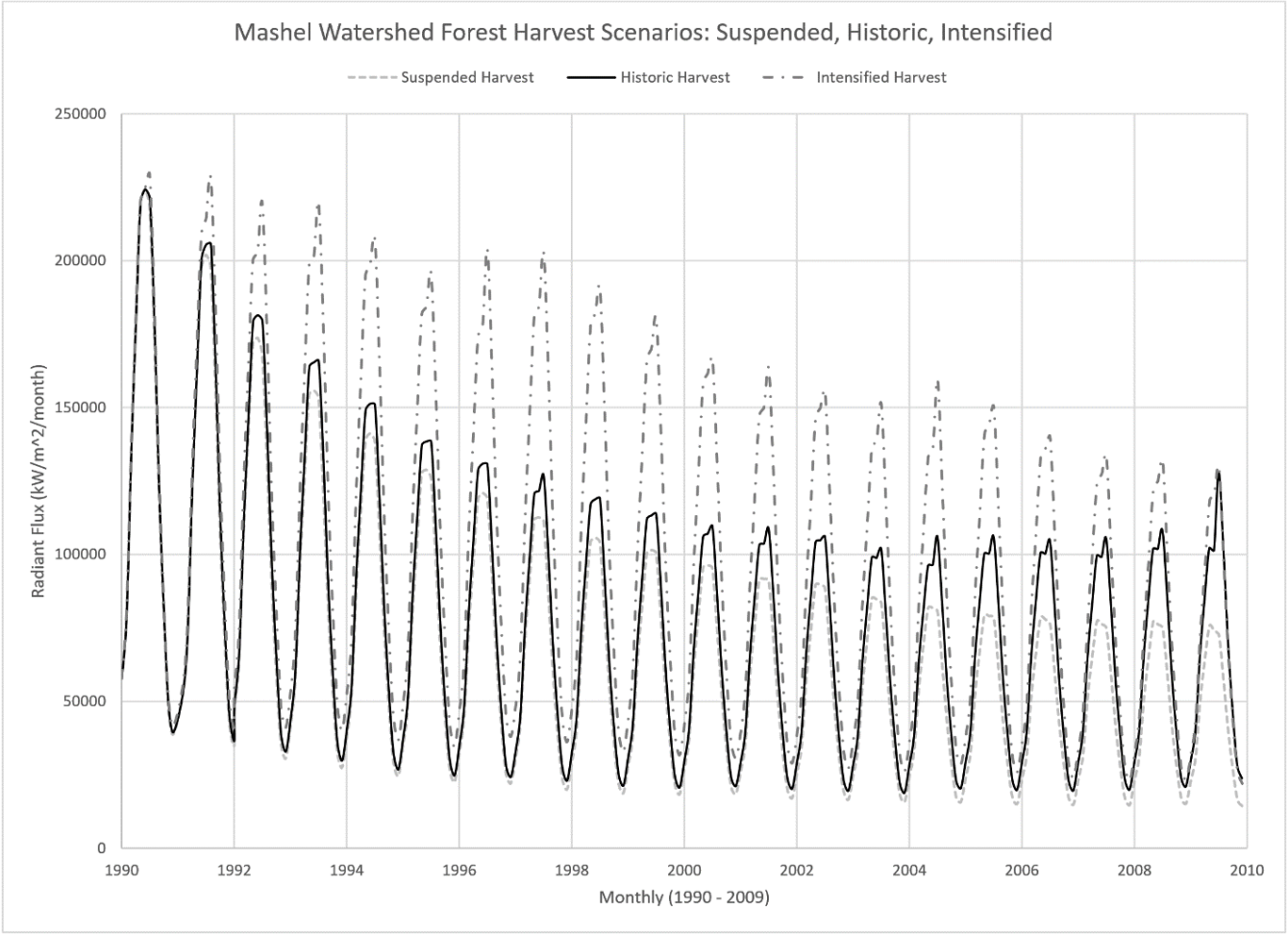

Figure 4-9: Spatially summed and daily to monthly aggregated results.

Daily ground-irradiance results spatially summed and aggregated to monthly values for the Mashel River Watershed from 1990 through 2008.

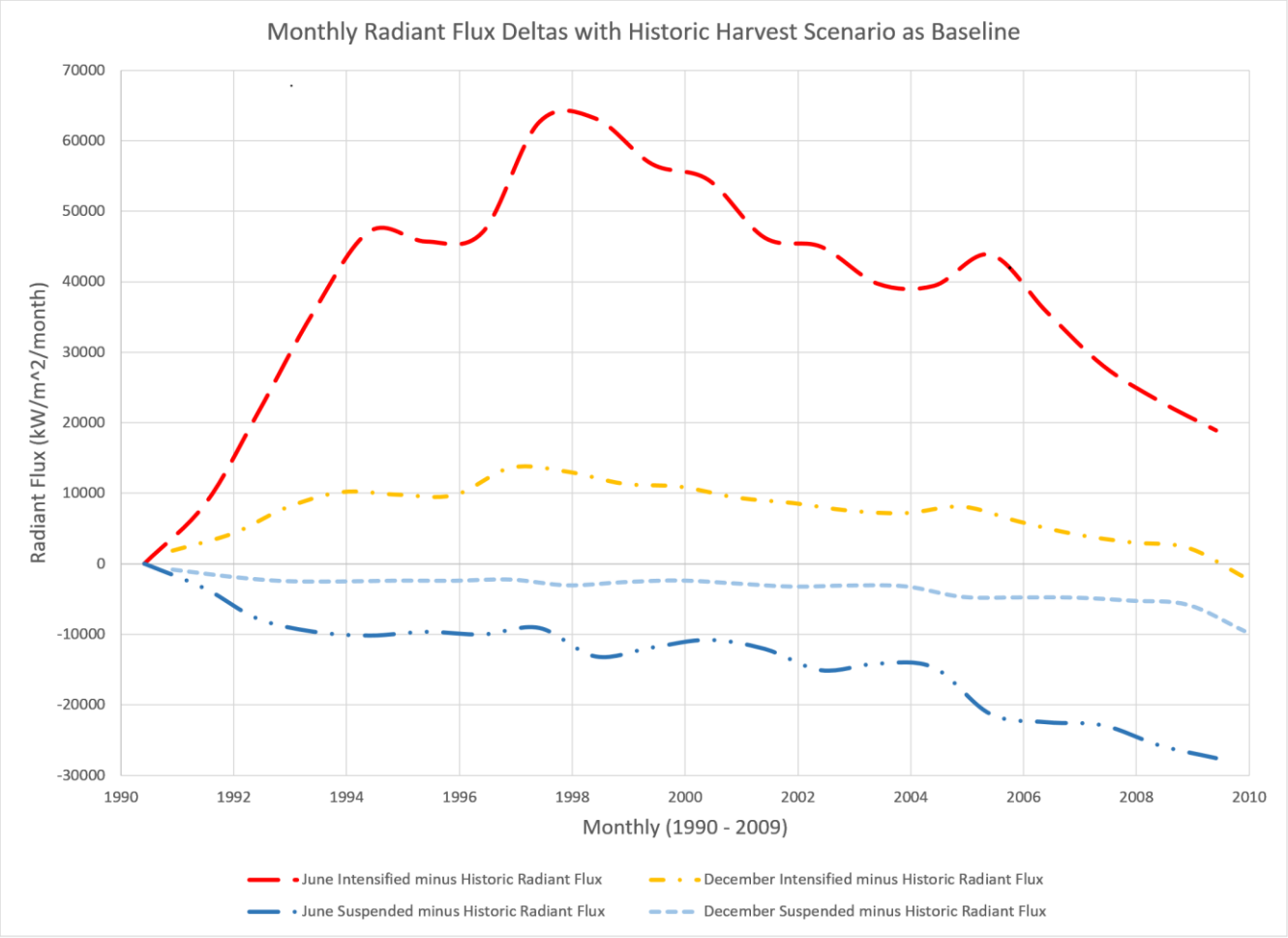

Figure 4-10: Monthly aggregated irradiance deltas for scenarios minus historic.

Mashel River Watershed monthly aggregated Penumbra irradiance deltas: Intensified minus Historic, and Suspended minus Historic.

4.12 Appendix

1. Mashel_HistoricHarvest_Summer_Day.wmv
2. Mashel_NoHarvest_Summer_Day.wmv
3. Mashel_IntensifiedHarvest_Summer_Day.wmv

5. Conclusion

The work presented here advances watershed scale ecological modeling in several ways. First, this work developed a new solar energy model called Penumbra. Penumbra was the blending of several solar energy modeling approaches to reach a compromised approach. This approach balances the complexity of ray tracing techniques with simplistic site knowledge techniques. Second, Penumbra was utilized to improve an existing ecological modeling methods soil temperature estimations. This soil temperature work not only improved the soil temperature estimate accuracies, but also provided realistic spatially-distributed soil temperature values. Third, Penumbra was integrated into VELMA, an ecohydrology model. As a proof of concept, this integration of models expands the possibilities in watershed scale ecological modeling. The dynamic interaction between VELMA's biomass estimations and Penumbra's irradiance estimations will allow for an array of advancements regarding watershed scale predictive modeling.

Penumbra as a stand-alone modeling tool can provide stakeholders the ability to simulate and understand their landscapes diverse solar energy interactions. These interactions can be simulated for topographic and object shadowing separately or combined. Penumbra possesses flexible temporal time stepping that allows users to model solar energy at fine temporal grains, but solar data can also be aggregated to any time step up to full days. These flexible temporal runtime parameters set the model apart from other solar energy modeling methods. Users can simulate their landscapes solar energy impacts at temporal scales matching their research goals. Penumbra was vetted against several different observed solar energy data sources. These results reveal Penumbra's abilities while providing users an understanding of potential simulation uncertainties.

Penumbra integrated into other ecological models can advance those models simulation accuracy and capabilities. Solar energy directly or indirectly impacts nearly all ecological processes. Many of these processes are spatially-distributed; therefore, spatially-distributed solar energy data are needed to accurately represent such processes. The increase in accuracy due to spatially-distributed solar energy was shown with the improvement of VELMA's soil temperature modeling approach. For VELMA, this integration will allow for improved sub-modeling of soil temperature, stream temperature,

habitat suitability, photosynthesis, snow dynamics, and any other ecological process where spatially-distributed solar energy has a significant impact on environmental process. Such an integration could benefit many other ecological models.

The Penumbra-VELMA integration has potential to advance predictive ecological modeling. The theoretical Mashel River Watershed demonstration exemplifies dynamic forest growth and disturbance affecting dynamic ground level solar energy estimations. The three Mashel River Watershed scenarios presented provided contrasting landscape scale solar energy resulting from contrasting forest management plans. This approach to ecological modeling has huge potential to leverage existing tools. The simulation results provide process-level details on solar energy response to forest growth and harvest, which could not feasibly be captured through experimentation or observation.

United modeling approaches, like the Penumbra-VELMA integration, have huge potential to benefit long-term ecological land management. As a decision support tool framework, Penumbra-VELMA can provide stakeholders the ability to simulate and understand a variety of landscape management plans prior to implementation of management activities that can take years to decades to come to fruition. Such knowledge is powerful when land management policies are irreversible.

No matter if Penumbra is utilized to develop spatially-distributed solar data that do not currently exist, or is integrated into ecological models to improve its sub-modeling, Penumbra adds to ecological modeling spatially diverse landscape scale solar energy estimates. These estimates include the shadowing from topographic and object shading. The simulation of such data at over large landscapes is a unique advancement for fields of science performing ecological modeling, especially for predictive purposes. With this new solar data, the interplay with other variables can be constructed into more meaningful process-based environmental relationships.

Entities involved in land management (private land-owners, watershed councils, tribes, local, state, and federal government) may have conflicting management goals, yet all share the need for decision support tools. These entities do share the common need for improved ecological tools that provide accurate assessments of these landscapes of interest. Penumbra was developed to be a decision support tool. Stream temperature Total

Maximum Daily Load (TMDL) levels are on the rise, bacterial TMDL levels are an important problem that threatens water quality, and though the remaining riparian zones might be protected, what is left may not be enough to turn the tide on environmental concerns surrounding stream health. I hope as a collaborative society we can advance models that can be leveraged as decision support tools. Then we may fully understand the value of our ecosystems and further understand the impact our land use decisions have on our landscapes. Only then may productive policies be agreed upon; policies that place dynamic ecosystem processes as the focal point of discussion.

6. Bibliography

Abdelnour, A., Stieglitz, M., Pan, F, McKane, R. (2011). "Catchment hydrological responses to forest harvest amount and spatial pattern." Water Resources Research 47(9): 1-18.

Angel, E; and Shreiner, D. (2012). “Interactive Computer Graphics: A Top-Down Approach with Shader-Based OpenGL.” 6th edition. Addison Wesley: Boston MA. pp. 264-265.

Bicknell, B.R., Imhoff, J.C., Kittle, J.L., Jr., Donigian, A.S., Jr., and Johanson, R.C., (1997), “Hydrological Simulation Program--Fortran: User's manual for version 11”: U.S. Environmental Protection Agency, National Exposure Research Laboratory, Athens, Ga., EPA/600/R-97/080, p. 755.

Bokhorst, S., Huiskes, A., Aerts, R., Convey, P., Cooper, E.J., Dalen, L., Erschbamer, B.A., Gudmundsson, J., Hofgaard, A., Hollister, R.D., Johnstone, J., Jonsdottir, I.S., Lebouvier, M., Van de Vijver, B., Wahren, C., Dorrepaal, E. (2013). "Variable temperature effects of Open Top Chambers at polar and alpine sites explained by irradiance and snow depth." Global Change Biology 19(1): 64-74.

Boyd, M., and Kasper, B. (2003). “Analytical methods for dynamic open channel heat and mass transfer: Methodology for heat source model Version 7.0.”

Brown, R., Ebersole, J., Brookes, A., Boxall, G., Massie, J. (2015). “Evaluating the Simulation of Metacommunities for Riverine Fishes (SMURF).” 145th Annual Meeting, Portland, Oregon, American Fisheries Society.

Caissie D. (2006). “The thermal regime of rivers: a review”. Freshwater Biology 51: 1389–1406

Carlson, H.S., and Jaeger, J.C. (1959). “Conduction of Heat in Solids.” 2nd edition. Clarendon Press, Oxford.

Cedar River LiDAR Bare Earth DEM and nDSM (computer file). (2014). “Cedar River Watershed & Floodplain, Lake Youngs Reservoir, & SCL/Tolt Reservoir Study Areas LiDAR”. Available: Puget Sound LiDAR Consortium, Seattle, WA http://pugetsoundlidar.ess.washington.edu/index.htm (January 13th, 2016).

Cushing, J.B., Winters, K.M.,Lach, D., (2015), May. “Software for scientists facing wicked problems lessons from the VISTAS project.” In Proceedings of the 16th Annual International Conference on Digital Government Research (pp. 61-70). ACM.

Detenbeck, N. E., A. C. Morrison, R. W. Abele, and D. A. Kopp (2016), "Spatial statistical network models for stream and river temperature in New England, USA." Water Resource., 52, pp. 6018–6040, doi:10.1002/2015WR018349.

Form B - Locations Worldwide: 44.915960°, -123.001439° (computer file). (1990). "Complete Sun and Moon Data for One Day." Available: Astronomical Applications Department U.S. Naval Observatory (USNO), Washington, D.C. http://aa.usno.navy.mil/data/docs/RS_OneDay.php (October 28th, 2016).

Fatichi, S., Vivoni, E. R., Ogden, F.L., Ivanov, V. Y., Mirus, B., Gochis, D., Downer, C. W., Camporese, M., Davidson, J. H., Ebel, B., Jones, N., Kim, J., Mascaro, G., Niswonger, R., Restrepo, P., Rigon, R., Shen, C., Sulis, M., Tarboton, D. (2016), "An overview of current applications, challenges, and future trends in distributed process-based models in hydrology." USA, Journal of Hydrology, 537, pp. 45–60, doi:10.1016/j.jhydrol.2016.03.026.

Glassner, A. S. (1989). "An Introduction to Ray Tracing." Academic Press pp.10-19, ISBN 0-12-286160-4.

Guzy, M. R., C. L. Smith, J. P. Bolte, D. W. Hulse and S. V. Gregory. (2008). "Policy research using agent based modeling to assess future impacts of urban expansion into farmlands and forests." Ecology and Society 13(1): 37.

Hartmann, D. L., Ockert-Bell, M.E., Michelsen, M.L. (1992). "The Effect of Cloud Type on Earth's Energy Balance: Global Analysis." Journal of Climate 5: pp. 1281-1304.

Heckbert, P. S. (1987). "Ray Tracing JELL-O Brand® Gelatin." Computer Graphics 21(4): pp. 73-74.

Holbert, K. E. and Srinivasan D. "Solar Energy Calculations*,"* Handbook of Renewable Energy Technology, *edited* by A. F. Zobaa and R. C. Bansal, World Scientific Publishing Co., (2011), Chapter 8, pp. 189-204, ISBN *978*-981-4289-06-1.

Java Tutorials. "Trail: The Reflection API". www.docs.oracle.com/javase/tutorial/reflect. Oracle, Web. December 20th, 2016.

Johnson, S. L. (2003). "Stream temperature: scaling of observations and issues for modelling." Hydrological Processes 17(2): pp. 497-499.

Kelly, D. J., Bothwell, M. L., Schindler, D. W. (2003). "Effects of Solar Ultraviolet Radiation on Stream Benthic Communities: An Intersite Comparison." Ecological Society of America 84(10): pp. 2724-2740.

Kennedy, R.E., Yang, Z., Cohen, W.B., Pfaff, E., Braaten, J. and Nelson, P., (2012). "Spatial and temporal patterns of forest disturbance and regrowth within the area of the Northwest Forest Plan." Remote Sensing of Environment, 122, pp.117-133.

Learning OpenGL. "Shadow-Mapping." www.learnopengl.com. Patreon, Web. October 02nd, 2016.

Li, G., Jackson C. R., Kraseski, K. A. (2012). "Modeled riparian stream shading: Agreement with field measurements and sensitivity to riparian conditions." Journal of Hydrology 428-429: pp. 142-151.

Lorensen, W. E. and H. E. Cline (1987). "Marching Cubes: A High Resolution 3D Surface Construction Algorithm." Computer Graphics 21(4): pp. 163-169.

Mayer, T. D. (2012). "Controls of summer stream temperature in the Pacific Northwest." Journal of Hydrology 475: pp. 323-335.

McKane, R.B., Brookes, A., Djang, K., Stieglitz, M., Abdelnour, A. G., Pan, F., Halama, J. J., Pettus, P. B., Phillips, D. L. (2014) "VELMA Version 2.0 – User Manual and Technical Documentation." U.S. Environmental Protection Agency, Office of Research and Development, National Health and Environmental Effects Research Laboratory, Western Ecology Division, Corvallis, Oregon, USA: p. 60.

Means, J. E. and T. E. Sabin (1989). "Height Growth and Site Index Curves for Douglas fir in the Suislaw National Forest Oregon." Western Journal of Applied Forestry 4(4): pp. 136-142.

Mellander, P.E., Stahli, M., Gustafsson, D., and Bishop, K. (2006) "Modelling the effect of low soil temperatures on transpiration by Scots pine", Hydrological Processes., 20, pp. 1929–1944.

Neitsch, S. L., Arnold, J. G., Kiniry, J. R., Williams, J. R. (2011). "Soil and Water Assessment Tool Theoretical Documentation Version 2009." T. W. R. Institute. College Station, Texas, USA, AgriLIFE Research & Extension pp. 32-38.

NRCS: National Water & Climate Center. (2016). "Snow Telemetry (SNOTEL) Data Collection Network." Online. U. S. D. o. Agriculture. Portland OR, NRCS National Water & Climate Center.

NSRDB Hourly Data 24232 Salem, OR (computer file). (1990). "NSRDB 1961-1990: Hourly Data Files." Available: National Renewable Energy Laboratory (NREL), Washington, D.C. http://rredc.nrel.gov/solar/old_data/nsrdb/1961-1990/hourly/1990/ (October 28th, 2016).

Oregon Crest to Coast (computer file). (2008). “EPA Oregon Cascade Mountain Crest-to-Coast transect.” Available: National Oceanic and Atmospheric Administration https://data.noaa.gov/dataset/oregon-crest-to-coast-environmental-monitoring-transect-dataset, ftp://islay.coas.oregonstate.edu/forestbiomass/mr200/ (June 15th, 2016).

Pan, F., Stieglitz, M. and McKane, R.B., (2012). “An algorithm for treating flat areas and depressions in digital elevation models using linear interpolation.” Water Resources Research, 48(6).

PRISM Climate Group, Oregon State University, www.prism.oregonstate.edu, Accessed 16 Feb 2016.

Redding, T. E., Hope, G. D., Fortin, M.-J., Schmidt, M. G., Bailey, W. G. (2003). "Spatial patterns of soil temperature and moisture across subalpine forest-clearcut edges in the southern interior of British Columbia." Canadian Journal of Soil Science (83): pp. 121–130.

Reich, P. B., Luo, Y., Bradford, J. B., Poorter, H., Perry, C. H., Oleksyn, J. (2014). "Temperature drives global patterns in forest biomass distribution in leaves, stems, and roots." Proceedings of the National Academy of Sciences, USA 111(38): pp. 13721-13726.

Rost, Randi J., Bill Licea-Kane. OpenGL Shading Language. 3rd Edition. (2010). Pierson Education Inc. Boston,MA pp. 385-386.

Rost, Randi J., Bill Licea-Kane. OpenGL Shading Language. 3rd Edition. (2010). Pierson Education Inc. Boston,MA pp. 698.

Seidl, R., Rammer, W., Scheller, R. M., Spies, T. A. (2012). "An individual-based process model to simulate landscape-scale forest ecosystem dynamics." Ecological Modelling 231: pp. 87-100.

Sun, N., Yearsley, J., Voisin, N., Lettenmaier, D. P. (2015): “A spatially distributed model for the assessment of land use impacts on stream temperature in small urban watersheds.”, Hydrological Processes., 29(10), pp. 2331-2345

Sun as A Source of Energy. (2015) “Part 4: Irradiation Calculations” www.itacanet.org/the-sun-as-a-source-of-energy/part-4-irradiation-calculations. ITACA, Web. June 15, 2015.

Tague, C. L., and L. E. Band (2004), “RHESSys: Regional hydro-ecologic simulation system—An object-oriented approach to spatially distributed modeling of carbon, water, and nutrient cycling.” Earth Interactions., 8(19), pp. 1–42.

Thornton, P.E., Running, S.W., White, M.A. (1997). “Generating surfaces of daily meteorological variables over large regions of complex terrain.” Journal of Hydrology 190: pp. 204-251. http://dx.doi.org/10.1016/S00022-1694(96)03128-9

Trenberth, K. E. (2002). “Earths Energy Balance.” The National Center for Atmospheric Research. Boulder, Colorado, USA pp. 5-7.

Upper Soda LiDAR Bare Earth DEM and nDSM (computer file). (2009). “Calapooia/South Santiam Study Areas LiDAR.” Available: Oregon Department of Geology and Mineral Industries, Portland, OR http://www.oregongeology.org/dogamilidarviewer (October 15th, 2016).

Ver Hoef, J.M., Peterson E.E., Clifford D., and Shah R. (2014) “SSN: An R package for spatial statistical modeling on stream networks.” Journal of Statistical Software, 56(3).

Waschmann, Ronald S., U.S. Environmental Protection Agency - Western Ecology Division. "Oregon Crest-to-Coast Climate Observations". NOAA National Centers for Environmental Information. doi:10.7289/V5TT4NWV. (15Jun2016).

WED-EPA. (computer file) “Crest-to-Coast Overview.” Available: National Oceanic and Atmospheric Administration https://data.noaa.gov/dataset/oregon-crest-to-coast-environmental-monitoring-transect-dataset, https://www.ncei.noaa.gov/data/epa/oc2c/docs/epa-oregon-crest-to-coast_overview_c20160616.pdf (December 21st, 2016).

Wigmosta, M.S., B. Nijssen, P. Storck, and D.P. Lettenmaier, (2002): “The Distributed Hydrology Soil Vegetation Model, In Mathematical Models of Small Watershed Hydrology and Applications.” V.P. Singh, D.K. Frevert, eds., Water Resource Publications, Littleton, CO., pp. 7-42.

Yearsley, J. (2012). "A grid-based approach for simulating stream temperature." Water Resources Research 48(3).